INTERNATIONAL STANDARD

ISO 21439

First edition
2009-02-15

Clinical dosimetry — Beta radiation sources for brachytherapy

Dosimétrie clinique — Sources de radiation bêta pour curiethérapie

Reference number
ISO 21439:2009(E)

PDF disclaimer

This PDF file may contain embedded typefaces. In accordance with Adobe's licensing policy, this file may be printed or viewed but shall not be edited unless the typefaces which are embedded are licensed to and installed on the computer performing the editing. In downloading this file, parties accept therein the responsibility of not infringing Adobe's licensing policy. The ISO Central Secretariat accepts no liability in this area.

Adobe is a trademark of Adobe Systems Incorporated.

Details of the software products used to create this PDF file can be found in the General Info relative to the file; the PDF-creation parameters were optimized for printing. Every care has been taken to ensure that the file is suitable for use by ISO member bodies. In the unlikely event that a problem relating to it is found, please inform the Central Secretariat at the address given below.

COPYRIGHT PROTECTED DOCUMENT

ISO copyright office
Case postale 56 • CH-1211 Geneva 20
Tel. + 41 22 749 01 11
Fax + 41 22 749 09 47
E-mail copyright@iso.org
Web www.iso.org

Published in Switzerland

Contents

Page

Foreword

ISO (the International Organization for Standardization) is a worldwide federation of national standards bodies (ISO member bodies). The work of preparing International Standards is normally carried out through ISO technical committees. Each member body interested in a subject for which a technical committee has been established has the right to be represented on that committee. International organizations, governmental and non-governmental, in liaison with ISO, also take part in the work. ISO collaborates closely with the International Electrotechnical Commission (IEC) on all matters of electrotechnical standardization.

International Standards are drafted in accordance with the rules given in the ISO/IEC Directives, Part 2.

The main task of technical committees is to prepare International Standards. Draft International Standards adopted by the technical committees are circulated to the member bodies for voting. Publication as an International Standard requires approval by at least 75 % of the member bodies casting a vote.

Attention is drawn to the possibility that some of the elements of this document may be the subject of patent rights. ISO shall not be held responsible for identifying any or all such patent rights.

ISO 21439 was prepared by Technical Committee ISO/TC 85, *Nuclear energy*, Subcommittee SC 2, *Radiation protection*.

Introduction

Clinical dosimetry covers the methods by which values of the relevant physical quantity, absorbed dose to water, can be measured at a given point by the use of calibrated instruments in a clinical setting. The application of beta radiation sources for brachytherapy requires new and skilled methods for adequate clinical dosimetry necessitated by the short range of the beta radiation. This causes large dose-rate gradients around beta radiation sources, and hence it is necessary that the detector volumes for absorbed-dose measurements be extremely small. This leads to the requirement for highly specialized detectors and calibration techniques, and it is necessary to scrutinize closely every calibration obtained in one beta radiation field and determine if it is applicable in another field.

It is necessary that an appropriate quality system be implemented and maintained in the hospital for clinical beta radiation source dosimetry. It is the responsibility of the medical physicist to carry out testing and calibration activities for any source in such a way as to meet the requirements for adequate dosimetry. This International Standard gives guidance on how to satisfy these needs.

Clinical dosimetry — Beta radiation sources for brachytherapy

1 Scope

This International Standard specifies methods for the determination of absorbed-dose distributions in water or tissue that are required prior to initiating procedures for the application of beta radiation in ophthalmic tumour and intravascular brachytherapy [1], [2], [3]. Recommendations are given for beta radiation source calibration, dosimetry measurements, dose calculation, dosimetric quality assurance, as well as for beta radiation brachytherapy treatment planning. Guidance is also given for estimating the uncertainty of the absorbed dose to water. This International Standard is applicable to "sealed" radioactive sources, such as plane and concave surface sources, source trains of single seeds, line sources, and shell and volume sources, for which only the beta radiation emitted is of therapeutic relevance.

The standardization of procedures in clinical dosimetry described in this International Standard serves as a basis for the reliable application of beta radiation brachytherapy. The specific dosimetric methods described in this International Standard apply to sources for the curative treatment of ophthalmic disease, for intravascular brachytherapy treatment, for overcoming the problem of restenosis and for other clinical applications using beta radiation.

This International Standard is geared towards organizations wishing to establish reference methods in dosimetry aiming at clinical demands for an appropriately small uncertainty of the delivered dose. This International Standard does not exclude the possibility that there can be other methods leading to the same or smaller measurement uncertainties.

2 Normative references

The following referenced documents are indispensable for the application of this document. For dated references, only the edition cited applies. For undated references, the latest edition of the cited document (including any amendments) applies.

ISO/IEC Guide 98-3, *Uncertainty in measurement — Part 3: Guide to the expression of uncertainty in measurement* (*GUM:1995*)

ISO/IEC Guide 99, *International vocabulary of metrology — Basic and general concepts and associated terms* (*VIM*)

ISO 6980-2, *Nuclear energy — Reference beta particle radiation — Part 2: Calibration fundamentals related to basic quantities characterizing the radiation field*

ICRU Report 51, *Quantities and Units in Radiation Protection Dosimetry*

3 Terms and definitions

For the purposes of this document, the terms and definitions given in ICRU Report 51, ISO Guide 99 and ISO 6980-2, and the following apply.

3.1
absorbed dose
D
quotient of $\mathrm{d}\bar{\varepsilon}$ by $\mathrm{d}m$, where $\mathrm{d}\bar{\varepsilon}$ is the mean energy imparted by ionizing radiation to matter of mass $\mathrm{d}m$, as given by Equation (1):

$$D = \frac{\mathrm{d}\bar{\varepsilon}}{\mathrm{d}m} \tag{1}$$

NOTE The absorbed dose is designated in units of joules per kilogram, with the special name of gray (Gy).

3.2
absorbed dose to water
D_{w}
quotient of $\mathrm{d}\bar{\varepsilon}$ by $\mathrm{d}m$, where $\mathrm{d}\bar{\varepsilon}$ is the mean energy imparted to water by ionizing radiation to a medium of mass $\mathrm{d}m$, as given by Equation (2):

$$D_w = \frac{\mathrm{d}\bar{\varepsilon}}{\mathrm{d}m} \tag{2}$$

NOTE The absorbed dose to water is designated in units of joules per kilogram, with the special name of gray (Gy).

3.3
acceptance test
contractual test carried out by the user on receipt of a new instrument or source(s) in order to verify compliance with contractual specifications

NOTE 1 An acceptance test of an instrument is carried out after new equipment has been installed, or major modifications have been made to existing equipment.

NOTE 2 An acceptance test of a source is carried out on each source before being put into service for the first time. If a consignment contains more than one source, it is carried out on all sources of a particular type.

3.4
active source length
ASL
length of the source over which the absorbed dose rate at a defined distance from the source axis is within a specified ratio of the maximum absorbed dose rate at this distance

3.5
afterloading
automatically or manually controlled transfer of one or more sealed radioactive sources between a storage container and pre-positioned source applicators for brachytherapy

3.6
average beta energy
E_{ave}
quotient of beta energy averaged over the distribution, Φ_E, of the beta particle fluence with respect to energy as given by Equation (3):

$$E_{ave} = \frac{\int_0^{E_{max}} E\,\Phi_E(E)\,dE}{\int_0^{E_{max}} \Phi_E\,dE} \quad (3)$$

where $\Phi_E = d\Phi/dE$

3.7
brachytherapy
intracavitary, interstitial, superficial (including ophthalmic), or intraluminal (e.g. intravascular) radiotherapy in the immediate vicinity of one or more sealed or unsealed radioactive sources

3.8
calibration
set of operations that establish, under specific conditions, the relationship between values of a quantity and the corresponding values traceable to primary standards

NOTE 1 For an instrument, a calibration establishes, under specific conditions, the relationship between values of a quantity indicated by a measuring instrument or measuring system and the corresponding values realized from the standards.

NOTE 2 For a source, a calibration establishes, under specific conditions, the value of a quantity produced by the source.

3.9
clinical target volume
CTV
gross tumour or target volume (GTV) with the addition of a margin that accounts for cells that are clinically suspected but have unproven involvement

NOTE In malignant disease, e.g. ophthalmic tumours, these oncological safety margins account for subclinical disease. In restenosis treatment, the CTV includes the full interventional length (IL) of the vessel with all vessel wall layers and with the addition of proximal and distal safety margins to include all tissue possibly injured during the interventional process.

3.10
detector test source
radiation source used for the determination of the long-term stability of a radiation detector

3.11
dosimeter
⟨beta radiation therapy⟩ equipment that uses detectors for the measurement of absorbed dose, or absorbed dose rate, in beta radiation fields as used in radiation therapy

NOTE A radiotherapy dosimeter contains the following components: one or more detector assemblies, a measuring assembly (including possibly a separate display device), one or more detector test sources (optional) and one or more phantoms (optional).

3.12
dwell time
time a radioactive source or source train remains at a selected treatment position

3.13
effective point of measurement
P_{eff}
point at which the absorbed dose rate in an undisturbed medium is determined from the detector signal

3.14
extrapolation chamber
ionization chamber capable of having a collection volume that is continuously variable to a vanishingly small value by changing the separation of the electrodes, which allows the user to extrapolate the measured ionization density to zero collecting volume

NOTE The extrapolation chamber serves as a primary standard, under proper conditions of use (see Annex C).

3.15
fluence
Φ
quotient of $\mathrm{d}N$ by $\mathrm{d}A_{\mathrm{s}}$, where $\mathrm{d}N$ is the number of particles incident on a sphere of cross-sectional area $\mathrm{d}A_{\mathrm{s}}$, as given by Equation (4):

$$\Phi = \mathrm{d}N/\mathrm{d}A_{\mathrm{s}} \tag{4}$$

3.16
gross tumour or target volume
GTV
macroscopic extent and location of target tissue that can be observed or visualized using applicable imaging modalities

NOTE In malignant disease, e.g. ophthalmic tumours, target tissue means the demonstrable tumour growth. In restenosis treatment, the GTV includes the full vessel extent injured during the interventional process.

3.17
influence quantity
quantity that can have a bearing on the result of a measurement without being the subject of the measurement

3.18
interventional length
IL
length of the vessel injured during the interventional process

3.19
lesion length
LL
stenotic or occluded length of the vessel segment as determined by the interventionalist

3.20
maximum beta energy
E_{max}
highest value of the energy of beta radiation emitted by a particular radionuclide that can emit one or several continuous spectra of beta radiation each with a characteristic maximum energy

3.21
measurement standard
instrument that defines, represents physically, maintains or reproduces the unit of measurement of a quantity (or multiple or sub-multiple of that unit) in order to transfer it to other instruments by comparison

3.22
planning target volume
PTV
clinical target volume (CTV) plus safety margins to account for physiological movements and changes, as well as for various set-up uncertainties

3.23
point of test
point at which the conventional true value is determined and at which the reference point of the dosimeter is placed for calibration and test purposes

3.24
primary standard
measurement standard (of the highest metrological quality) that defines, represents physically, maintains or reproduces the unit of measurement of a quantity (or a multiple or sub-multiple of that unit) in order to transfer it to other instruments by comparison

NOTE 1 The primary standard is operated by a national laboratory under reference conditions and its accuracy has been verified by comparison with the comparable standards of institutions participating in the International Measurement System.

NOTE 2 A primary standard realizes the quantity being measured without reference to any other standard of the same type.

3.25
ionizing radiation
emission and propagation of energy through space or through a material medium in the form of electromagnetic waves or particles that have the potential to ionize an atom or molecule through atomic interactions

3.26
radiation detector
equipment, generally a sub-assembly, or substance that, in the presence of radiation, provides by either direct or indirect means a signal or other indication suitable for use in measuring one or more quantities of the incident radiation

3.27
reference absorbed dose to water
D_{o}
absorbed dose to water at the reference point

3.28
reference conditions
set of influence quantities for which the calibration is valid without any correction

NOTE The reference conditions for the quantity being measured may be chosen consistent with the properties of the instrument being calibrated. The quantity being measured is not an influence quantity.

3.29
reference isodose length
RIL
vessel length at the reference distance enclosed by a certain defined percentage isodose of the reference dose at P_{Ref}

NOTE 1 The reference distance is measured from the source axis to a line parallel to the source axis on which P_{Ref} is located.

NOTE 2 For example, ESTRO recommends the 90 % isodose.

3.30
reference lumen diameter
RLD
diameter of the vessel lumen after angioplasty as determined by angiography in a representative plane within the planning target volume

3.31
reference orientation of a detector
orientation of the dosimetry detector with respect to the direction of the incident radiation stated by the manufacturer

3.32
radionuclide purity
proportion of the total activity present in the form of the stated radionuclide

NOTE The radionuclide purity is generally expressed as a percentage.

3.33
reference point
P_{ref}
⟨for source calibration⟩ point in a source radiation field at which the reference absorbed dose rate is specified, and which is also used for normalization of relative measurements

3.34
reference point of a detector
point of a detector that is placed at the point of test for calibrating or testing purposes

NOTE The distance of measurement refers to the distance between the reference points of the radiation source and of the detector.

3.35
routine calibration
calibration appropriate to a routine application of a source or an instrument

NOTE A routine calibration may be of a confirmatory nature when it is performed either to check the calibration carried out by the manufacturer together with an instrument, or to check whether the calibration is sufficiently stable during the continued, long-term use of a source or an instrument. When considering the most practical way to perform a routine calibration, results obtained in a type test can turn out to be helpful, for example in selecting the phantom.

3.36
secondary standard
standard whose value is assigned by comparison with a primary standard of the same quantity

3.37
source applicator
⟨brachytherapy⟩ device to position one or more radiation sources at the intended treatment positions

NOTE The radiation source may be a fixed part of the applicator, and the applicator may, furthermore, include protective shielding and/or a source guide.

3.38
source train
sequence of sealed radioactive sources, possibly separated by non-radioactive spacers, that is specified by a single value and calibrated as a whole

3.39
special calibration
calibration of a source or an instrument for a special case similar to that performed in connection with a type test

NOTE A special calibration is performed, for example, if the source or instrument is used under special circumstances or if the routine or type testing provides insufficient information.

3.40
standard test conditions
conditions under which all influence quantities and instrument parameters have their standard test values

NOTE Ideally, calibrations should be carried out under reference conditions. As this is not always achievable (e.g. for ambient air pressure) or convenient (e.g. for ambient temperature), a (small) interval around the reference values may be used. In principle, corrections should be made for the deviations of the calibration factor (if dimensionless) or calibration coefficient (if the instrument indication has different units from the calibration quantity) from its value under reference conditions caused by these deviations. In practice, the uncertainty aimed at serves as a criterion to determine whether it is necessary to take an influence quantity into account by an explicit correction or whether its effect may be incorporated into the uncertainty. During type tests, all values of influence quantities that are not the subject of the test are fixed within the interval of the standard test conditions.

3.41
test
⟨of an instrument⟩ measurement intended to confirm that an instrument is functioning correctly and/or the quantitative determination of the variations of the indication of the instrument over a range of radiation, electric and environmental conditions

NOTE Four distinct categories of instrument testing, of which calibration is a part, are generally recognized: type test, acceptance test, special calibration, routine calibration.

3.42
test
⟨of a source⟩ measurement intended to confirm that a source is functioning correctly and/or that the encapsulation is intact, and/or the quantitative determination of the variations of the field of the source over a range of radiation, electric and environmental conditions

NOTE Four distinct categories of source testing, of which calibration is part, are generally recognized: type test, acceptance test, special calibration, routine calibration.

3.43
traceability
property of the result of a measurement or the value of a standard whereby it can be related to stated references, usually national standards or International Standards, through an unbroken chain of comparisons each having a stated uncertainty

3.44
transfer standard
standard used as an intermediary to compare standards and establish traceability

3.45
treatment parameter
factor that describes one aspect of the irradiation of a patient during radiotherapy, such as radiation energy, absorbed dose, treatment time

3.46
treatment time
time between initiation and termination of irradiation, excluding any time in the ready state after interruption

3.47
type test
⟨of an instrument⟩ test intended to determine the characteristics of a particular type or model of a production instrument

NOTE 1 This type test involves extensive testing over a wide range of quantities that can have a bearing on the result of a measurement without being the objective of the measurement: the “influence quantities”. For ionizing radiation detectors, such influence quantities are, for instance, energy, angle of incidence, dose or dose rate and radiation type, usually under a variety of environmental conditions.

NOTE 2 A type test is normally performed on a prototype or on an instrument taken at random from a production batch and intended to be typical of the type. A type test will normally be carried out by National or Secondary Standard Laboratories, which may make the information available to the instrument user.

3.48
type test
〈of a source〉 test intended to determine the characteristics of a particular type or model of a production source

NOTE 1 This type test involves extensive testing for a number of conditions that can have a bearing on the result of an irradiation.

NOTE 2 A type test is normally performed on a prototype or on a source taken at random from a production batch and intended to be typical of the type. A type test will normally be carried out by National or Secondary Standard Laboratories, which may make the information available to the source user.

3.49
water equivalence
property of a material that approximates the radiation attenuation and scattering properties of water for a specified range of radiation energies

3.50
water-equivalent material
material that absorbs and scatters a specified radiation quality to the same degree as water for a specified range of radiation energies

3.51
water phantom
water-equivalent phantom
object made from water or a water-equivalent material having essentially the same radiation interaction properties as liquid water with respect to the dosimetric procedure under consideration

4 Beta radiation sources and source data

4.1 Ophthalmic and dural brachytherapy sources

Brachytherapy has been used since the beginning of the 20th century when applications using radium and radon seeds in skin applicators were performed. Besides beta radiation, these natural radioactive sources emit alpha and gamma radiation. A typical indication is the control of the formation of keloids. The development of artificial, less radiotoxic radioactive sources allowed an increase in the activity concentration and thus a reduction in treatment time, and an improvement in radiation protection as well. With the experience of ophthalmic brachytherapy using cobalt-60 (^{60}Co) applicators, beta radiation from strontium-90/yttrium-90 (^{90}Sr + ^{90}Y) planar and later curved applicators also started being used in the 1950s for the treatment of lesions of the eye, such as pterygia. Often referred to as “plaques”, in this International Standard, they are referred to as “applicators” or “radioactive ophthalmic brachytherapy sources”.

In the 1980s, radiotherapy for eye malignancies (e.g. uveal melanoma, retinoblastoma, hemangioma) [4], [5], [6], [7], [8], [9] was found to offer a therapeutic alternative to enucleation, being at least equally effective in controlling tumour growth and at the same time eye- and vision-sparing. For such ophthalmic treatments, a number of different beta emitters, and also photon sources, were used in the past, e.g., strontium-90/yttrium-90 (^{90}Sr+^{90}Y), ruthenium-106/rhodium-106 (^{106}Ru+^{106}Rh), cobalt-60 (^{60}Co), iridium-192 (^{192}Ir), gold-198 (^{198}Au) and radium-226 (^{226}Ra). Presently ^{106}Ru + ^{106}Rh ophthalmic brachytherapy sources are widely used, especially in Europe, and remain commercially available. Also ^{90}Sr + ^{90}Y ophthalmic brachytherapy sources are applied for a few cases [10], although they are currently not being manufactured.

For completeness, we mention that in the US, custom-made ophthalmic brachytherapy sources employing iodine-125 (^{125}I) or palladium-103 (^{103}Pd) are mainly used. Also, eye applicators which combine iodine-125 and ruthenium-106/rhodium-106 have recently been introduced into the clinical routine at Essen University Hospital [11]. Clinical dosimetry of this applicator and photon sources are both beyond the scope of this International Standard.

Very recently, thin yttrium-90 (^{90}Y) foil applicators have been used to treat spinal dura after tumour removal to control microscopic residual disease [12].

4.2 Intravascular brachytherapy sources

In intravascular brachytherapy (IVB), the vessel section injured by the interventional process of widening is treated with either beta or photon radiation [13], [14], [15]. In the coronary artery tree, the injured section lengths are usually on the order of 2 cm to 4 cm in arteries with diameters of 2 mm to 4 mm. It is also necessary to treat longer or more complex target volumes (long lesions up to 9 cm, multifocal lesions or bifurcations) in coronaries and in large peripheral vessels (tens of centimetres). This requires line sources with a very narrow diameter, less than 1 mm, able to fit through a brachytherapy catheter. Typical arrangements include encapsulated line sources mounted on the end of wires that can be used to insert and remove the sources to and from the treatment volume. Line sources may also be realized from linear arrays of "seeds," which can be delivered to the target site either manually or automatically. Radionuclides that have been used for these sources include ^{32}P, ^{90}Sr + ^{90}Y, and ^{90}Y. The physical length of these sources varies (3 cm to 6 cm) to adequately cover the target volume. Stepping short wire sources (0,5 cm to 2 cm) are used to treat longer target volumes.

Other sources have been applied to the restenosis problem, however they were for the most part unsealed and their dosimetry is beyond the scope of this International Standard. For completeness, they include ^{188}Re and ^{186}Re radioactive liquid, ^{133}Xe gas-filled balloons, ^{32}P-coated balloons and radioactive stents [14]; no further details on these sources are given in this International Standard.

4.3 Characteristics of radionuclides

Table 1 shows a compilation of half-lives (with uncertainties), and maximum and average energies for the different beta radiation sources most commonly used for clinical applications [16].

Table 1 — Properties of radionuclides in the most commonly used clinical beta radiation sources

Beta emitter	Half life d	E_{max} MeV	E_{avg} MeV	Major photon radiation with percentage per decay
^{90}Sr	10 523 ± 22	0,546	0,195 8	none
^{90}Y	2,667 ± 0,008	2,280 1	0,933 6	none
^{32}P	14,263 ± 0,003	1,710 5	0,694 9	none
^{106}Ru	373,59 ± 0,15	0,039 4	0,010	none
^{106}Rh	(3,449 ± 0,009) E-4	3,541 0	1,410	0,512 MeV (20 %) 0,622 MeV (10 %) 1,0 MeV (1,6 %) 1,13 MeV (0,4 %) 1,55 MeV (0,2 %)

4.4 Source specification

4.4.1 General

The manufacturer of brachytherapy sources shall provide the following information:

— reference data set (RDS) of the given source type, and

— calibration data (CD) of the specific source.

NOTE Appropriate documents containing the required data include the source certificate (SC) (as given in ISO 2919 [175] and IAEA No. TS-R-1 [17]) and the “Instructions for use”.

The manufacturer is liable for his products according to legal requirements. Thus, the reference data set and the calibration data shall contain all data on which treatment planning at the required level is based. The measurement information required in the calibration data is important also for the clinical user who is required to make an independent verification of the source properties.

See Annex B for examples of data sheets.

4.4.2 Reference data set

4.4.2.1 General

The RDS shall contain at least

— the manufacturer's name, and address;

— the radionuclide, half life and maximum beta energy of the nuclide, and major photon radiation components and energies;

— a statement of radionuclide purity;

— source type identification, nominal dose rate and nominal contained activity;

— design of the source, including dimensions and composition (both radioactive core and encapsulation).

4.4.2.2 Reference data set for area sources

An RDS specifically for area (ophthalmic concave or planar) sources shall contain at least

— the active and physical diameters, window thickness and material, radius of curvature, dimensions of cutouts (e.g. see Annex B: product data sheet);

— typical values of the relative axial dose rate (depth dose distribution) with a resolution of at least 1 mm starting closer than 1 mm from the applicator surface to the bremsstrahlung background;

— typical two-dimensional distribution of the relative dose rate with a resolution of at least 10 % (in at least one plane including the source axis and, in the case of asymmetric sources, in a second orthogonal plane through the cutout), as well as in at least one plane perpendicular to the source axis preferably through the reference point.

4.4.2.3 Reference data set for line sources

An RDS specifically for line (intravascular seed arrays, wire or balloon) sources shall contain at least

— the seed number (if applicable), nominal inactive and active source length and diameter, number and position of markers on active and dummy sources, design and dimensions of the catheter and relevant tolerances;

— typical values of the relative radial dose rate as a function of the distance from the source axis with a resolution of at least 0,1 mm from 0,5 mm to the bremsstrahlung background, including values at about 50 %, 75 %, and 125 % of the range of the beta radiation;

— typical values of the relative longitudinal dose rate, along a line parallel to the source axis through P_{ref};

— support for three-dimensional dosimetry for intravascular sources (optional) (see 5.4).

4.4.3 Calibration data

4.4.3.1 General

Calibration data (CD) shall contain at least the reference dose rate at the calibration date/time with uncertainty (expanded with $k = 2$), with the method of determination and with a statement on the traceability to a primary standard.

4.4.3.2 Calibration data for area sources

Calibration data specifically for area (ophthalmic concave or planar) sources shall contain at least

— tabulated values of the absorbed dose rate to water (relative or absolute) as a function of distance from the applicator surface along the source axis, with a resolution of at least 1 mm, starting closer than 1 mm from the applicator surface and extending to the bremsstrahlung background, with uncertainty (expanded with $k = 2$) and method of determination;

— relative dose rate distribution at 1,0 mm distance from the surface normalized to the value at the axis with uncertainty (expanded with $k = 2$) and method of determination, and values of derived source non-uniformity (see 5.7.3) and source asymmetry (see 5.7.4);

— relative dose rate distribution in planes perpendicular to the source axis (to allow comparison with measurements in the clinic; see 11.1.6) (optional);

— source data to support three-dimensional dose distribution calculation (optional).

4.4.3.3 Calibration data for line sources

Calibration data specifically for line (intravascular seed arrays, wire or balloon) sources shall contain at least

— relative radial dose rate distribution (measured on a line vertical to the source axis through P_{ref} with resolutions of at least 0,5 mm);

— relative longitudinal dose rate distribution (measured at a line parallel to the source axis through P_{ref});

— statement on active source length;

— value of source non-uniformity (see 5.7.3);

— statement on equatorial anisotropy (see 5.7.5).

5 Dose calculation parameters and formalisms

5.1 General

In 5.2 to 5.7 are introduced the relevant radiation-field parameters and formalisms for expressing dose distributions about beta radiation sources. In this International Standard, discussion is limited to four source geometries: point, line, planar and concave.

5.2 Parameters of the radiation field

5.2.1 General

It is often convenient to parameterize the radiation field rather than to express the absorbed dose rate as a function of position around the source. An obvious first step in this parameterization is to use the absorbed dose rate at the reference point, and then use a relative value of the absorbed dose rate at other points. These relative values do not change with time (as does the absorbed dose rate for radionuclide sources) and presumably are the same from source to source for the same radionuclide and source construction.

5.2.2 Reference absorbed dose to water

The choice of the reference distance for the reference absorbed dose (rate) to water is based on the geometry of the sources used, the characteristic of the near-field dose distribution of the applied beta nuclides and the distance of clinical interest. Therefore, the reference point for planar beta radiation sources is located 1 mm from the source surface and for concave sources, 2 mm from the source surface, both on a line passing through the centre of the source area. The choice of 2 mm for the reference point distance for concave applicators, rather than the 1 mm recommended by the ICRU Report 72 [18], is justified by the difficult source geometry, which makes measurements at the closer distance a problem. For beta radiation point and line sources, the reference point is located at a distance of 2 mm measured from the source centre, and for line sources it is perpendicular to the source axis [18], [19], [20], [21],[22], [23].

The absorbed dose rate at the reference point, P_{ref}, defined as the reference absorbed dose rate to water, is denoted by $\dot{D}_0(\vec{r}_0)$, where $\vec{r}_0$ is the location of the reference point. The absorbed dose rate at any arbitrary location, $\vec{r}$, about the source is then given by Equation (5):

$$\dot{D}(\vec{r}) = \dot{D}_0(\vec{r}_0)R(\vec{r}) \tag{5}$$

where $R(\vec{r})$ is the relative absorbed dose rate function.

5.2.3 Dose distribution coordinate systems

The choice of coordinate system in which to express $\vec{r}$ is usually guided by the source geometry. For point-like sources, it is convenient to use spherical coordinates, $\vec{r}(r,\theta,\phi)$; however for planar, concave and line sources, a cylindrical coordinate system, $\vec{r}(\rho,z,\phi)$, is better adapted, especially if the source exhibits symmetry around the source axis. In this case, the absorbed dose rate varies only in the radial direction ("away" from the axis of a line source or the central axis of an area source) and in the axial direction ("along" a line source, or away from the surface of an area source). Equation (5) then reduces to the form given in Equation (6):

$$\dot{D}(\rho,z) = \dot{D}(\rho_0,z_0)R(\rho,z) \tag{6}$$

where ρ and z are the radial and axial coordinates, respectively, and (ρ_0, z_0) are the coordinates of the reference point. The function $R(\rho,z)$, when given in a tabular format, is commonly known as an "away and along" table. Figure 1 illustrates the three coordinate systems used. It is important to note the opposite meanings of away and along for the line source versus the area source geometries. The reference coordinates in the recommended systems for the various beta radiation source geometries are shown in Table 2.

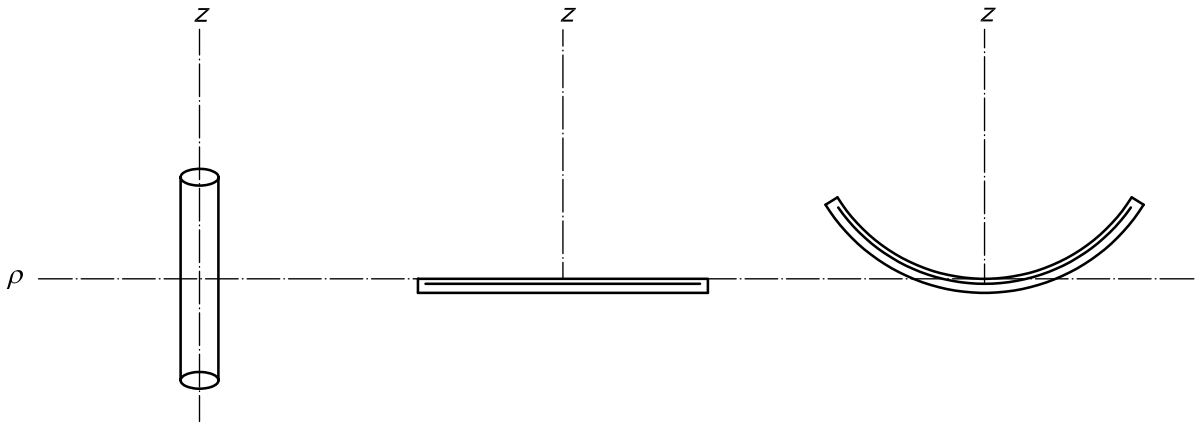

Figure 1 — Cylindrical coordinate systems for beta radiation source geometries

Table 2 — Reference points, P_{ref}, for beta radiation sources

Source geometry	ρ mm	z mm
Line source	2	0
Planar source	0	1
Concave source	0	2

The formalisms discussed assume cylindrically symmetric sources. For cylindrically non-symmetric sources (e.g. notched applicators), it is necessary that the formalisms be extended to include the dependence on the azimuthal angle, ϕ. For such sources, the Z axis should be specified by the manufacturer.

5.3 Radial dose profile

In spherical coordinates for a symmetric point like source, Equation (5) reduces to the form of Equation (7):

$$\dot{D}(r) = \dot{D}_0 R(r) \tag{7}$$

where $R(r)$ is known as the radial dose profile and is analogous to the central-axis depth dose function in radiotherapy with beam sources.

For line sources, it is possible to define a similar function, which corresponds to the $z = 0$ column of an “away and along” table. In this case, Equation (7) takes the form of Equation (8):

$$\dot{D}(\rho,z) = \dot{D}_0 R(\rho) H(\rho,z) \tag{8}$$

where $H(\rho,z)$ is the off axis dose function, normalized to unity for $z = z_0 = 0$. The derivation of Equations (9) and (10) should be obvious:

$$R(\rho) = \dot{D}(\rho,z_0) / \dot{D}_0 \tag{9}$$

and

$$H(\rho,z) = \dot{D}(\rho,z) / \dot{D}(\rho,z_0) \tag{10}$$

Because of the very high dose-rate gradients close to seed and line sources, a different approach is used for field parameterization of these sources (see 5.4).

For area sources, this is expressed in the form of Equation (11):

$$\dot{D}(\rho,z) = \dot{D}_0 R(z) H(\rho,z) \tag{11}$$

where

$H(\rho,z)$ is the off-axis dose function, normalized to unity for $\rho = \rho_0 = 0$;

$$R(z) = \dot{D}(\rho_0,z)/\dot{D}_0\,; \tag{12}$$

$$H(\rho,z) = \dot{D}(\rho,z)/\dot{D}(\rho_0,z)\,. \tag{13}$$

5.4 Normalization of relative-dose data for seed sources

5.4.1 General

The protocol recommended by the AAPM TG 60 Report [22] for the calculation of the three dimensional dose distributions around beta radiation sources used in intravascular brachytherapy is based on the older TG-43 protocol [24], developed to apply only to photon-emitting sources like seeds used for interstitial brachytherapy. Therefore, the formalism has been expressed in spherical coordinates assuming symmetry about the source axis. The positions are represented in the remaining two coordinates, r and θ. Figure 2 shows a representation of this coordinate system. Using this formalism, the absorbed dose rate, $\dot{D}(r,\theta)$, is given by Equation (14):

$$\dot{D}(r,\theta) = \dot{D}_0(r_0,\theta_0)\cdot\frac{G(r,\theta)}{G(r_0,\theta_0)}\cdot g(r)\cdot F(r,\theta) \tag{14}$$

This approach is chosen for field parameterization rather than the “away and along” table approach [see Equation (8)] because use of the geometry function removes much of the high cell-to-cell variation in the “away and along” tables, making interpolations more accurate, as described in 5.4.2 to 5.4.4.

5.4.2 Geometry function, $G(r,\theta)$

The geometry function accounts for the variation of dose due to an idealized activity distribution of the source. It should be emphasized that it is only a convenient construct, meant to make the interpolations of the other parameters more accurate by removing the inverse square dependence of the dose rate distribution. The value of the geometry function is calculated under the line source approximation as given in Equation (15):

$$G(r,\theta) = \frac{\beta}{Lr\sin(\theta)} \tag{15}$$

where

L is a length, usually taken as the active source length;

β is the angle subtended by the source length, L, at the point (r, θ).

Referring to Figure 2, it can be seen that $\beta = \theta_2 - \theta_1$. The geometry function is meant to represent the absorbed dose distribution in the absence of scattering and absorption for a line source of length, L.

5.4.3 The radial dose function, $g(r)$

The radial dose function represents the variation of the absorbed dose rate along the perpendicular bisector of the source, and includes the effects of absorption and scatter in water. It can be calculated from the radial dose profile, $\dot{D}(r,\theta_0)$, using Equation (16):

$$g(r) = \frac{\dot{D}(r,\theta_0)}{\dot{D}(r_0,\theta_0)} \cdot \frac{G(r_0,\theta_0)}{G(r,\theta_0)} \tag{16}$$

The first quotient is simply the radial dose profile, $R(r)$, expressed in polar coordinates.

The radial dose function can be given in the form of a polynomial function, which is evaluated at the desired radial distance, r. This function is unity for r_0.

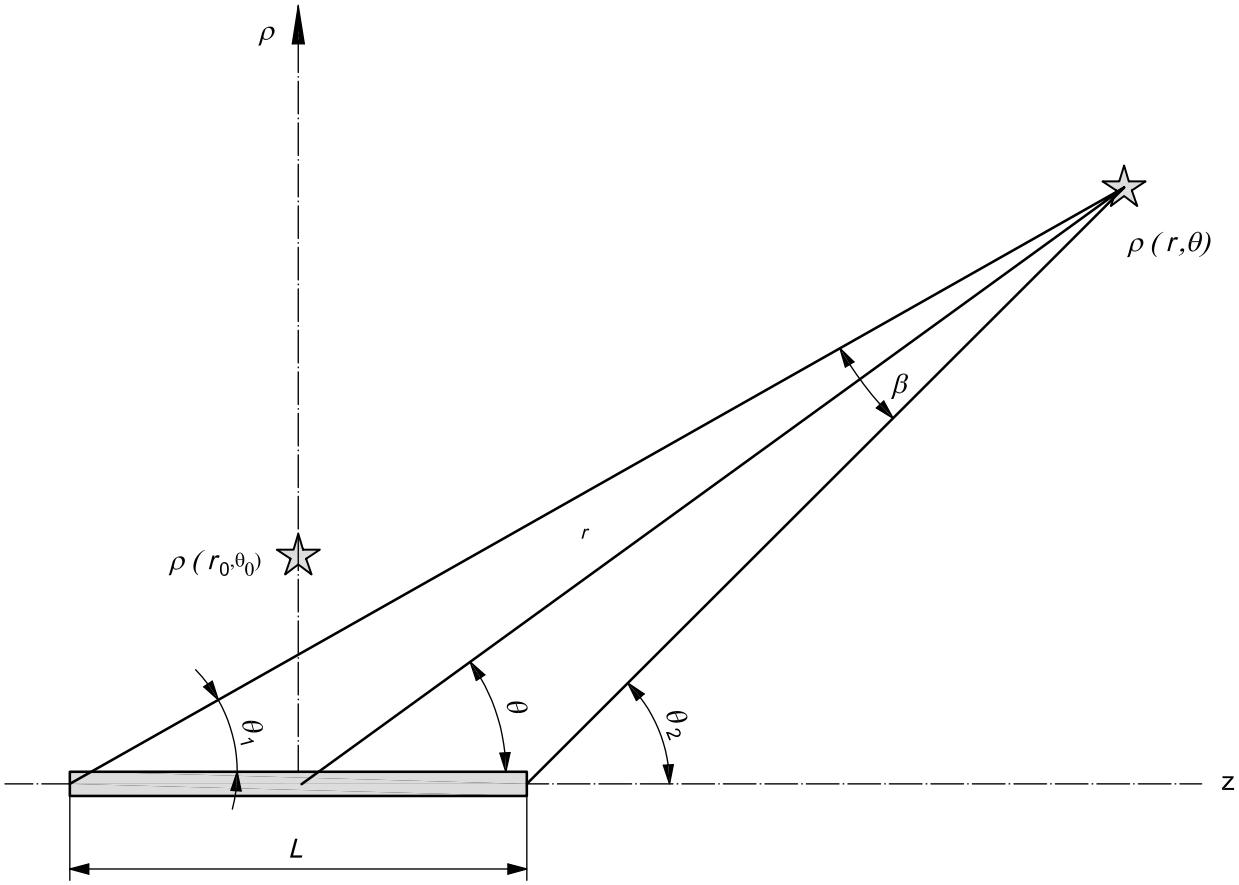

Figure 2 — TG-43 protocol coordinate system

5.4.4 The anisotropy function, $F(r,\theta)$

The anisotropy function represents the variation of the absorbed dose rate around the source in the θ direction and includes the effects of absorption and scatter in water. It can be calculated from the off-axis dose profile, appropriately converted to polar coordinates using Equation (17):

$$F(r,\theta) = \frac{\dot{D}(r,\theta)}{\dot{D}(r,\theta_0)} \cdot \frac{G(r,\theta_0)}{G(r,\theta)} \tag{17}$$

Again, the first quotient is simply the off-axis dose function, $H(r,\theta)$, normalized to unity at θ_0. The anisotropy function is given in tabular format, where it is possible to interpolate the radial distance and the angle to obtain the value of the function at the desired coordinates.

5.5 Adaptation of the TG-43/60 formalism for a long beta radiation line source

5.5.1 General

The application of the TG-43/60 formalism breaks down in the case of a long beta line source or an entire source arrangement consisting of several seeds [26], [27]. As already introduced in 5.4, the AAPM TG 43/TG 60 formalism should be used for single-seed sources or small segments of a wire source. One solution to the breakdown problem is to use the results of calculations for small segments of line sources. One of the motivations for calculating only small segments is the possibility of modelling dose distributions from non-uniform sources, as well as to study the effect of changes in source length. Furthermore, using a 2,5 mm wire segment, there are no problems with a breakdown in the AAPM TG 43 formalism [25]. In addition, it is possible to make dose-profile calculations for a curved source, as can also be done with the seed-based sources, using the TG-43/60 formalism. This is a very powerful argument for not changing the formalism, but rather using data for a shorter wire segment to model the dose distribution for a longer source.

5.5.2 Introduction of cylindrical coordinates and new terminology for functions

Schaart, *et al*., [26] have proposed an adaptation of the formalism that appears to work well for intravascular line sources but that preserves the essential advantages of the AAPM TG 43/TG 60 approach. The new formalism is conceptually similar to the AAPM TG 43/TG 60 formalism. However, the parameters of the new formalism are redefined to avoid the singularity problem described above. Furthermore, the new formalism is defined in cylindrical coordinates, which better match the source-target geometry. This has the advantage that an evenly spaced matrix of data points within the region of interest is easily obtained using equidistant intervals along the axes.

In the cylindrical coordinate formalism, the dose-rate distribution about a beta radiation line source in water is expressed as given in Equation (18):

$$\dot{D}(\rho,z) = \dot{D}_0 \cdot \frac{G(\rho,z)}{G(\rho_0,z_0)} \cdot g(\rho) \cdot F(\rho,z) \tag{18}$$

Here, $\dot{D}_0$ denotes the source strength that is defined as the absorbed dose rate in water at the reference point, i.e. at $\rho_0 = 2$ mm and $z_0 = 0$. Similar to the older TG-43 formalism, a geometry function is used to suppress the influence of the inverse square law on the other parameters. The general definition of the geometry function has been given in 5.4.2. Since the dose rate along a long, uniform beta radiation line source is uniform and independent of source length except near the ends of the source, it is appropriate to use the geometry function for an infinite line source, as originally proposed by Schaart, *et al*. [26]. In this approximation, the geometry function reduces to the form of Equation (19):

$$G(\rho,z) = G(\rho) = \frac{1}{\rho} \tag{19}$$

The transverse dose function, $g(\rho)$, which is normalized to unity at the reference point, is defined as given in Equation (20):

$$g(\rho) = \frac{G(\rho_0,z_0)}{G(\rho,z_0)} \frac{\dot{D}(\rho,z_0)}{\dot{D}(\rho_0,z_0)} \tag{20}$$

The transverse dose function plays a role similar to that of the radial dose function in that it characterizes the dose-rate distribution along the transverse bisector of the source. However, the transverse dose function is a function of the cylindrical radial distance, ρ, instead of the spherical distance, r. Therefore, if the above geometry function is used, $g(\rho)$ characterizes the entire dose distribution about a uniform beta line source, except in the dose fall-off regions near the ends of the source.

The non-uniformity function, $F(\rho,z)$, which is normalized to unity on the transverse axis, is defined as given in Equation (21):

$$F(\rho,z)=\frac{G(r,z_0)}{G(r,z)}\,\frac{\dot{D}(\rho,z)}{\dot{D}(\rho,z_0)} \tag{21}$$

If the geometry function in Equation (19) is used, the first term on the right-hand side vanishes so that the non-uniformity function completely describes the axial variation of the dose rate in terms of the ratio of the dose rate at a point and the dose rate on the transverse axis at the same radial distance. Thus, this function accounts not only for the dose fall-off near the source ends, but also for any dose-rate non-uniformity that can result from variations in, for example, the activity distribution or the encapsulation thickness along the length of the source.

5.6 Reference data sets

Reference values of relative dose-rate data are used both for simple manual calculation as well as for treatment-planning software. While they can be obtained by comparisons and averages of independently performed theoretical modeling calculations, for values obtained from measurements of real sources, it is necessary that high accuracy and reproducibility be achieved in order to avoid unacceptably high uncertainties in the resulting data. This issue should be assessed whenever reference-source data are presented.

At the present time, there are no published tabulations of reference-data sets for ophthalmic brachytherapy sources. However, some representative data for a planar $^{90}Sr+{}^{90}Y$ source and a concave $^{106}Ru+{}^{106}Rh$ source, taken from ICRU Report 72 [18], are given in Annex A.

For two beta radiation intravascular brachytherapy sources, reference data have been published [27]. These data are shown in Annex A for $^{90}Sr+{}^{90}Y$ seed sources and for ^{32}P wire sources. In addition, calculated data are also given in Annex A for ^{32}P wire segments that can be used to build up an arbitrarily long source.

Also, as an aid to the calculation of $G(r,\theta)$, a sample table is given for a 2,5 mm source. Note that the quantity $r^2G(r,\theta)$ is tabulated. This is an interesting quantity since it indicates any deviations from the inverse square law due to the line source approximation.

5.7 Parameters for source uniformity characterization

5.7.1 General

Real radiation sources are characterized by a less than perfectly uniform distribution of the radioactive material within the source volume. Additionally, the influences of encapsulation and its mechanical tolerances are more important for beta radiation than for photon sources. For this reason, parameters to characterize this non-uniform distribution are required to set limits on acceptable non-uniformities. Moreover, these limits can represent boundary criteria for the use of nominal dose-rate values.

5.7.2 Average reference absorbed dose rate to water for a line source

With the assumption of a uniform dose-rate distribution, the concept of reference absorbed dose rate, while defined at a point, can be extended to the useful length of a beta radiation source. And *vice versa*, the average absorbed dose rate of a beta radiation line source can be defined by the average of the absorbed dose rates at a distance of 2 mm from the source axis over the active length source minus a margin at each end of the source [28]. For ^{32}P sources, this margin shall be taken as 2,5 mm, while for $^{90}Sr+{}^{90}Y$ sources, the margin shall be taken as 3,0 mm. To distinguish this averaged quantity from the reference absorbed dose rate, $\dot{D}_0$, the symbol $\dot{D}_{avg}$ is used.

5.7.3 Source non-uniformity

For area sources that have rotational symmetry, source non-uniformity at a given distance from the source surface is expressed as the percentage value of the maximum deviation of absorbed dose rate from the absorbed dose rate on the source axis ($\rho = 0$) within a radius given by 0,8 R_{50}, where R_{50} is the radius of the 50 % isodose contour. Mathematically, the source non-uniformity, U_{F}, expressed as a percentage, is given by Equation (22) [28]:

$$U_{\mathrm{F}} = \max \frac{\left(\left| \dot{D}_{\mathrm{min}} - \dot{D}_{\mathrm{p=0}} \right|, \left| \dot{D}_{\mathrm{max}} - \dot{D}_{\mathrm{p=0}} \right| \right)}{\dot{D}_{\mathrm{p=0}}} \times 100 \tag{22}$$

Central to this definition is the concept of field centre, the algorithm for the determination of which is given in detail in ICRU Report 72 [18].

Uniformity measurements for area sources should be performed at a distance of 2 mm or less from the source surface in water-equivalent material. In practice, such a measurement parallel to, or on the surface of, a concave applicator is quite difficult to perform. Practical guidance in performing these measurements is given in 11.1.6.

For line sources, a similar concept is used, except that the deviation is determined and expressed relative to the average absorbed dose rate and the values compared restricted to those within the active source length less the margins given in 5.2.2. Thus, line source uniformity, U_{L}, expressed as a percentage, is given by Equation (23) [28]:

$$U_{\mathrm{L}} = \max \frac{\left(\left| \dot{D}_{\mathrm{min}} - \dot{D}_{\mathrm{ave}} \right|, \left| \dot{D}_{\mathrm{max}} - \dot{D}_{\mathrm{ave}} \right| \right)}{\dot{D}_{\mathrm{ave}}} \times 100 \tag{23}$$

5.7.4 Source asymmetry for rotationally symmetric area sources

Another useful parameter for characterizing source uniformity is the source asymmetry, U_{AS}, expressed as a percentage, as given by Equation (24) [28]:

$$U_{\mathrm{AS}} = \max \left[\frac{\dot{D}_{\mathrm{max}}(\rho) - \dot{D}_{\mathrm{min}}(\rho)}{\dot{D}_{\mathrm{ave}}(\rho)} \right] \times 100 \tag{24}$$

where $\dot{D}_{\mathrm{ave}}(\rho)$ is the average of values around the circle defined by radius, ρ, at measurement depth, z. The distance from the source surface should be the same as used for the determination of non-uniformity.

5.7.5 Equatorial anisotropy for line sources

Analogous to source asymmetry, this parameter describes the variation in uniformity as measured at a fixed value of ρ, in a plane perpendicular to the source axis passing through the source centre ($z = 0$). U_{EA}, expressed as a percentage, is given by Equation (25):

$$U_{\mathrm{EA}} = \max \left[\frac{\dot{D}_{\mathrm{max}}(\rho,0) - \dot{D}_{\mathrm{min}}(\rho,0)}{\dot{D}_{\mathrm{ave}}(\rho,0)} \right] \times 100 \tag{25}$$

6 Calibration and traceability

6.1 Measurand

The measurand absorbed dose to water, which is the clinically relevant quantity and is now being used in external beam dosimetry worldwide, shall also be employed to calibrate beta radiation brachytherapy sources. It is the most relevant quantity biologically and should be used in radiotherapy in general. Primary and secondary standards for realizing and disseminating the unit “gray” shall be designed for this measurand.

6.2 Traceability

To ensure that dose measurements performed by different users with different dosimeters are comparable, it is necessary that the instruments used be properly calibrated with the stated uncertainty, and that the measurements at the user's sites be traceable to a primary standard. This can be done either by a direct calibration of the user's instruments against the primary standard or in a two- or multiple-step process by transferring the unit “gray” to secondary and transfer standards. It is necessary to recognize that each additional transfer step increases the uncertainty of the measurement at the clinical site.

6.3 Reference point

For ophthalmic beta radiation sources, it is necessary that calibrations be performed at the reference point, P_{ref}, of $z = 1$ mm for planar sources [18] and $z = 2$ mm for concave sources, as measured on the central axis of the source (see 5.2.2 and 5.2.3).

For intravascular brachytherapy beta radiation sources, it is necessary that calibrations be performed at the reference point, P_{ref}, of 2 mm measured from the source centre perpendicular to the source axis [18], [19], [20], [21], [22].

6.4 Primary standards

For beta radiation fields, the extrapolation chamber is used as the primary standard. A detailed description of the procedure for absorbed dose to water by means of extrapolation chambers is given in Annex C.

6.5 Secondary standards

For beta radiation, a secondary standard can be either a dosimetric system of proper accuracy calibrated by a national laboratory or a suitably calibrated radioactive beta radiation source whose radiation field is characterized by measurements performed at the national laboratory. The secondary standard can be used for the calibration of transfer standards or the user's dosimetry system. An example of a beta radiation secondary standard is described in detail in Clause C.7.

6.6 Transfer standards

Transfer standards or devices are used to transfer the unit of the measurement quantity from the well defined reference conditions of a primary or secondary standard to the conditions of a dose measurement in practice, where the actual values of the influence quantities can significantly differ from the reference conditions during calibration of the transfer standard. Thus, it is necessary to know the performance of the standard with respect to the relevant influence quantities, so that variations in the response of the instrument due to variations of influence quantities can be accounted for by correction factors. This requires a detailed investigation of such a transfer standard, which, for example, may be performed by a type test. Examples of dosimetry systems used as transfer devices are described in Clause D.1.

6.7 Calibration of therapeutic beta radiation sources

6.7.1 General

A measurement geometry as close to the clinical situation as possible shall be selected for the reference absorbed dose rate calibration. Thus, the measurement of the reference absorbed dose rate with a calibrated detector should be carried out in a water phantom whenever possible.

It is recommended that the calibration of therapeutic beta radiation sources be based on a dose-measuring system traceable to a national or international standard. An example of such a system is a $^{90}Sr + ^{90}Y$ secondary standard and a certified scintillation dose ratemeter.

6.7.2 Calibration of ophthalmic beta radiation sources

The calibration of an ophthalmic beta radiation source should be performed with a system calibrated by a national metrology institute or traceable to a primary standard, or with a measuring system that is calibrated in terms of absorbed dose to water relative to such a certified system by means of a $^{90}Sr + ^{90}Y$ secondary standard. It is anticipated that $^{106}Ru + ^{106}Rh$ may also be available as a secondary standard in the future. As an alternative, one may use other well characterized radiation fields, such as a ^{60}Co therapy beam or therapy electron beam spectra, whose dose rates at the depth of measurement are determined with instrumentation traceable to a primary standard [29]. Care should be taken to ensure that the system responds the same to the calibration beams as to the beta radiation source. It is necessary to stress that such procedures can result in an increased uncertainty because of the uncertainty in the energy and beam-quality dependence of detector response.

From the practical point of view, it is convenient to perform a calibration procedure by determining a complete depth dose distribution of the beta radiation source. Thus, the comparison of the measured curve with a standard depth dose distribution allows one to identify systematic deviations immediately.

A major requirement for any detector used for calibrations is that the dimensions of the sensitive volume are sufficiently small to allow one to neglect the variations in dose deposition within the sensitive volume (see 7.2.1). Although the dose gradient near a beta radiation applicator source follows an almost exponential fall off in the radial direction away from the source surface, usually the dose distribution is nearly constant in the two other dimensions. Thus the detector need only to be thin in one dimension, and the integration effect of the detector in the other dimensions can be neglected or taken into account by a simple unfolding procedure.

6.7.3 Calibration of intravascular beta radiation sources

For intravascular brachytherapy beta radiation sources, calibration should be done by using a recommended [19] system calibrated by a national metrology institute or traceable to a primary standard, or with a measuring system that is calibrated in terms of absorbed dose to water relative to such a certified system. For reference distances for dose specification, see Table 2. For intravascular brachytherapy sources, the reference distance is 2 mm from the source centre ($\rho = 2$ mm, $z = 0$ mm). Calibrations are performed in terms of absorbed dose to water. Reference conditions for calibration are the position of the source in the middle of a water phantom with dimensions of at least $15\ \text{cm} \times 15\ \text{cm} \times 15\ \text{cm}$ and a specific position of measurement at a radial distance, P_{ref}, measured from the middle of the source axis to the centre of the detector.

7 Dose measurements in-phantom and measurement corrections

7.1 Measurements in water or a water-equivalent phantom

It is useful to define three different types of measurements, corresponding to the three components of the complete three-dimensional representation of the radiation field:

a) absolute dose rate at the reference location;

b) relative dose rate along the perpendicular bisector;

c) relative dose rate at points off the perpendicular bisector.

When considering line sources, it should be noted that all the formalisms so far assume that the radiation field is symmetric around the source axis. To verify this assumption, it is prudent to assess this assumption of uniformity by a fourth class of measurements: relative dose rate around the source axis at the reference distance (or some suitable substitute).

Absorbed dose to tissue is prescribed, but measurements can be made only in materials that approximate the scattering and absorption properties of tissue. Tissue equivalence describes the degree to which the material matches the tissue; it is usually quantified by a comparison of mass-energy absorption coefficients (for photons) and stopping powers (for beta radiation) over the energy range of interest. Since there is considerable variation in tissue composition and density in the human body, water is commonly used as the reference medium for performing the measurements. The use directly in water poses problems for some detectors, and it is necessary that they be enclosed in some sort of waterproof covering, which might or might not be water-equivalent for the radiation type and energy range being measured. Also, accurate source-detector positioning is more difficult in a water phantom. For this reason, recourse is often made to solid phantoms made from water-equivalent plastic. Such phantoms offer very reproducible positioning, within the limits achievable by precision machining. Accuracy of positioning is governed by how well the distances between source and detector can be measured. Some commonly used plastics are discussed in the next section.

Because of the difficult characteristics of near-field dosimetry, it is well worth the effort for the researcher to take great care in the design and setup of source-detector combinations. For precise positioning, solid phantoms are preferred, although the use of solid water analogues comes at the price of increased uncertainty because of the differences in radiation absorption and scattering between the solid medium and water. Precise machining is important, particularly for beta radiation measurements because of the possibility of beta radiation streaming in any air gaps, which results in loss of absorbed dose at the measurement point. Charge build-up can also be an issue for the higher-dose rate beta radiation sources, so the use of a conducting material can be a consideration. When catheters are used instead of bare sources, the position of the source within the catheter should be taken into account. In cases when this positioning might not be reproducible, as in the case of loose seeds injected hydraulically, multiple irradiations should be performed and the results averaged. When measurements of intravascular brachytherapy sources are performed in a water phantom, it is convenient to use after-loading techniques. Care should be taken so that the catheter into which the source is loaded does not change position when a source is inserted. It is helpful to use a cathetometer for performing precise measurements between the source and the measurement plane. For measurements of concave ophthalmic brachytherapy sources, again, water is the preferred medium, but recourse can also be made to solid phantoms of water-equivalent material of spherical shape to conform to the applicator. These phantoms can be cut to accept dosimeters (see, for example, Reference [29]). Appropriate water-equivalent materials for phantom construction are discussed in Clause D.2.

7.2 Detectors for beta radiation

7.2.1 Near-field dosimetry

Dosimetric measurements in close proximity to beta radiation brachytherapy sources are very difficult to perform. These extremely inhomogeneous dose distributions with a steep slope over several orders of magnitude of dose within a few millimeters require the measurement of absorbed dose within very small volumes. Thus, in order not to disturb the physical situation being measured, it is necessary that the dosimetry detector be as tiny and as water-equivalent as possible [31]. Although for central axis depth dose measurements for planar and concave beta radiation applicators where the lateral-dose gradient is not large, very thin and flat detectors can be used. Dose measurements close (less than 5 mm) to an ophthalmic brachytherapy source and intravascular sources require the use of detectors providing spatial resolutions on the order of 0,1 mm to 1,0 mm for all dimensions. Such small dimensions require great sensitivity (for active devices) or can involve long irradiation times (for passive devices). In addition, it is necessary that the detector probe-packaging material, especially the front cover, be very thin to achieve precise depth dose or off-axis dose measurements, and should be water-equivalent as well. Further requirements are accuracy in absolute dose measurement (capable of being calibrated), precision and linearity of response over several orders of

magnitude of dose (rate). The spatial variation of the dose distributions inside the detector volume is usually not negligible. The effective point of measurement of the absorbed dose (or dose rate) depends on the distance to the source and the detector orientation as well. It is necessary that possible energy dependence or anisotropy of response be taken into account. Thus, it is necessary that the effective reference point of dose measurement in the vicinity of a brachytherapy source be determined and considered for each detector, for each type of radiation field, for each position inside the field and probably for each orientation of the detector probe (see 7.4).

7.2.2 Possible detectors for calibration of beta radiation sources

The requirements of 7.2.1 allow only the smallest volume plastic scintillator systems, radiochromic films, and appropriately small silicon diodes of routine use for source calibration. Other detectors, such as small-volume ionization (including extrapolation) chambers, MOSFET detectors, liquid ion chambers, alanine films, gel dosimeters, small-volume diamonds and, for some applications, ultra-thin thermoluminescent dosimeters (TLD's) may also be used, but are not recommended for routine measurements (see Annex D).

7.3 Conversion of absorbed dose in solid phantoms to absorbed dose to water

Absorbed dose measurements of therapeutic beta radiation sources are often performed in solid phantoms made from low-atomic-number materials such as A-150 plastic, WT1, polystyrene or polymethylmethacrylate (PMMA) (see 7.1). The depth dose distribution in such a solid phantom is generally different from that in water, therefore requiring a correction. Monte Carlo calculations, in which the phantom medium is replaced by water, can be used for such corrections. Another possibility is to correct through scaling.

Traditionally, beta radiation measurements made in low-atomic-number media other than water were scaled by expressing depths and distances in terms of areal density, that is, mass per unit area (see, for example, Reference [30]). A more accurate scaling method has been proposed by Cross [32] in the late 1960s. Cross proposed that the depth-dose distributions of plane and point-like beta radiation sources in different low-Z media are very similar and can be related to one another via a scaling factor based on distance. Since then, this so-called scaling method has been used for a variety of applications and the results in low-Z media appear to be accurate to within 2 % to 3 % for the types of sources just mentioned [33]. Recently, the applicability of the scaling method has been extended to line sources with zero or finite diameter by Schaart [34].

The similarity between beta radiation depth-dose distributions in different media can be understood as follows. At beta radiation energies, the mass stopping power, S/ξ , of low-Z media is dominated by the mass electronic (or collisional) stopping power S_{el}/ξ . According to the well-known Bethe formula, S_{el}/ξ is approximately proportional to the electron density, $N_{\mathrm{A}}Z/M$, where N_{A} is Avogadro's number, Z is the atomic number and M the molar mass of the medium [33], [35]. The electron density tends to decrease with increasing Z; so if the transport of electrons were determined only by S_{el}/ρ , one would expect them to penetrate more deeply (in terms of areal density) into higher-Z materials. This is, for example, reflected in the increase of the continuous slowing down range, R_{CSDA}, (in units of mass per area) with increasing Z. It can also be seen from Bethe's equation that the variation of, S_{el}/ρ, with Z is nearly independent of its variation with energy. As a result, the ratio of the stopping powers experienced by an electron in two different materials is nearly the same at all energies. One can, therefore, expect that the dose distributions in different media are related by a scaling factor based on distance equal to this ratio.

it is necessary that the influence of electron scattering be taken into account as well, however. As follows from the expression by Mott, the single-scattering cross-section per nucleus is approximately proportional to Z^2 [33]. Since the scattering events are statistically independent, one may argue that the mean-square angle of deflection per unit areal density due to nuclear scattering, also called the mass scattering power, is proportional to $N_{\mathrm{A}}Z^2/M$ [33], [35]. This phenomenon tends to increase the mean path length (and therefore the energy loss) per unit areal density with increasing Z.

The net result appears to be a decrease of the average depth of penetration (in units of mass per area) with increasing Z [36], [37]. More importantly, Mott's equation shows that the relative angular distribution of the scattering probability is nearly the same for all low-Z elements. The same is therefore true for materials composed of multiple low-Z elements. It then follows that the scattering probability per unit energy loss of such materials is approximately proportional to an effective atomic number defined by Equation (26) [32]:

$$\bar{Z} = \frac{\sum_i N_i Z_i^2}{\sum_i N_i Z_i} \tag{26}$$

where

N_i is the relative number of nuclei of charge Z_i.

Furthermore, it follows from Mott's and Bethe's equations that this variation with $\bar{Z}$ is nearly independent of the variation with electron energy. Thus, by approximation, the ratio of the scattering probabilities per unit energy loss of different low-Z materials is independent of angle and remains constant with electron energy.

Cross, therefore, proposed that the dose distributions in different media can be related by a distance scaling factor, equal to the product of the stopping power ratio and some function of $\bar{Z}$ [32]. This function is obtained empirically by deriving scaling factors relative to water from experimental or calculated dose distributions and dividing these by the appropriate mass stopping power relative to water, S/S_{w}. Since stopping power ratios vary somewhat with energy, the ratio of the ranges of 500 keV electrons, R_{w}/R, is usually taken as the average mass stopping power relative to water. It appears that the results can then be fitted by Equation (27) [33]:

$$\eta = (0{,}777 + 0{,}037\,56\,\bar{Z} - 0{,}000\,66\,\bar{Z}^2)\frac{S}{S_{\mathrm{w}}} \tag{27}$$

Scaling factors obtained from Equation (27) are given in Table D.2 for several different media [33]. The estimated standard uncertainty in these values is 1,5 %. These scaling factors can be used to scale the dose distributions between different, homogenous low-Z media, provided that the source geometry shows a sufficient degree of symmetry. For an (effectively) infinite, planar beta radiation source, the dose distribution in water as a function of the distance, x (expressed in units of length), to the source can be calculated from the dose distribution, $D(x)$, in a different low-Z medium as given in Equation (28) [32], [33]:

$$D(x) = \eta \cdot D_{\mathrm{w}}\left(\eta \frac{\xi}{\xi_{\mathrm{w}}} x\right) \tag{28}$$

where

η is the scaling factor, or relative attenuation, of the medium relative to water;

ξ is the density of the medium;

ξ_{w} is the density of the water.

It is noted that the same relationship holds for broad, parallel beta-particle beams incident on a slab of material. In this case, the variable, x, is the depth of penetration, expressed in units of length, into the material (see, e.g., ISO 6980-2 for a detailed example).

For a point source, the scaling relationship is given in Equation (29) [32], [33]:

$$D(r) = \eta^3 \cdot \frac{\xi^2}{\xi_{\mathrm{w}}^2} \cdot D_{\mathrm{w}}\left(\eta \frac{\xi}{\xi_{\mathrm{w}}} r\right) \tag{29}$$

were r is the distance to the point source, expressed in units of length. For the more general case of a source with spherical symmetry and finite diameter, it has been shown that Equation (39) holds [34]:

$$r^2 \cdot D(r) = \eta \cdot [r_s + \eta \frac{\xi}{\xi_w}(r - r_s)]^2 \cdot D_w(r_s + \eta \frac{\xi}{\xi_w}[r - r_s]) \quad (30)$$

where r_s is the outer radius of the source, expressed in units of length.

For a line source having a diameter of zero and a length larger than twice the range of the beta particles, the depth-dose distributions in different media are related as given in Equation (31) [34]:

$$D(\rho) = \eta^2 \cdot \frac{\xi}{\xi_w} \cdot D_w(\eta \frac{\xi}{\xi_w}\rho) \quad (31)$$

where ρ is the radial distance to the longitudinal source axis, expressed in units of length. For the more general case of a cylindrically symmetric source with a finite diameter and a length exceeding twice the beta-particle range, Equation (32) holds [34]:

$$\rho \cdot D(\rho) = \eta \cdot [\rho_s + \eta \frac{\xi}{\xi_w}(\rho - \rho_s)] \cdot D_w(\rho_s + \eta \frac{\xi}{\xi_w}[\rho - \rho_s]) \quad (32)$$

where ρ_s is the outer radius of the source, expressed in units of length.

7.4 Effective point of measurement in the detector

A detector with a finite volume yields a reading proportional to the absorbed dose averaged over the volume of the detector.

For water-equivalent detectors, the average absorbed dose, D_{avg}, over a detector with a volume, V_{det}, is given by Equation (29):

$$D_{avg} = \frac{1}{V_{det}} \int_{V_{det}} D_w(\vec{r})\, dV \quad (33)$$

where

dV is an infinitesimal volume at point $\vec{r}$ within the detector volume;

$D_w(\vec{r})$ is the absorbed dose at that point.

The effective point of measurement, P_{eff}, is the point in water with the same absorbed dose as the average absorbed dose over the detector, i.e. $D_w(P_{eff}) = D_{avg}$.

An equivalent way of defining the effective point of measurement is to calculate the average electron fluence, $\Phi_{Avg,Det}$, within the detector volume and define P_{eff} as the point in the undisturbed medium with the same electron fluence as $\Phi_{Avg,Det}$. In this case, the electron fluence includes the beta particles emitted from the source and electrons liberated by bremsstrahlung.

The effective point of measurement for a particular source/detector geometry can be assessed with reference dosimetry data. Generally, if the detector is reasonably thin (less than 1 mm in the dimension of the highest dose gradient), differences between the effective point of measurement and the centre of the detector sensitive volume are minimal. Recent investigations [90] at the Technische Bundesanstalt (PTB) with plastic scintillator detectors showed that, due to the shift of the effective point of measurement regarding the reference point of the detector, it is necessary to expect a maximum systematic deviation of 1 % or 2,5 % in the case of dosimetry of eye applicators or line sources, respectively [38]. The results are based on the

assumptions that the diameter and length of the detector is on the order of 1 mm, the reference point is the middle of the detector, and that the calibration is done in a radiation field from a planar source at a depth of 2 mm in water-equivalent material (for example, by means of the PTB primary standard for planar sources).

8 Theoretical modelling

8.1 Point-dose kernels

Theoretical modelling is increasingly being used to supplement measurements and type tests. One convenient method to model distributed sources is to consider the dose distribution produced by a point radioactive source in a unit density (water) medium. Such a source produces a spherically symmetric radiation field which is a function of a single spatial variable, r, the distance to the point source. As first given by Loevinger and Berman [38], the absorbed dose distribution for a beta radiation point source, when expressed in terms of fraction of the emitted energy that is absorbed per unit mass of the medium, is known as the point-dose kernel, and is given by Equation (34):

$$\dot{D}(r) = QK_1 n_\beta E_{\text{avg}} \Phi_\beta(r) \tag{34}$$

where

Q is the source activity, expressed in disintegrations per second;

K_1 is a conversion factor, equal to $1{,}602 \times 10^{-10}$ Gy·g/MeV;

n_β is the number of beta particles emitted per disintegration;

E_{avg} is the average energy of the beta radiation spectrum;

Φ_β is the beta point kernel.

The beta point kernel is given by Equation (35):

$$\Phi_\beta(r) = \int_0^{E_{\text{max}}} (E_0 / E_{\text{avg}}) S_\beta(E_0) \Phi(r, E_0) \mathrm{d}E_0 \tag{35}$$

where

$S_\beta(E_0)$ is the beta radiation spectrum with end point energy equal to E_{max};

$\Phi(r,E_0)$ is the point kernel for the monoenergetic source of energy E_0.

Monoenergetic point kernels are either measured [40], [41] or calculated [42], [43], [44], [45], [46]. With a knowledge of the monoenergetic point kernels, one can calculate the dose distribution produced in a medium from an extended source by an integration of the point dose kernels over the source volume (see, for example, Reference [47]). This approach is valid only for the unit density medium (water) in which the monoenergetic point kernel has been calculated, and it is necessary to resort to approximations when considering non-water media. The validity of these approximations can be tested by a comparison with Monte Carlo approximations, as shown in a recent work [48]. In general, point-dose kernel calculations produce reasonable results for seed and line brachytherapy sources, but poor results for planar and concave sources, due to the greater amount of non-water media for the latter. Point-dose kernel calculations have the distinct advantage over Monte Carlo calculations in speed of calculation, thus making them attractive for real-time dosimetry calculations. Some examples of such calculations for intravascular brachytherapy sources are given by Seltzer [47].

8.2 Monte Carlo simulation

8.2.1 General

The Monte Carlo method is based on the idea that if all materials and dimensions of a dosimetric problem are known and all the probabilities of the various possible radiation interactions are known, then particles can be tracked and scored as they are transported from the source through the geometry of the problem. A random-number generator is used to sample the starting coordinates, direction and energy of a particle and, subsequently, all parameters needed to model the various interactions and secondary radiations as the particle is being tracked. Obviously, the more "histories" (source particles) that are tracked, the more accurate are the resulting calculations. A review of the Monte Carlo method with emphasis on therapeutic beta radiation dose calculations has recently been published [47]. Several other reviews and discussions of the Monte Carlo method can be found in the literature [33], [48], [49], [50], [51], [52], [53], [54].

With the advent of faster and faster computers, Monte Carlo calculations are becoming more and more attractive for determining dose distributions for brachytherapy sources. Using Monte Carlo calculations, three-dimensional dose distributions can be calculated in complex geometries involving multiple materials and with high spatial resolution. The latter advantage is particularly important in the case of beta radiation brachytherapy sources that can exhibit very large dose-rate gradients near the source. It is, therefore, not surprising that many authors have recently used this technique for the calculation of dose distributions about clinical beta radiation sources [25], [48], [55], [56], [57], [58], [59], [60], [61], [62], [63], [64], [65], [66], [67,], [68], [69], [70], [71], [72], [73], [74], [75].

Several general-purpose Monte Carlo codes, which have proven useful for calculations on beta radiation sources, are available today. A brief review of the most commonly used Monte Carlo codes used in clinical beta radiation dosimetry is provided in Clause E.1.

Although a variety of well-validated codes are currently available, this does not mean that correct results are obtained easily. This can be illustrated, for example, by a recent study on ophthalmic beta radiation sources in which large discrepancies were reported between the results obtained with different codes and between simulations and experiments [48]. Similar discrepancies were observed for an IVB source in another recent study [59]. As another example, discrepancies of up to 30 % have been reported between the dose distributions calculated about an $^{90}Sr + {}^{90}Y$ intravascular beta radiation source with three different codes [63]. On the other hand, many studies have been published that show good agreement between simulations and experiments and between results obtained with different Monte Carlo codes. A recent meta-study of published dose measurements and simulations on intravascular sources provides interesting examples of both very good agreement and significant discrepancies [27].

Differences between the results obtained with different codes can arise from differences between the input data (problem geometry, source emission spectrum, etc.) and from intrinsic differences between the radiation transport algorithms and cross-section libraries. Many codes use a condensed-history approach to simulate the transport of electrons, see Clause E.4 for more details. In this case, the results can additionally be affected by artefacts arising from the limitations of the multiple-scattering algorithms used by the code. Well known examples are boundary-crossing and step-size artefacts, see Clause E.4. Thus, to avoid systematic errors, it is important for the user of any Monte Carlo code to understand these limitations.

Monte Carlo dose calculations on clinical sources should always be verified by measurements. As a Monte Carlo dose calculation yields the dose rate per unit contained activity, experimental verification can be achieved by comparison with a dose measurement on a source whose contained activity has been measured.

8.2.2 Reporting Monte Carlo dose calculations

Monte Carlo dose calculations should be reported in such a way that sufficient information is provided for others active in the field to be able to reproduce the work performed. In practice, this requires a detailed description of the problem itself, the code used and all relevant transport parameters. For the specific case of Monte Carlo (beta radiation) dose calculations, the following list provides an overview of various aspects that should be covered in sufficient detail. It is noted, however, that this list might not be exhaustive and that, depending on the problem and the code used, it can be necessary to include additional items to provide a complete description of the work performed:

— name and version of code used, platform on which the code is run, and any relevant installation options;

— particle types and interactions included in the simulation; for example, a “coupled electron-photon simulation” means that both electrons and photons are being transported, and that photons produced by electrons, and electrons produced by photons, are taken into account in the simulation;

— specifications of the physics models (transport algorithms) that have been used for all types of particles simulated (only applicable if the code used offers multiple options);

— overview of the interaction processes that are taken into account in the simulation; in some codes, all interaction processes are switched off by default, which means that it is necessary that the user be cautious to include all processes necessary to obtain good results; in other codes, all interaction processes are switched on by default, and the user has the option to switch off (irrelevant) processes in order to decrease calculation times; in both cases, it is important to specify completely which settings are used;

— in the case of a condensed-history simulation of electron (or any other charged particle) transport, the values of all multiple-scattering parameters that can be set by the user; many codes require the user to set a number of parameters that control the multiple-scattering algorithms; examples are parameters that determine or limit the step size and/or the fractional energy loss per electron step, that control the number of substeps per step, that allow the user to choose among different electron transport algorithms or among different options for sub-modules of the transport algorithm, that specify whether to use a special boundary-crossing algorithm, etc.; such parameters can have a significant influence on the end result, and it is, therefore, very important to describe which settings have been used, even if those are default values, this should be clearly stated;

— specification of the cross-section libraries used for all types of particle simulated; the radiation interaction data form a crucial part of the input for any simulation and, therefore, the data used should be clearly specified;

— complete description of the problem geometry, including all relevant dimensions and, preferably, including a diagram;

— elemental composition (i.e., the relative amount of each chemical element present in a material), the mass density and any other relevant properties of all materials used in the simulation; depending on the code used, other relevant material properties can include the physical state, e.g. condensed (solid or liquid) vs. non-condensed (gas) and the conduction state (conductor or non-conductor), properties that are of importance for calculating electron stopping powers;

— geometry and dimensions of the model used for the source and, for all types of particles emitted, the energy spectrum and the angular distribution; in the case of a radioactive source, the source dimensions correspond to those of the radioactive volume and the angular distribution of the emitted radiation are isotropic; manufacturers are encouraged to make this information available to researchers so that more valid results of modeling can be obtained;

— description of the methods used to score the dose (or any other quantity of interest), including a complete description of the scoring geometry (this is typically a grid of scoring voxels in dose calculations);

— cut-off energy (i.e., the energy below which particles of a given type are stopped, depositing their remaining energy on the spot) for all types of particles used in the problem; in some codes, cut-off energies can be set for individual materials or geometric regions; if this is the case, a complete description should be given; some codes employ range cuts rather then cut-off energies, in which case, a complete description of all range cuts used in the problem should be provided;

— any other cut-offs used in the problem; some codes allow the user to specify additional cuts, such as a cut for the particle importance or for the time-of-flight of a particle;

— maximum energy for all types of particles used in the problem, if applicable; some codes allow the user to specify maximum energies in order to avoid the unnecessary calculation of transport data beyond the energy range of interest during the initiation phase of the run;

— complete description of all variance-reduction techniques used; examples include source biasing, biasing of secondary particle production (e.g. bremsstrahlung), Russian roulette and particle splitting, forced collisions, etc.; clearly, since excessive use of variance-reduction methods can distort the end result of a simulation, it is very important to provide a complete and thorough description of all variance-reduction techniques that have been applied;

— comparison to measurements (if they exist), at least by reference;

— associated uncertainties for all results; as discussed in 9.6, an accurate and complete assessment of all relevant components of uncertainty is generally not limited to the standard deviation that most codes provide together with the calculated mean of the quantity of interest, but can include many other components of uncertainty that, in general, it can be necessary to quantify via type B evaluation methods (see ISO Guide 98-3).

9 Uncertainties in source calibrations

9.1 General

To make measurements comparable, it is necessary to state the quality of a measurement in terms of the uncertainty of measurement. ISO Guide 98-3 (GUM) introduces a unifying method for evaluating and stating measurement uncertainties. This method has been accepted by all calibration services in the world and has become a standard in the field of metrology.

The determination of uncertainties of absolute calibration, absolute dose measurements and relative dose measurements should be performed according to the ISO Guide 98-3 procedure.

9.2 Uncertainty of primary standards

Primary standards for absorbed dose rate from beta radiation brachytherapy sources are maintained in the US, Germany, and the Netherlands (see Annex C). Quoted expanded uncertainties[1)] ($k = 2$) are in the range of 7,5 % to 11 % [77], [78], [79], [80].

9.3 Uncertainty of secondary standards

In beta radiation dosimetry, secondary standards usually take the form of sources calibrated by a primary laboratory. Thus, the uncertainty in these standards corresponds to the value assigned by the primary laboratory.

9.4 Uncertainty of transfer standards

9.4.1 General

Transfer standards are calibrated against either primary or secondary standards and, as such, they have the associated uncertainties of these standards. To this it is necessary to add the uncertainties due to the calibration process, which include reading reproducibility, material effects (phantom and detector), volume averaging, positioning and, in the case of secondary standard sources, source non-uniformity. It is necessary that all these effects be considered in the determination of the overall uncertainty of an absolute clinical dosimetry measurement.

1) The expanded uncertainty is obtained by multiplying the combined standard uncertainty by a coverage factor, k.

9.4.2 Radiochromic film

The relative combined standard uncertainty of the results of radiochromic film used for relative measurements can extend from 4 % to 7 % ($k = 1$) [18], [29], [55], [81]. This is a best-case estimate and users are cautioned to determine the uniformity of a sample of each lot prior to use. For absolute measurements, it is necessary to take the combined standard uncertainty of the absolute calibration procedure into account (see D.1.1).

9.4.3 Plastic scintillation detector

The relative combined standard uncertainty of plastic scintillation detectors for relative measurements can extend from 3 % to 6 % ($k = 1$) [82], [83]. For absolute measurements, it is necessary to take the combined standard uncertainty of the absolute calibration procedure into account (see D.1.2).

9.4.4 Thermoluminescence dosimeter (TLD)

The relative combined standard uncertainty of TLD detectors for relative measurements can extend from 3 % to 5 % ($k = 1$) [84]. For absolute measurements, it is necessary to take the combined standard uncertainty of the absolute calibration procedure into account (see D.1.3).

9.4.5 Diode detector

The relative combined standard uncertainty of diode detectors for relative measurements of $^{106}Ru + {}^{106}Rh$ concave applicators is quoted as 4,5 % [85]. This value is comparable to the other methods given and, as with them, for absolute measurements, it is necessary to take the combined standard uncertainty of the absolute calibration procedure into account (see D.1.4).

9.4.6 Well ionization chamber

The well ionization chamber (WIC) is a special type of transfer device, yielding a quantity related to the average reference absorbed dose rate. The relative combined standard uncertainty of well ionization chambers for relative measurements of reference absorbed dose for IVB sources is about 2 % to 3 % [21], [86], subject to the caveat that the measured reference absorbed dose rate is characteristic of an average value over the source length, and hence its relationship to reference absorbed dose rate at the source centre is extremely dependent on the source uniformity (see 5.7.3). For absolute measurements, it is necessary to calculate the combined standard uncertainty of the absolute calibration procedure and the effect of source uniformity (see D.1.5).

9.5 Relationship of dosimetry uncertainty to positional error

For the examples given above, it can be seen that combined expanded uncertainties for clinical dosimetry measurements of beta radiation brachytherapy sources are in the range of 10 % to 20 %. This rather large value can be looked at in the light of the relationship between the dosimetry uncertainty and the positional uncertainty, given by the gradient of the relative depth-dose distribution [18]. At a 2 mm depth in water, these gradients range from about 20 %/mm for $^{106}Ru + {}^{106}Rh$ concave sources to about 90 %/mm for $^{90}Sr + {}^{90}Y$ seed trains. Using these values, it is seen that the 10 % to 20 % uncertainties correspond to positional uncertainties of less than 1 mm, usually much smaller than the positional errors associated with source placement during therapy.

9.6 Uncertainty in theoretical modeling

Uncertainty in theoretical modeling is considered in detail in Clause E.3.

10 Treatment planning and reporting

10.1 General

Prescribing, recording and reporting is the key for later evaluation and for obtaining a better understanding of radiotherapy. It is necessary to clearly describe a minimal set of relevant parameters to prescribe the dose to specified dose reference points in the specified target volume and to structures at risk, as well as to record and report the doses delivered [13]. It is necessary that these parameters be specific, well determined and uniformly documented. In beta radiation brachytherapy, very steep distributions of dose are applied with a drop of dose of several orders of magnitude within a few millimeters. Thus, it is not sufficient to report just one dose value.

10.2 General aspects of treatment planning

The most complete treatment planning for brachytherapy requires a full three-dimensional description of the dose distribution around the source. Factors and functions are mainly applied in treatment planning systems together with various imaging modalities. Detailed aspects of treatment planning are considered in Annex F.

10.3 Documentation in ophthalmic brachytherapy

It is necessary that planning be done pre-placement, and it is sometimes necessary to make adjustments post-placement in order to account for the actual source placement.

For one-dimensional treatment planning, the plan report should include the depth-dose profile on the central axis of the source, dose to the prescription point, the tumour apex (if different from prescription point), the centre of the tumour base (inner sclera-uvea), and other relevant critical structures (e. g. optic nerve and optic disk, macula, retina, lens and cornea).

For two-dimensional treatment planning, the plan report should include all the information required with one-dimensional plans plus 2D dose distributions in planes that include the central axis of the tumour/applicator superimposed on two-dimensional images of the tumour (for example an ultrasound B-scan), as well as doses to the critical structures. Three-dimensional plans can include isodose distributions in selected planes as well as dose volume histograms for the tumour and critical structures, in addition to the dose information for the standard points of interest.

10.4 Uncertainty of the dose delivered in ophthalmic brachytherapy

The clinical outcome strongly depends on precise dose delivery to the target volume, while sparing healthy surrounding tissues. Issues that vitiate this situation include dosimetric uncertainties, uncertainty in measuring the tumour dimensions (like determination of the apical height using ultrasound) and uncertainties arising from the positioning of the applicator, both laterally and radially (poor contact with the eye). Positioning can be evaluated post irradiation by visual examination of the irradiated eye. Close attention should be paid to these issues by applicator users.

As an example of the impact of positioning errors, Table 3 gives predicted changes in delivered dose for a typical applicator applied to an idealized tumour with an apex height of 5 mm, a basal diameter of 15,6 mm and a chord length of 17,3 mm.

Table 3 — Typical dose errors associated with positional errors

Applicator shift		Relative dose change at the apex %	Relative dose change at the inner sclera %	
			Central point of the tumour	Tumour rim
radial	1 mm	−32	−22	−41
	2 mm	−56	−39	−61
lateral	1 mm	−1	0	29 to −44
	2 mm	−2	0	43 to −72

10.5 Documentation in intravascular brachytherapy

10.5.1 General

Based on and extending the AAPM TG 60 recommendations [22], [23] and taking into account the recommendations from the DGMP-Report 16, [19] and from the GEC-ESTRO EVA-Recommendations [20], a set of relevant parameters is defined describing the spatial and temporal distributions of the absorbed dose delivered to target structures or potential structures at risk (e.g. the vasa vasorum), independent of the irradiation technique or source used, and under conditions which are closely related to the clinical ones, and which can easily be determined.

10.5.2 Target volume

There are still ongoing discussions concerning different cells as possible targets for vascular radiation therapy. Although the endothelial cells in the intima have been considered first, the proliferating smooth-muscle cells and/or the myofibroblasts have been held responsible by the majority of investigators for initiating neointimal thickening and/or restenosis and, thus, often the media and/or adventitia are assumed to be the target layers.

Furthermore, it is necessary to irradiate the full length of the vessel section injured by the interventional process (e.g. by dilatation, stenting, rotablation, atherectomy). It is necessary to establish sufficiently wide longitudinal safety margins, according to the anatomical topographical and physiological uncertainties (at least 5 mm to 10 mm for coronaries and more than 10 mm to 15 mm for peripherals) to avoid edge recurrence due to an under-dosage in a part of the injured section of the vessel.

Until an overall consensus can be reached to determine target cells and mechanisms of vascular radiotherapy, the entire vessel wall containing plaque/intima, media and adventitia in the injured section of the vessel (including sufficiently long safety margins) should be considered to form the target volume; see Table 4.

Table 4 — Target volume in intravascular brachytherapy

Site of injured artery	Position and length
Vessel wall	Plaque/intima, media, and adventitia
Clinical target volume (CTV)	Whole vessel wall in injured section of artery
Planning target volume (PTV)	CTV plus sufficiently wide safety margins
Safety margins	e.g. >5 mm to 10 mm for coronary arteries, >10 mm to 15 mm for peripheral arteries
Structure at risk (potential)	Endothelium of vasa vasorum

Intravascular ultrasound, IVUS, is the ideal tool to visualize the individual vessel wall architecture quantitatively, to guide vascular brachytherapy and to yield the spatial information on target structures and potential structures at risk immediately prior to vascular brachytherapy in real time and under irradiation treatment conditions as seen from the assumed position of the source [86]. Thus, for clinical trials and routine treatments to be reported, IVUS is strongly recommended.

10.5.3 Reporting the spatial distribution of dose delivered

For all kinds of vascular brachytherapy, the dose should be prescribed in terms of absorbed dose to water at a system related to a reference point, P_{ref}, to enable better comparison. For coronary application, P_{ref} is a point at a radial reference distance of $\rho = 2$ mm from the centre of the source while $\rho = 5$ mm is recommended for intra-peripheral applications, see Table 5. Also, it is necessary to state the corresponding radial depth dose distributions in water, taking into account typical diameters of employment of a centring balloon filled with a contrast agent (e.g. CO_2), of a balloon filled with radioactivity (e.g. ^{133}Xe) or containing radioactivity in its balloon wall or of a radioactive stent. These typical diameters can be 2,0 mm and 3,0 mm for coronary applications, or 6,0 mm and 8,0 mm for peripheral vessels.

Table 5 — Reporting the spatial distribution of dose

Clinical application	Coronary arteries	Peripheral vessels
Dose quantity and unit	Absorbed dose to water, expressed in gray	
Reference dose	Dose at P_{ref}	
Reference point: P_{ref} (system related)	2 mm in water (radial distance from source center)	5 mm in water (radial distance from source center)
Reported dose (target related)	Dose at 1 mm tissue depth	Dose at 2 mm tissue depth
Relative distribution of dose in (partial) target volumes	Dose-volume histogram, or dose triplet: D_{mean}, D_{min}, D_{max}	

For the biology-based evaluation of clinical results, it is necessary to report a target-tissue-related dose. Thus, it is necessary that the dose distributions delivered to the target structures be reported preferably as dose-volume histograms (DVH). As an alternative, the mean dose (D_{mean}) and the dose variation (D_{min}, D_{max}) should be stated. To allow more detailed evaluation, the DVH or the dose triplet should be specified, both for the whole target volume and for partial target structures, such as plaque/intima, media and adventitia. In order to determine D_{min}, it is necessary that the borders of target structures be defined clearly or a certain radial distance be specified.

At the least, it is necessary to state a dose value relative to the target tissue. For better evaluation, the dose at 1 mm tissue depth should be stated as representative for the whole coronary artery vessel wall and at 2 mm for peripherals. If no centring balloon or stenting is applied, the mean dose could be stated delivered at 1 mm tissue depth within the whole target volume (or 2 mm, respectively).

10.5.4 Reporting the temporal distribution of dose delivered

It is necessary to describe the temporal distribution of dose, e.g. by stating the absorbed dose rate at the specification point, the irradiation time and, if necessary, the number of fractions (see Table 6).

Table 6 — Reporting the temporal distribution of dose

Clinical application	Temporary	Permanent implants (radioactive stents)
Dose rate quantity, unit	Absorbed dose rate to water in gray per min	
Reference point: P_{ref} at radial distance of	2 mm (coronary arteries) 5 mm (peripheral arteries)	
Dose: biologically relevant physically relevant	Dose at P_{ref}	Dose at P_{ref}: integrated over e.g. 48 h integrated over 28 days
Dose rate	Dose rate at P_{ref}	Maximum dose rate at P_{ref}
Irradiation time: biologically relevant physically relevant	Time, including interruptions, total time	Time for delivering 90 % of dose or 3 $T_{1/2}$

For temporal intravascular radiotherapy with catheter-based systems the irradiation time should include the time of interruptions, e.g. to overcome ischemia. For permanent implants, the irradiation time can be defined as the irradiation time for a certain amount of dose. AAPM TG 60 [22] had recommended accumulating the absorbed dose over a physically relevant period of time of 28 days. A shorter period of time, e.g. 48 h, seems to be more relevant biologically.

10.5.5 Source localization

The extremely steep dose fall-off in vascular brachytherapy, the tortuous and pulsating shape of the vessel, the irregular vessel wall architecture and the mostly eccentric position of the source in relation to the target structures cause large dose variations. Thus, the determination of the relevant parameters is a challenge.

10.6 Reporting uncertainties in intravascular brachytherapy

Uncertainties include dosimetric uncertainties, uncertainty in measuring the vessel dimensions [like determination of the reference lumen diameter (RLD) [20] using angiography], and uncertainties arising from the positioning of the source, both along and across the vessel. The use of a centring catheter alleviates the positional uncertainty within the lumen. Due to the very high dose gradients, evaluated uncertainties can be very large (> 100 %); however, the treatment dosage window seems to be large enough to allow such errors with no detriment to outcome.

11 Clinical quality control

11.1 Acceptance tests

11.1.1 General

The acceptance test shall be carried out by the user during the initial delivery for each source to demonstrate that it conforms with the specifications stated by the manufacturer in the calibration certificate. Results of absolute measurements shall be traceable to a national standard.

11.1.2 Acceptance level

Agreement within the uncertainties ($k = 1$) is the basis for intercomparison of all dosimetric quantities on which an acceptance test is performed. This assumes a careful analysis of all type A and B uncertainties by both the user and the manufacturer before an acceptance level for the given quantity can be stated explicitly. Reasonable assessments of uncertainty are expected, in the range of the examples given in 9.4, and in no case are to exceed ±20 % ($k = 1$).

11.1.3 Recommended equipment

11.1.3.1 General

In 7.2 and Annex D, dosimetry detectors and systems are briefly described. Those that are suitable for the dosimetric measurements of beta radiation from brachytherapy sources are calibrated plastic scintillators, calibrated radiochromic film, plus an appropriate phantom and scanning device, calibrated diodes, calibrated TLDs and, for line sources only, calibrated well chambers in combination with uniformity measurements with radiochromic film and a densitometer.

11.1.3.2 Scintillator systems

Recommendations concerning scintillator systems include the following.

— Detector (active scintillator volume) should not exceed 1 mm in any dimension.

— For a monofiber system without compensation of background light (Cerenkov effect), the background light should not exceed 10 % of the scintillator light.

11.1.3.3 Radiochromic film

Recommendations concerning radiochromic film include the following.

— Use film as specified in AAPM TG55 [81] and the latest recommendations by the manufacturer.

— If a document scanner is used for a film readout for absolute dosimetry, it should be used in the transmission mode, have at least 12 bit per colour image depth and it should not alter the image data in any way. It is necessary that the analysis software properly handle information in TIFF file format.

11.1.3.4 Diodes

Recommendations concerning diode measurements include the following.

— Detector (active volume) should not exceed 1 mm in any dimension.

— An understanding of the energy and angular response and change in response with time and possibly with the accumulated dose is important.

11.1.3.5 TLDs

Recommendations concerning TLD measurements include the following.

— Detector volume should not exceed 1 mm in any dimension.

— An understanding of the energy and angular response is important.

11.1.3.6 Phantoms

Recommendations concerning phantoms include the following.

— If a solid phantom is used, it should be precisely machined (< 0,1 mm air spaces) of one of the materials specified in Clause D.2, and preferably should be supplied by the source manufacturer.

— If water is used, the detector positioning should be accurate and reproducible to better than 0,1 mm.

11.1.3.7 Well ionization chambers

Recommendations concerning well ionization chambers (only for IVB) include the following.

— The chamber should be designed to measure mainly the beta radiation.

— Use an appropriate insert. Note the necessity that the insert and chamber be calibrated as a pair.

— Set the correct length on insert, such that the centre of the line source or source train is at the centre of "sweet" length (position range of maximum response of the chamber). When this is done, the response for many chambers is proportional to the length of the source.

— Use a chamber with a sufficiently long "sweet" length relative to the source length.

— Use an appropriately calibrated electrometer or measuring assembly.

For a full description of the use of well ionization chambers for source calibration see Reference [84].

11.1.4 Verification of the reference absorbed dose rate to water

Using one of the detector systems recommended above that has been calibrated in an adequate radiation field representative of the source being measured, the reference dose rate shall be determined directly. The simplest way to accomplish this is to use a device fixing the source and the selected detector in a phantom in such a way that the required geometry and reference distance are reproducibly achieved. It can be more practical to carry out measurements along the source axis (which are required anyway to check the relative data) and make an interpolation to the reference point. In this way, the calculation of the effective point of measurement with all density corrections for the phantom material of the detector itself and within the detector probe can be done without restrictions on the design of the setup.

For intravascular brachytherapy sources, direct measurement of the reference absorbed dose rate to water is regarded as being preferable to measurements made with calibrated, well ionization chambers, with the proviso that a sufficient number of direct measurements is made to sample the entire active length over all equatorial angles. However, measurements with well ionization chambers, complemented by radiochromic film to demonstrate uniformity, $U_{\mathrm{L}} < 10$ %, are very convenient and can be implemented if the combined uncertainty are rated as acceptable. For replacement sources measured with well ionization chambers, a statement from the manufacturer is required that there has been no change in the design or in the material of the source or encapsulation. For sources that have a U_{L} that exceeds 10 %, measurements with a well ionization chamber are not appropriate and either the source should be exchanged or the reference absorbed dose rate should be verified by a direct measurement.

11.1.5 Verification of the relative depth dose

It is recommended to measure a complete set of depth dose distribution(s) using one of the systems of 11.1.3 either in water or water-equivalent plastic. At least four points between 1 mm and 7 mm should be measured to specify the shape of the depth-dose curve. One point should be as close to the source surface as possible. If the data have been measured at coordinates differing from those in the certificate, the comparison should be based on the appropriate data fit-function.

11.1.6 Source non-uniformity tests

For ophthalmic beta radiation brachytherapy sources, sufficient measurements parallel to the source surface at the distance of 1,0 mm should be made for a meaningful determination of source non-uniformity covering the relevant area defined in 5.7.3. For planar sources, this is most easily done using radiochromic film. For concave sources, measurements with small strips of thin (single-emulsion) radiochromic film parallel to the surface imbedded in a 1 mm thick shell, or in several planes perpendicular to the source axis, can be performed. Indications of non-uniformity can be observed from films irradiated in such planes. For measurements with scintillators or diodes in water, the effective point of measurement, which depends on detector orientation with respect to the field gradient, shall be verified. If film is used, measurements should be averaged over suitable areas to avoid pixel-to-pixel variations in signals causing failure; in no case should the averaging be over areas larger than 1 mm diameter. The lateral distance between measurements should be no greater than 2 mm.

For intravascular beta radiation brachytherapy sources, the dose (rate) uniformity should be checked at at least five measuring points along the linear source at the radial distance of the calibration reference point, P_{ref}. As with area sources, this test is most easily performed with radiochromic film.

11.1.7 Source asymmetry tests

In the case of planar sources, the same measurements used for uniformity testing may be used to assess source asymmetry (see 5.7.4).

For concave sources, it is not necessary that the film measurements be performed parallel to the source surface but should be analyzed with regard to the relevant radial distance to the source axis. For notched sources, there should be mirror symmetry about the axis through the notch. Because asymmetry is defined on a circle, film measurements both in a plane or parallel to the source surface may be used.

11.1.8 Equatorial anisotropy tests for line sources

This is most easily checked with a point detector (scintillator or diode) by rotating the source while the detector is fixed and examining the variation in signal. It is necessary to take care that the distance between the detector and source remains constant during this measurement, which can also be performed in air.

11.1.9 Active source length and active area

This is most easily performed with autoradiography and can be assessed with a ruler (for line sources) or minimal image analysis (for planar area sources). For concave sources, the results of the source non-uniformity tests may be used for measurements of active area.

11.1.10 Mechanical source specifications

As well as the dosimetric characteristics, the user should also check the stated geometric dimensions of the source, such as the size and shape (e.g., presence of cutouts) of a concave applicator, or the length (or number of seeds) of a line source.

11.1.11 Contamination (leakage)

As with any sealed radioactive source, it is necessary that leakage tests [88], [89] be performed to verify that the radioactive source containment is in accordance with local regulations.

11.1.12 Failure of acceptance test

Recommended limiting values for both U_{L}, U_{AS} and U_{EA} are 20 %. It is expected that with improvements in manufacturing technology, this value can be lower in the future.

If the acceptance test is failed, the clinical physicist should have a second independent test performed, and if the result of the measurement is consistent with the initial result, consult the manufacturer to confirm the

stated value. If the discrepancy is not resolved, then a qualified third party (another hospital with experience in these measurements or an independent calibration laboratory accredited for these calibrations) can be consulted to check the measurements. In the end, it is the ultimate responsibility of the clinical physicist/physician to decide whether or not to use the source, and if so, which value is used for therapy.

11.2 Constancy checks

All beta radiation brachytherapy sources shall be tested for removable contamination in accordance with local regulations.

11.2.1 Ophthalmic brachytherapy sources

Before and after each use, ophthalmic brachytherapy sources should be examined for wear or damage. Cleaning and sterilization should be carried out according to the recommendations of the manufacturer because they can damage the source encapsulation [88].

11.2.2 Intravascular brachytherapy sources

For subsequent deliveries of intravascular sources of the identical type, the user should perform consistency checks and compare them with the detailed measurements performed during the initial acceptance test and the reference data set. The tests of the relative depth dose distribution and the dose rate uniformity can be performed with the equipment calibrated for the initial acceptance test at the calibration reference point, P_{ref}, and at least three additional measuring points, two of them within the range of the beta-particle radiation (e.g. at approximately 50 % and 75 % of this range) and one beyond the range (e.g. at approx. 125 %) to check the purity of the beta radiation emitter.

The manufacturers are obligated to develop reliable check procedures. The user should ensure the reliability of the results from the measuring procedures by periodical internal control measurements. Routine calibrations shall be integrated in the hospital's QA system.

For these sources, the following tests shall be performed:

— check of device functions according to the manufacturer's recommendations;

— before each application, check of the complete source transfer and the safe positioning of the radiation sources in the source guide catheter using dummy sources;

— after each treatment or in case of suspicion of damage, check for contamination;

— every quarter, verification check of the entire measuring procedure with all steps for data collection and processing, especially with regard to correction, precision, and long-time stability;

It is necessary that the results of these internal checks be documented and stored according the requirements of the established Quality Management (QM) system of the user. If deviations are identified, corrective and preventive measures shall be introduced.

Annex A
(normative)

Reference data

Table A.1 — Relative measured axial depth-dose distributions in water for a planar $^{90}Sr + ^{90}Y$ source and for a concave $^{106}Ru + ^{106}Rh$ source

NOTE See Reference [18].

Depth in water z mm	Relative measured axial depth	
	$^{90}Sr + ^{90}Y$ planar source	$^{106}Ru + ^{106}Rh$ concave source
0	1,752	1,353
0,5	1,342	1,297
1	1	1,212
1,5	0,734	1,110
2	0,533	1
2,5	0,383	0,889
3	0,272	0,781
4	0,127	0,587
5	0,052	0,428
6	0,018	0,302
7	—	0,206
10	—	0,053

Table A.2 — List of values of the radial-dose function, $g(r)$, for $^{90}Sr + ^{90}Y$ single-seed sources and ^{32}P wire segments

NOTE See References [25] and [27].

r or ρ mm	Radial-dose function $g(r)$		Transverse-dose function $g(\rho)$
	$^{90}Sr + ^{90}Y$ 2,5 mm seed	^{32}P 2,0 mm segment	^{32}P 20 mm or 27 mm wire
0,5	1,134	1,199	1,862
1	1,096	1,249	1,634
1,5	1,067	1,164	1,322
2	1	1	1
2,5	0,909	0,802	0,713
3	0,803	0,603	0,480
3,5	0,692	0,424	0,303
4	0,578	0,276	0,177
4,5	0,466	0,166	0,094
5	0,362	0,091	0,045
5,5	0,272	0,046	0,018
6	0,198	0,024	0,006
6,5	0,139	0,015	0,002
7	0,092	0,010	—
8	0,30	—	—
9	0,01	—	—

Table A.3 — Geometry function, $G(r,\theta)$, multiplied by r^2 for a length, L, of 2,5 mm

r mm	Geometry function, multiplied by r^2 for a length, L, of 2,5 mm, at various values of θ $G(r,\theta)$									
	θ degrees									
	0	10	20	30	40	50	60	70	80	90
0,5	—	3,430	1,653	1,079	0,807	0,656	0,566	0,513	0,485	0,476
1	—	5,723	2,518	1,595	1,187	0,969	0,843	0,769	0,729	0,717
1,5	3,273	2,620	1,892	1,463	1,207	1,046	0,944	0,880	0,845	0,834
2	1,641	1,576	1,431	1,277	1,147	1,049	0,977	0,930	0,903	0,894
2,5	1,333	1,310	1,251	1,176	1,102	1,039	0,990	0,955	0,934	0,927
3	1,210	1,198	1,165	1,121	1,074	1,030	0,995	0,969	0,953	0,947
4	1,108	1,103	1,088	1,067	1,043	1,019	0,998	0,982	0,973	0,969
5	1,067	1,064	1,055	1,042	1,028	1,013	0,999	0,989	0,982	0,980
7	1,033	1,032	1,028	1,021	1,014	1,007	1,000	0,994	0,991	0,990
10	1,016	1,015	1,013	1,010	1,007	1,003	1,000	0,997	0,995	0,995

Table A.4 — Reference values for the anisotropy function, $F(r,\theta)$, for a single $^{90}Sr + {}^{90}Y$ seed with a length, L, of 2,5 mm

NOTE See Reference [27].

r mm	Reference values of the anisotropy function for a $^{90}Sr + {}^{90}Y$ seed at various values of θ $F(r,\theta)$															
	θ degrees															
	0	5	10	15	20	25	30	35	40	45	50	55	60	70	80	90
0,25	—	—	—	—	—	—	—	—	—	—	—	1,040	1,034	1,018	1,005	1
0,5	—	—	—	—	—	—	—	—	—	—	—	1,018	1,012	1,006	1,001	1
1	—	—	—	—	—	1,098	1,06	1,035	1,021	1,012	1,007	1,004	1,001	1,000	1,000	1
1,5	0,832	0,789	0,781	0,745	0,780	0,836	0,879	0,911	0,934	0,951	0,964	0,974	0,981	0,992	0,998	1
2	0,789	0,777	0,765	0,742	0,743	0,767	0,803	0,842	0,878	0,908	0,932	0,952	0,967	0,987	0,997	1
2,5	0,746	0,745	0,743	0,744	0,755	0,774	0,803	0,835	0,867	0,896	0,922	0,942	0,959	0,983	0,996	1
3	0,740	0,742	0,748	0,755	0,769	0,788	0,813	0,841	0,870	0,896	0,921	0,941	0,958	0,983	0,996	1
4	0,766	0,770	0,775	0,786	0,800	0,818	0,839	0,863	0,885	0,908	0,929	0,947	0,962	0,984	0,996	1
5	0,793	0,800	0,806	0,816	0,828	0,844	0,863	0,882	0,903	0,922	0,939	0,955	0,968	0,986	0,996	1
6	0,829	0,833	0,839	0,845	0,856	0,871	0,889	0,905	0,921	0,939	0,953	0,965	0,976	0,989	0,998	1
7	0,876	0,882	0,896	0,900	0,909	0,921	0,933	0,942	0,955	0,967	0,977	0,986	0,989	0,996	1,001	1
8	0,972	1,006	0,990	1,001	1,003	1,000	1,015	1,019	1,015	1,011	1,021	1,016	1,016	1,011	1,002	1

Table A.5 — Reference values for the anisotropy function, $F(r,\theta)$, for a ^{32}P source segment with a length, L, of 2,5 mm

NOTE See Reference [25].

r mm	Reference values of the anisotropy function for a ^{32}P source with a length, L, of 2,5 mm, at various values of θ $F(r,\theta)$								
	θ degrees								
	10	20	30	40	50	60	70	80	90
1	—	—	—	0,949	0,970	0,985	0,994	0,999	1,000
1,5	—	—	0,872	0,928	0,964	0,984	0,995	1,000	1,000
2	—	0,719	0,831	0,914	0,957	0,982	0,995	1,000	1,000
2,5	—	0,714	0,827	0,905	0,959	0,982	0,995	1,001	1,000
3	—	0,714	0,824	0,905	0,960	0,985	0,995	1,000	1,000
3,5	0,619	0,739	0,840	0,915	0,964	0,984	0,998	1,001	1,000
4	0,650	0,764	0,856	0,936	0,975	0,998	1,004	1,004	1,000
4,5	0,684	0,794	0,888	0,971	1,001	1,017	1,016	1,010	1,000
5	0,722	0,831	0,919	0,985	1,015	1,018	1,015	1,001	1,000

Table A.6 — Reference values for the non-uniformity function, $F(\rho,z)$, for the 20 mm and 27 mm ^{32}P wire sources

NOTE See Reference [27].

z mm		Reference values for the non-uniformity function $F(\rho,z)$									
Length of ^{32}P wire source [a]		ρ mm									
27 mm	20 mm	0,6	1,0	1,5	2,0	2,5	3,0	3,5	4,0	4,5	5,0
±3,5	±0,0	9,982E-01	1,000E+00	1,001E+00	1,002E+00	1,002E+00	9,993E-01	9,992E-01	9,992E-01	1,000E+00	1,001E+00
±4,0	±0,5	9,982E-01	1,000E+00	1,001E+00	1,002E+00	1,002E+00	9,977E-01	9,992E-01	9,996E-01	1,000E+00	1,001E+00
±4,5	±1,0	9,988E-01	1,000E+00	1,001E+00	1,002E+00	1,002E+00	9,972E-01	1,001E+00	1,000E+00	1,001E+00	1,002E+00
±5,0	±1,5	9,988E-01	1,000E+00	1,001E+00	1,002E+00	1,002E+00	9,999E-01	1,003E+00	1,001E+00	1,001E+00	1,003E+00
±5,5	±2,0	9,999E-01	1,000E+00	1,001E+00	1,002E+00	1,002E+00	1,002E+00	1,004E+00	1,002E+00	1,002E+00	1,004E+00
±6,0	±2,5	1,000E+00	1,001E+00	1,001E+00	1,002E+00	1,002E+00	1,002E+00	1,004E+00	1,003E+00	1,003E+00	1,004E+00
±6,5	±3,0	1,001E+00	1,001E+00	1,001E+00	1,002E+00	1,002E+00	1,002E+00	1,003E+00	1,004E+00	1,003E+00	1,003E+00
±7,0	±3,5	1,002E+00	1,001E+00	1,001E+00	1,002E+00	1,002E+00	1,003E+00	1,003E+00	1,005E+00	1,003E+00	1,001E+00
±7,5	±4,0	1,003E+00	1,001E+00	1,001E+00	1,001E+00	1,001E+00	1,005E+00	1,003E+00	1,005E+00	1,002E+00	1,000E+00
±8,0	±4,5	1,003E+00	1,001E+00	1,001E+00	1,001E+00	1,001E+00	1,005E+00	1,003E+00	1,004E+00	1,001E+00	9,990E-01
±8,5	±5,0	1,002E+00	1,001E+00	1,000E+00	1,000E+00	1,000E+00	1,004E+00	1,001E+00	1,001E+00	1,000E+00	9,987E-01
±9,0	±5,5	1,001E+00	9,998E-01	9,990E-01	9,985E-01	9,985E-01	1,001E+00	9,981E-01	9,981E-01	9,994E-01	9,985E-01
±9,5	±6,0	9,988E-01	9,982E-01	9,969E-01	9,959E-01	9,950E-01	9,955E-01	9,931E-01	9,932E-01	9,963E-01	9,965E-01
±10,0	±6,5	9,955E-01	9,954E-01	9,931E-01	9,909E-01	9,886E-01	9,872E-01	9,846E-01	9,846E-01	9,891E-01	9,892E-01
±10,5	±7,0	9,905E-01	9,907E-01	9,865E-01	9,812E-01	9,769E-01	9,733E-01	9,691E-01	9,692E-01	9,733E-01	9,730E-01
±11,0	±7,5	9,840E-01	9,827E-01	9,741E-01	9,632E-01	9,554E-01	9,484E-01	9,415E-01	9,410E-01	9,447E-01	9,425E-01
±11,5	±8,0	9,757E-01	9,686E-01	9,506E-01	9,312E-01	9,175E-01	9,059E-01	8,960E-01	8,948E-01	8,972E-01	8,932E-01
±12,0	±8,5	9,625E-01	9,403E-01	9,053E-01	8,755E-01	8,547E-01	8,396E-01	8,280E-01	8,260E-01	8,274E-01	8,223E-01
±12,5	±9,0	9,307E-01	8,764E-01	8,214E-01	7,852E-01	7,609E-01	7,466E-01	7,355E-01	7,325E-01	7,346E-01	7,296E-01
±13,0	±9,5	8,169E-01	7,342E-01	6,822E-01	6,545E-01	6,369E-01	6,295E-01	6,218E-01	6,187E-01	6,217E-01	6,186E-01
±13,5	±10,0	4,925E-01	4,927E-01	4,940E-01	4,948E-01	4,936E-01	4,973E-01	4,950E-01	4,925E-01	4,973E-01	4,963E-01
±14,0	±10,5	1,661E-01	2,504E-01	3,050E-01	3,351E-01	3,514E-01	3,642E-01	3,675E-01	3,675E-01	3,730E-01	3,729E-01
±14,5	±11,0	5,774E-02	1,101E-01	1,660E-01	2,051E-01	2,293E-01	2,452E-01	2,526E-01	2,557E-01	2,607E-01	2,595E-01
±15,0	±11,5	2,651E-02	5,083E-02	8,573E-02	1,163E-01	1,382E-01	1,521E-01	1,604E-01	1,657E-01	1,691E-01	1,656E-01
±15,5	±12,0	1,442E-02	2,639E-02	4,462E-02	6,248E-02	7,790E-02	8,861E-02	9,515E-02	9,977E-02	1,016E-01	9,638E-02
±16,0	±12,5	7,922E-03	1,447E-02	2,358E-02	3,232E-02	4,157E-02	4,954E-02	5,353E-02	5,481E-02	5,561E-02	5,122E-02
±16,5	±13,0	4,079E-03	7,647E-03	1,194E-02	1,613E-02	2,095E-02	2,521E-02	2,781E-02	2,668E-02	2,654E-02	2,473E-02
±17,0	±13,5	1,931E-03	3,617E-03	5,130E-03	7,632E-03	9,694E-03	9,621E-03	1,178E-02	1,233E-02	1,067E-02	1,020E-02
±17,5	±14,0	8,565E-04	1,594E-03	1,598E-03	3,231E-03	3,674E-03	4,644E-03	4,912E-03	5,469E-03	4,358E-03	3,672E-02

[a] For the 27 mm source, $F(\rho,z) = 1$ for $0 < z < 3{,}5$ mm; $F(\rho,-z) = F(\rho,z)$ for both sources.

Annex B
(informative)

Reference data sheet examples

B.1 Ophthalmic brachytherapy source

Product information for a ^{106}Ru ophthalmic brachytherapy source is described in this subclause.

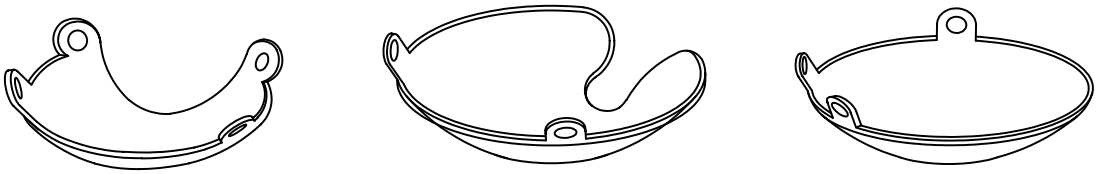

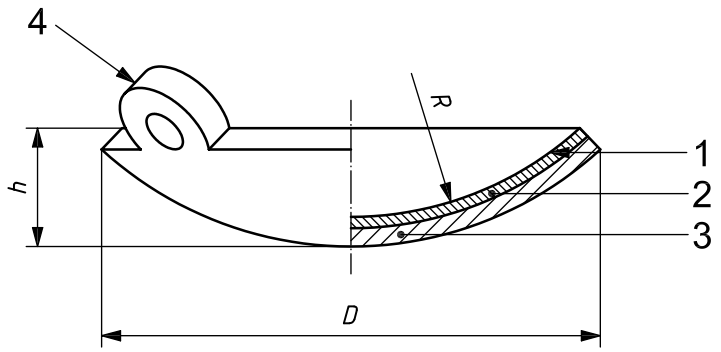

Key

1 radiation window
2 radioactive part
3 backing
4 suture holes

NOTE 1 See Table B.1 for values of D, h, and R.

NOTE 2 Figures are reproduced by permission of Eckert & Ziegler BEBIG GmbH.

Figure B.1 — Source construction

Table B.1 — Source geometric parameters

Type	Diameter D mm	Height h mm	Radius R mm	Number of suture holes (eyelets)	Angle between eyelets degrees
CCZ	11,6	2,3	12	2	180
CCY	11,6	2,3	12	3	120
CCX	11,6	2,3	12	2	90
CXS	11,6 [a]	2,3	12	2	90
CCA	15,3	3,3	12	2	90
CCD	17,9	4,3	12	2	90
CCB	20,2	5,4	12	2	90
CGD	22,3	6,1	13	3	90/145
CCC	24,8	8,0	13	2	90
COB	19,8	5,2	12	2	90
COD	25,4	7,5	14	2	90
COE	19,8	5,2	12	2	90
COC	25,4	7,5	14	2	90
CIA	15,3	3,3	12	2	180
CIB	20,2	5,4	12	2	180
CIB-2	20,2	5,4	12	4	120/60

[a] Active diameter for CXS is 7,9 mm.

The source has the following characteristics:

— radionuclide: $^{106}Ru/^{106}Rh$;

— half-life: 1 year;

— maximum energy: 3,54 MeV;

— nominal dose rate at the centre of the concave side: 120 mGy/min;

— source thickness: 1 mm;

— radiation window: 0,1 mm silver foil.

Available source designs are shown in Figure B.2.

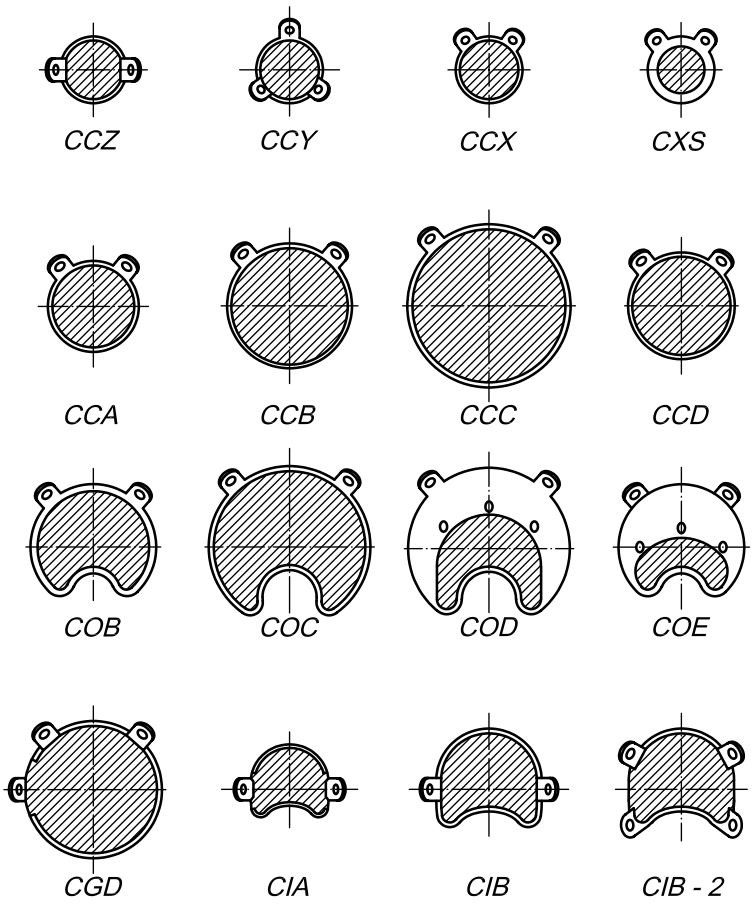

Figure B.2 — Available source designs

A depth-dose profile for a type CCB plaque is shown in Figure B.3.

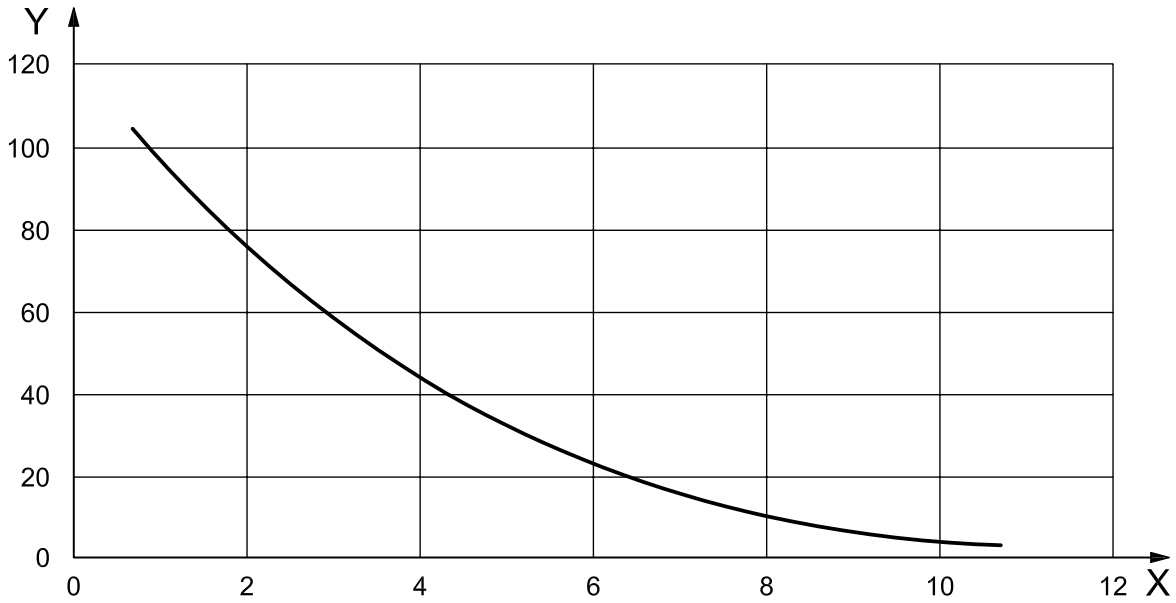

Key

X distance from plaque surface, expressed in millimetres

Y dose rate, expressed in mGy/min

Figure B.3 — Depth-dose profile for a type CCB plaque

Uniformity data for a type CIB plaque are shown in Figure B.4.

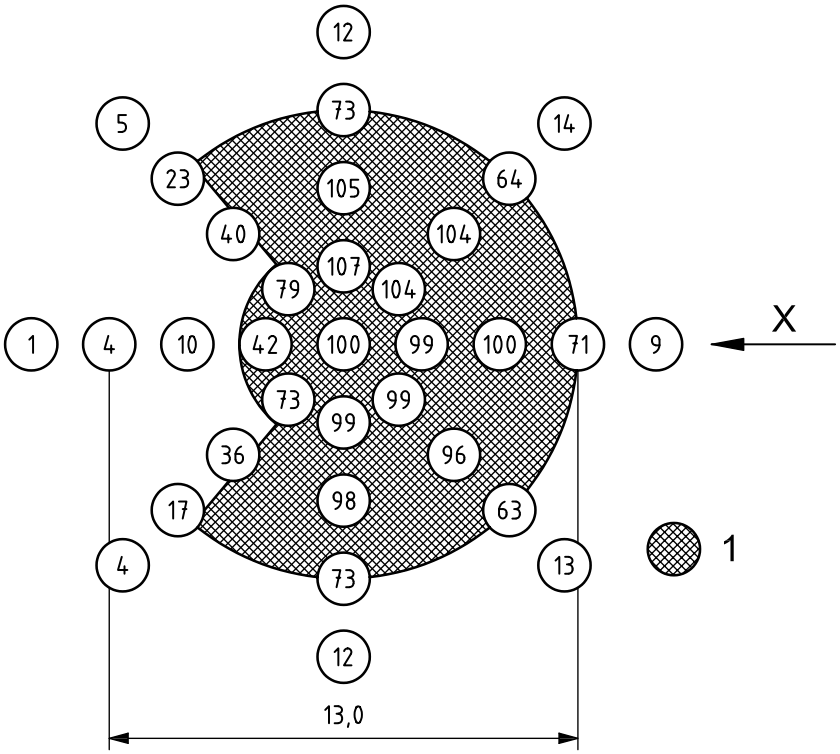

Key

X reference direction

1 application

Figure B.4 — Uniformity data for a type CIB plaque

B.2 Intravascular brachytherapy source

B.2.1 Reference data sheet

— Source model number: _____.

— Radionuclide: ^{32}P (phosphorus-32):

  — radionuclide purity: 99,9 %,

  — chemical purity: 99,9 %.

  The ^{32}P solid, active source is encased in a Nitinol capsule. The distal end of the Nitinol source wire encapsulates the active source. A 1 mm tungsten marker is located on each end of the active source and a Nitinol plug is welded into the distal end of the wire cavity. The minimum Nitinol tube wall thickness is 0,063 5 mm (0,002 5 in). The source wire outer diameter is 0,46 mm (0,018 in) and its length is 2 430 mm.

— Nominal source radioactive length: 20 mm.

— Active source diameter: 0,24 mm (0,009 5 in).

The source construction is shown in Figure B.5.

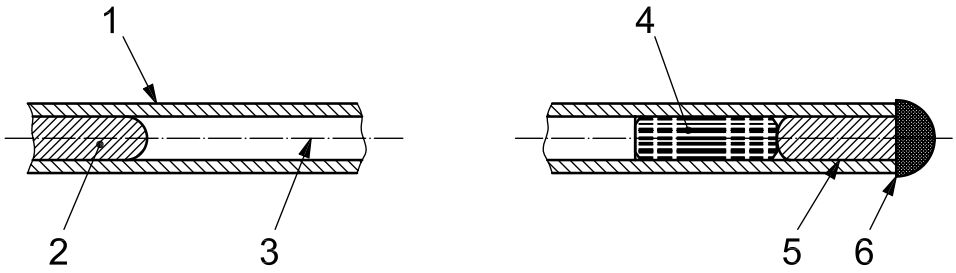

Key

1 Niti tube: ∅ 0,018 mm, 0,003 val nom.
2 Niti wire
3 ^{32}P source: ∅ 0,24 mm; length, 27 ± 0,25 mm
4 tungsten wire marker: OD 0,010; length, 1,00 ± 0,25 mm
5 nickel-titanium plug: OD 0,010; length 1,00 ± 0,25 mm
6 hemispherical weld, tube and plug together

Figure B.5 — Source construction

B.2.2 Source calibration data

B.2.2.1 Method of calibration

The dose rate in water, expressed in grays per minute, is measured at the reference point and the contained activity is measured using a NIST-calibrated well chamber with Guidant insert.

B.2.2.2 Uncertainty in calibrated dose rate and activity

The reference dose rate and contained activity was determined using instruments with calibration factors traceable to the National Institute of Standards and Technology. The overall uncertainty in the determination of the reference dose rate and contained activity is estimated to be within ± 15 % and ± 5,4 %, respectively, both at the 95 % confidence interval for the following conditions:

— measured reference dose rate: 36 Gy/min (2 mm from source axis in water along the orthogonal bisector);

— measured contained activity: 7,00 GBq (189 mCi);

— calculated reference dose rate per GBq: 5,14 Gy/min per GBq;

— calibration date and time: 2001 July 27, 00:00:01 GMT.

B.2.3 Spatial dose distribution data

B.2.3.1 Relative depth dose values

Table B.2 shows the depth dose data for the Guidant 20 mm ^{32}P source in water. The dosimetry data were calculated using the Monte Carlo method and validated using the NIST extrapolation chamber and radiochromic film in a polystyrene phantom. Estimated uncertainties of dose interpretations for the Monte Carlo method and radiochromic film are ± 2 % and ± 16 %, respectively. These data were compiled at the National Institute of Standards and Technology (NIST), Gaithersburg, Maryland, USA. The data are plotted in Figure B.7.

Table B.2 — Depth dose data for the Guidant 20 mm ^{32}P source in water

Depth [a] mm	Relative dose rate at P_{ref}
0,49	7,09E+00
1,00	3,15E+00
1,39	1,95E+00
1,89	1,12E+00
2,00	1,00E+00
2,39	6,54E-01
2,89	3,74E-01
3,39	2,06E-01
3,89	1,07E-01
4,39	5,15E-02
4,89	2,21E-02
5,39	8,05E-03
5,89	2,47E-03
6,39	5,91E-04
6,90	1,23E-04
7,40	5,20E-05
7,90	3,71E-05
8,40	3,27E-05
9,40	2,71E-05
10,00	2,49E-05
[a] Radial distance from the source axis.	

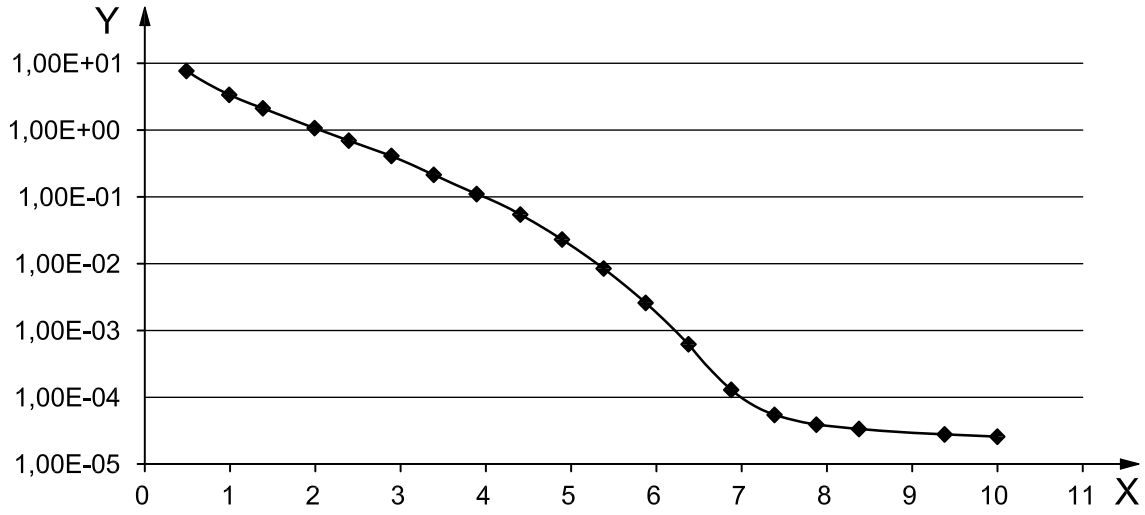

Key

X radial distance from the source axis in water, expressed in millimetres

Y relative dose rate

Figure B.6 — Depth-dose data

B.2.3.2 Dose distribution in water

B.2.3.2.1 Guidant ^{32}P source

Figure B.7 depicts the calculated dose rate profiles (relative to the reference dose rate at $\rho = 2$ mm) for the Guidant 20 mm ^{32}P source (model GDT-P32-1) at various radial distances from the source axis in water. The X-axis reference point is located at the source bisector, and the source active length (50 % isodose) extends to ± 10 mm. Data were generated at NIST using the Monte Carlo method.

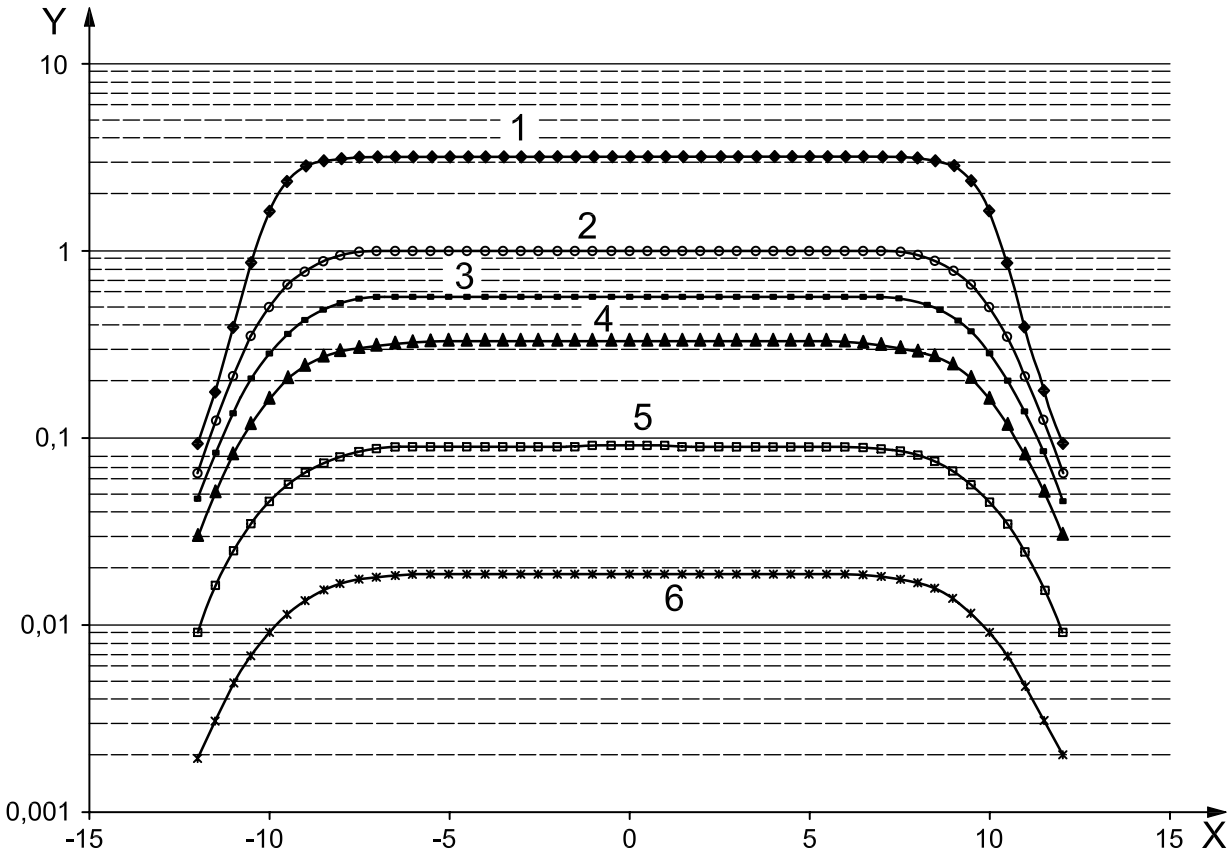

Key

X distance along the source axis, expressed in millimetres

Y relative dose rate

Radial distance from the source axis in water:

1 1,0 mm

2 2,0 mm

3 3,0 mm

4 4,0 mm

5 5,0 mm

6 6,0 mm

Figure B.7 — Dose distributions in water as a function of radial distance from the source axis

B.2.3.2.2 ^{32}P source wire

a) Figure B.8 is an example of a relative dose map of a 20 mm ^{32}P source wire at a depth of 2,12 mm from the centre of the source stepped once using the source delivery unit (SDU), resulting in a 40 mm equivalent source length (radiochromic film data).

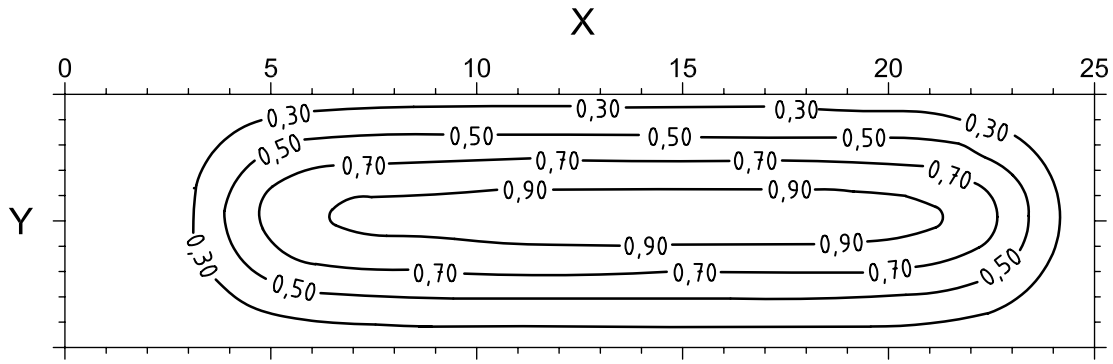

a) Single position

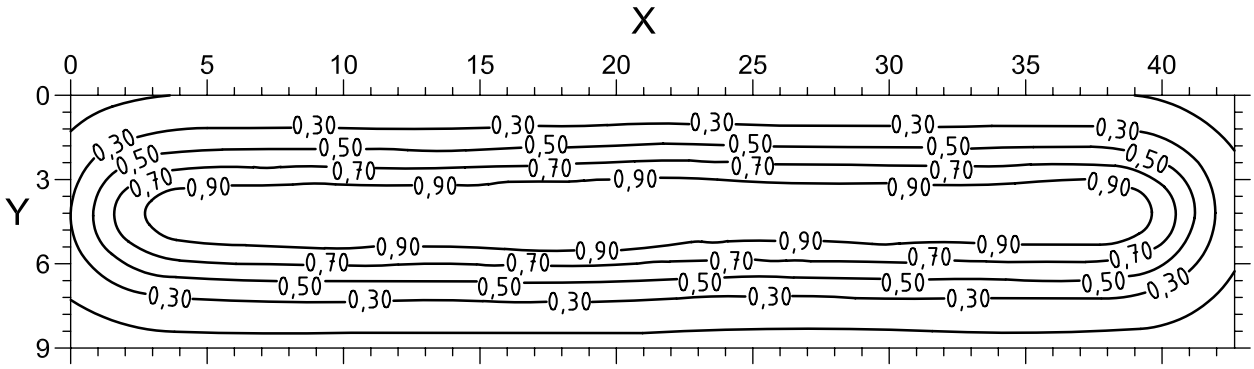

b) Two positions

Key

X axis, mm

Y y-axis, mm

Figure B.8 — Spatial dose distributions

B.2.3.3 Example of a source certificate

Source Certificate (example)

Model number: _____ **Serial number:** _____

Radionuclide: _____

Ref. dose rate: _____ Gy/min **Ref. distance is 2 mm from source axis in water**

Contained activity: _____ GBq or _____ mCi

Calibration date (yyyy/mm/dd): _____ **Time:** 00:00:01 GMT

Source active length: _____ mm

Axial (Longitudinal) Dose Rate Uniformity: Values are measured at the 2 mm reference depth over the central region of the source for a total of *xx* measurements, each separated by *xx* mm. The percent maximum and minimum relative to the average is ___ % and ___ %, respectively. The measurements have an estimated expanded uncertainty (2σ) of $\pm xx$ %.

Radiation output (from the center of the source in a radial direction):

Absorbed dose rate per unit activity in air at 5 cm = _____ µGy/min/MBq

Absorbed dose rate per unit activity in air at 100 cm = _____ µGy/min/MBq

Test for freedom from surface contamination and leakage:

Method: ISO 9978:1992(E) 5.3.1, wet wipe test

Result: < 185 Bq (5 nCi) **Date** (yyyy/mm/dd): _____

ISO classification: _____

Package certification statement: Requirements, address, and contact name.

Name: _____ Radiation safety officer **Date:** _____

Approval signature: _____ **Date** (yyyy/mm/dd): _____

Annex C
(informative)

Primary standards for beta radiation dosimetry

C.1 The extrapolation chamber

The extrapolation chamber is the primary measurement device for specifying absorbed dose rate to water in beta radiation fields. It is a parallel plate ionization chamber that consists of components that allow the attainment of a variable ionization volume by movement of one of the plates towards the other. A typical design [89], which utilizes a fixed entrance window and a movable collecting electrode, is shown in Figure C.1.

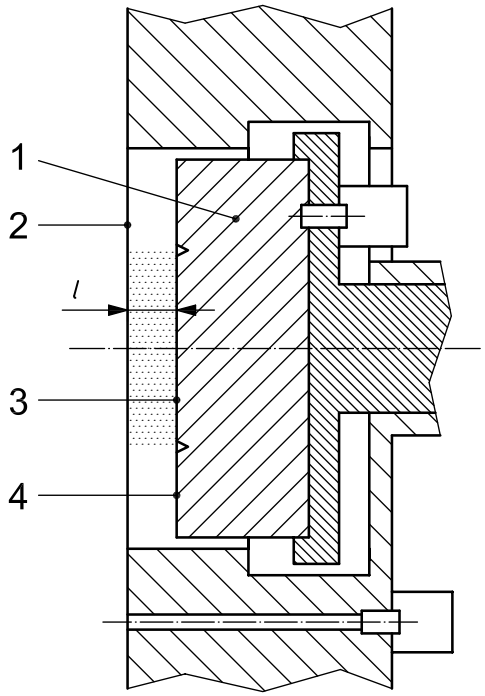

Key

1 piston
2 entrance window
3 collecting electrode
4 guard ring
l chamber depth

Figure C.1 — Schematic cross-section of the main parts of an extrapolation chamber

The entrance window also serves as the high-voltage electrode, and consists of a very thin conducting plastic foil. It is necessary that the window be thin enough so as not to unduly attenuate the beta radiation, yet strong enough so as to not be deformed by attraction to the grounded collecting electrode. The collecting electrode is maintained at ground potential and defines the cross-sectional area of the ionization volume. It is necessary that it be made of conducting material or have a conducting coating and be surrounded by, and electrically insulated from, a guard region. It is necessary that this insulation be thin enough so as not to perturb the electric field lines in the chamber volume, which ideally are uniform, and everywhere perpendicular to the two

electrodes. In the design shown in Figure C.1, the collecting electrode is constructed from polymethylmethacrylate (PMMA) that has a thin coating of conductive material in which a narrow groove has been inscribed to define the collecting area. Note the necessity that the collecting area be smaller than the active source area in order to properly specify the area of the source over which the dose rate is being determined [29]. It is necessary that the device be equipped with an accurate means to determine incremental changes in the distance between the two electrodes, hereafter referred to as the chamber depth; a micrometer attached to the piston that drives the collecting electrode is usually employed. A bipolar, variable-voltage DC power source is used to supply the high voltage to the collecting electrode and a low-noise electrometer is used to measure the current collected by the collecting electrode.

C.2 Principle of the determination of the absorbed dose rate to water for beta radiation

The determination of the absorbed dose rate to water due to beta radiation measured with an extrapolation chamber is derived from the general relationship given in Equation (C.1):

$$\dot{D}_{\mathrm{w}} = \frac{\bar{W}}{e} S_{\mathrm{w,a}} \left[\frac{\Delta I}{\Delta m_{\mathrm{a}}} \right]_{\mathrm{BG}} \tag{C.1}$$

where

ΔI is the increment of the ionization current;

Δm_{a} is the increment of the mass of air in the collecting volume under Bragg-Gray (BG) conditions.

Unfortunately Bragg-Gray (BG) conditions are generally not realized in measurements of the beta radiation reference radiation fields and, to overcome this difficulty, various corrections are applied such that the expression for the determination of the absorbed dose rate to water takes the form of Equation (C.2):

$$\dot{D}_{\mathrm{w}} = \frac{\left(\bar{W}/e\right) S_{\mathrm{w,a}}}{\xi_{\mathrm{a0}}\, A_{\mathrm{ce}}} \left[\frac{\mathrm{d}}{\mathrm{d}l} \Pi k' I(l) \right]_{l=0} \Pi k \tag{C.2}$$

where

$\bar{W}$ is the mean energy required to produce an ion pair in air;

e is the elementary charge (the recommended value of the quotient, $\bar{W}/e$, is 33,97 J/C);

ξ_{a0} is the density of air at the reference conditions of temperature, pressure and relative humidity;

A_{ce} is the effective area of the collecting electrode;

$S_{\mathrm{w,a}}$ is the ratio of the mean mass-electronic stopping powers in water and air [see Equation (C.3)];

Πk is the product of the correction factors that are independent of the chamber depth;

$\Pi k'$ is the product of the correction factors that vary with the chamber depth;

$\left[\frac{\mathrm{d}}{\mathrm{d}l} \Pi k' I(l) \right]_{l=0}$ is the limiting value of the slope of the function of the corrected current versus the chamber depth, l.

The ratio of the mean mass-electronic stopping powers in water and air, $S_{w,a}$, is given by Equation (C.3):

$$S_{w,a} = \frac{\int_0^{E_{max}} (\Phi_E)_w \, (S/\xi)_{el,w} \, dE}{\int_0^{E_{max}} (\Phi_E)_w \, (S/\xi)_{el,a} \, dE} \tag{C.3}$$

where

$(\Phi_E)_w$ is the spectrum of electrons at the reference point of the extrapolation chamber;

$(S/\xi)_{el,w}$ is the mass-electronic stopping power for an electron with kinetic energy E in water;

$(S/\xi)_{el,a}$ is the corresponding quantity for air.

It is assumed that secondary electrons (delta rays) deposit their energy where they are generated so that they do not contribute to the electron fluence. The upper limit of the integrals is given by the maximum energy, E_{max}, of the beta radiation in the fluence spectrum and the lower limit corresponds to the lowest energy in the spectrum, here indicated by a zero. In principle, this spectrum also includes any electrons set in motion by bremsstrahlung photons but these are usually of negligible importance.

Values for $S_{w,a}$ and spectra in different depth of water-equivalent material have been calculated for a planar $^{90}Sr + {}^{90}Y$ source by means of Monte Carlo methods (MCNP-4C) [77].

C.3 The NIST beta radiation primary standard

A special, in-house manufactured extrapolation chamber is used at NIST to determine the reference absorbed dose rate to water from beta radiation brachytherapy sources. The chamber features removable collecting electrodes that allow measurement of both planar sources and intravascular sources. For the latter measurements, the source is inserted in a hole in a tissue-equivalent plastic block (A150) with the centre of the source at a distance of 2 mm from the block surface. At this depth, the radiation field from a seed or wire source is such that a collecting electrode diameter of 1 mm can be used to measure absorbed dose rate. For measurements of planar sources, a 4 mm collecting electrode is used [29], [77]. Corrections are applied for the difference in backscatter between the collecting electrode material (carbon) and water, for variations in temperature and pressure from reference conditions and for the effect of beta radiation divergence within the chamber volume. To keep the latter correction as minimal as possible, extremely small chamber depths of 0,15 mm or less are used.

The relative expanded uncertainty ($k = 2$) of the absorbed dose rate to water at a depth of 2 mm in water-equivalent material is 7 % for the extrapolation chamber with the 4 mm collecting electrode used for planar beta radiation sources. For the same chamber equipped with the 1 mm collecting electrode used for determining reference absorbed dose rate from intravascular sources at a depth of 2 mm in water-equivalent material, the relative expanded uncertainty ($k = 2$) is 10 % [77].

C.4 The PTB primary standard for beta radiation planar sources

The primary standard for planar beta radiation sources at PTB is a further development of a conventional extrapolation chamber as described in principle in Clause C.1. The beta radiation source, being a 7,5 GBq or 750 MBq $^{90}Sr + {}^{90}Y$ source with an active area 15 mm in diameter, is situated in a container providing radiation protection, and can be positioned at reproducible distances from a reference plane in order to be able to vary the absorbed dose rate at this reference plane and in any depth of water-equivalent material between 0 mm and 8 mm. The radial dose-rate distribution is additionally measured for each of the different layer thicknesses with the aid of a special ionization chamber of high spatial resolution. Thus, complete three-dimensional $^{90}Sr + {}^{90}Y$ beta reference radiation fields in water-equivalent material with water absorbed dose

rates between 30 mGy/min and 10 Gy/min are available and can be used for the calibration of transfer dosimeters, such as radiochromic dye film, scintillation dosimeters or TLD. In the future, the specification of similar reference radiation fields for $^{106}Ru + ^{106}Rh$ is planned. The relative expanded uncertainty ($k = 2$) of the absorbed dose rate to water in 2 mm water-equivalent material is 6,9 %.

C.5 The PTB primary standard for beta radiation brachytherapy sources — Multi-electrode extrapolation chamber

A new primary standard has been developed that enables the realization of the unit of the measurand absorbed dose to water in the vicinity of beta radiation brachytherapy sources [78]. In the course of its development, the recommendations of the American Association of Physicists in Medicine (AAPM) Task Group 60 [22] and the Deutsche Gesellschaft für Medizinische Physik (DGMP) Arbeitskreis 18 [19] were taken into account. The primary standard is based on a newly designed multi-electrode extrapolation chamber (MEC), which meets, in particular, the requirements of high spatial resolution and small uncertainty. In contrast to a conventional extrapolation chamber, the central part of the MEC is a segmented collecting electrode that was manufactured in the clean room centre of PTB by means of electron-beam lithography on a wafer. About thirty collecting electrodes (for example 1 mm by 1 mm in size) are arranged in the centre of the wafer and a precise displacement device consisting of three piezoelectric macro-translators is incorporated to move the wafer collecting electrodes against the entrance window. An upper estimation of the relative expanded uncertainty ($k = 2$) of the absorbed dose rate to water in 2 mm water-equivalent material is 6,0 % [78] (see C.8).

C.6 The NMi beta radiation primary standard

This standard of the Nederlands Meetinstitut (NMi) is similar to the NIST extrapolation chamber in that the collecting electrode remains stationary while the entrance window is moved to change the collecting volume. A precision three-dimensional stage moves the source to allow centring, field mapping and maintenance of the position relative to the entrance electrode as the volume is changed. The collecting electrode is 1 mm in diameter and constructed from D400 water-equivalent plastic. A relative expanded uncertainty of 11 % ($k = 2$) has been assigned to the calibration of planar sources [91].

C.7 The PTB beta radiation secondary standard with planar source

The same type of $^{90}Sr + ^{90}Y$ beta radiation sources as described in Clause C.4 are commercially available as secondary standards. The source and the radiation containment are built under licence by a German manufacturer, AEA Technology[2)]. In the same way as for the PTB primary standard for planar sources, the beta radiation field of these secondary standards is determined at the PTB at various depths in water-equivalent material by means of the described extrapolation chamber. Thus, the user gets $^{90}S + ^{90}Y$ reference radiation fields traceable to a primary standard, which can be used for calibrations of transfer dosimeters at the hospital site.

C.8 Example of a detailed uncertainty budget in accordance with ISO Guide 98-3

The following is a detailed consideration of the uncertainties associated with the measurement of an area source with the PTB primary standard for area brachytherapy sources (see Clause C.4) using the procedures specified in ISO Guide 98-3.

2) This is an example of a suitable product available commercially. This information is given for the convenience of users of this International Standard and does not constitute an endorsement by ISO of this product.

The physical model for the calculation of the absorbed dose rate to water, $\dot{D}_{\mathrm{w}}$, expressed in grays per second, can be expressed as given in Equation (C.4):

$$\dot{D}_{\mathrm{w}} = S_{\mathrm{w,a}} \cdot \left(\bar{W}/e\right) \Big/ A_{\mathrm{ce}} \Big/ \xi_{\mathrm{a0}} \cdot M \cdot K_{\mathrm{ad}} \cdot K_{\mathrm{hu}} \cdot K_{\mathrm{sat}} \cdot K_{\mathrm{di}} \cdot K_{\mathrm{ad}} \cdot K_{\mathrm{d}} \cdot K_{\mathrm{ba}} \cdot K_{\mathrm{is}} \cdot K_{\mathrm{f}} \cdot K_{\mathrm{2D}} \quad \text{(C.4)}$$

where

$\bar{W}$ is the mean energy required to produce an ion pair in air;

e is the elementary charge; (the quotient, $\bar{W}/e$, is expressed in joules per coulomb;

$S_{\mathrm{w,a}}$ is the ratio of the mean mass stopping power ratio in water to air;

A_{ce} is the effective area of the collecting electrode, expressed in square metres;

ξ_{a0} is the density of dry air at the reference conditions, expressed in kilograms per cubic metre;

M is the gradient of the extrapolation curve at zero electrode spacing, expressed in amperes per metre;

K_{ad} is the correction of the air density;

K_{hu} is the correction of the relative humidity of the air;

K_{sat} is the saturation correction;

K_{di} is the correction of the divergence of the beta-particle field;

K_{d} is the correction of electrode spacing;

K_{ba} is the correction of the difference backscatter between tissue and the material of the collecting electrode;

K_{is} is the correction for the air gap between phantom surface and entrance window;

K_{f} is the entrance window correction;

K_{2D} is the two-dimensional dose rate profile correction.

The result of the evaluation is given in Table C.1. In this analysis, the relative expanded uncertainty ($k = 2$) of the absorbed dose rate to water in 2 mm water-equivalent material is 6,9 %.

Table C.1 — Uncertainty budget

Quantity	Value	Standard uncertainty	Type and probability distribution	Sensitivity coefficient	Uncertainty contribution Gy/s	Relative contribution %
$\bar{W}/e$	33,97 J/C	0,068	B, normal	0,004	$272 \cdot 10^{-6}$	0,4
$S_{w,a}$	1,120	0,006	B, normal	0,13	$7,55 \cdot 10^{-4}$	2,2
A_{ce}	$80,0 \cdot 10^{-6}$ m^2	$80 \cdot 10^{-9}$ m^2	A, combined	–1 800	$-1,4 \cdot 10^{-3}$	8,4
ξ_{a0}	1,203 kg/m^3	$2,00 \cdot 10^{-3}$ kg/m^3	B, normal	–0,12	$-230 \cdot 10^{-6}$	0,2
M	$300,00 \cdot 10^{-9}$ A/m	$4,50 \cdot 10^{-9}$ A/m	B, normal	$470 \cdot 10^3$	$2,1 \cdot 10^{-3}$	18,8
K_{ad}	1,000 0	$289 \cdot 10^{-6}$	B, rectangular	0,14	$41 \cdot 10^{-6}$	0,0
K_{hu}	1,000 0	$577 \cdot 10^{-6}$	B, rectangular	0,14	$81 \cdot 10^{-6}$	0,0
K_{sat}	1,000 0	$2,89 \cdot 10^{-3}$	B, rectangular	0,14	$410 \cdot 10^{-6}$	0,7
K_{di}	1,080 0	0,023 1	B, rectangular	0,13	$3,0 \cdot 10^{-3}$	38,3
K_d	1,000 0	$5,77 \cdot 10^{-3}$	B, rectangular	0,14	$810 \cdot 10^{-6}$	2,8
K_{ba}	1,000 0	$5,77 \cdot 10^{-3}$	B, rectangular	0,14	$810 \cdot 10^{-6}$	2,8
K_{is}	1,000 0	$5,77 \cdot 10^{-3}$	B, rectangular	0,14	$810 \cdot 10^{-6}$	2,8
K_f	1,000 0	$4,62 \cdot 10^{-3}$	B, rectangular	0,14	$650 \cdot 10^{-6}$	1,8
K_{2D}	1,100 0	0,017 3	B, rectangular	0,13	$2,2 \cdot 10^{-3}$	20,8
$\dot{D}_w$	0,140 9 Gy/s	—	—	—	$4,86 \cdot 10^{-3}$	—

Annex D
(informative)

Detectors and phantom materials for clinical dosimetry of beta radiation brachytherapy sources

D.1 Detectors

D.1.1 Radiochromic film dosimeter

Radiochromic films fulfil some of the requirements of an ideal beta radiation detector [18], [30], [55]. A comprehensive survey on radiochromic film [92] was followed by a survey on radiochromic film dosimetry published by the AAPM TG 55 [81]. Radiochromic film of several types is available under the trade name GAFCHROMIC™ 3). The layered design of the various films along with their elemental composition is provided in Table D.1. The films consist of one or two thin layers of radiosensitive emulsion of the order of 6 µm to 38 µm thick, either coated onto or sandwiched between usually transparent polyester backing of 60 µm to 100 µm.

The film sensitivity is a nearly linear function of the emulsion thickness. The initially almost colourless emulsion of radiochromic films darkens with irradiation and requires no processing, producing a coloured monochrome image. As the film is extremely fine-grained, it can be read with a high-resolution densitometry at spacings of tens of micrometers. The absorbance spectrum of the older GAFCHROMIC™ emulsion (HD-810, MD-55, and HS) exhibits a major peak at a wavelength of about 660 nm, and a minor peak at 610 nm. Thus, the film is most sensitive at these wavelengths. The absorption properties of radiochromic film allow the effective use of a helium-neon laser densitometer with wavelength 633 nm for optical-density measurements, except for the newly released EBT film, which exhibits its major peak around 635 nm, but has polarization artefacts that present problems with highly polarized laser beams.

A scanning densitometer, in principle most transmission-type scanners, can be used for off-line radiation-field mapping, i.e., to measure the density point-by-point over the film surface [93]. Producing a high-resolution 2D distribution of the film transmission or optical density allows its conversion into a 2D dose-rate distribution, while a series of films positioned at different distances from the source result in a 3D dose-rate matrix. On the other hand, films for brachytherapy beta radiation dosimetry, especially the ones used for ophthalmic brachytherapy sources, are often as small as 3 mm to 5 mm in diameter. Cutting such small films poses a challenge [30], as well as does the process of densitometry. The most convenient way of creating the 2D distributions is scanning the films using a flatbed scanner. Scanners that move the film in the scanning process are extremely inconvenient for such small films, since it is necessary that the film be attached to some kind of backing. Document scanners in the transmission mode have been successfully used for this purpose. The main requirements for a document scanner are listed in 11.1.3.

In order to optimize the film response using a colour document scanner, the film should be scanned in the highest colour mode (48 bit for most scanners) with all the image corrections by the scanner turned off and the results saved as an uncompressed tiff file. Then the red channel should be extracted from the resulting tiff file. It is necessary that the dosimeter-densitometer combination be calibrated, but it is usually sufficient to perform one calibration per production lot of radiochromic film.

Non-linearity of the response function density vs. dose is often due to limitations in the densitometry [94]. It is important to mark the direction of the film in the cutting process (the long or the short axis of the sheet) and always place all the films so that the mark is in the same direction on the scanner. This requirement should be

3) GAFCHROMIC™ is the trade name of a product supplied by International Specialty Products. This information is given for the convenience of users of this document and does not constitute an endorsement by ISO of the product named. Equivalent products may be used if they can be shown to lead to the same results.

followed for the calibration films as well as for the measurements. Mixing the scanning directions of the calibration films and the measurements can result in dose errors of up to 30 % [95], [96]. The scanning field of document scanners exhibits a certain unflatness in the direction of the lamp (perpendicular to the scanning direction). This unflatness might not be significant for small brachytherapy films placed close to the centre of the scanner. On the other hand, using large films requires a correction developed by the manufacturer. The latest film dosimetry software packages provide certain corrections for use of radiochromic film with document scanners as well as the ability to extract the red channel.

The radiochromic image exhibits a certain degree of so called post-exposure growth, which is a change of optical density over time. The effect is very significant (up to 20 %) in the first hours after exposure, but then slows down to less than a percent per day. The latest EBT film, which has a different chemistry, was found to be more stable. Therefore, the densitometry of radiochromic film should follow a strict protocol of scanning all films at a certain time after irradiation (usually 24 h to 48 h).

The advantages of radiochromic film include good water-equivalence for electrons, insensitivity to visible light, high resolution (about 1 200 line-pairs/mm), self-processing with optical density increasing approximately linearly with dose over several orders of magnitude (subject to the limitations in the densitometer mentioned above), and recently, availability of large sheets (20 cm $\times$ 25 cm). However, users should be aware of several concerns in this application. These include, but are not limited to, the following:

— variations in the thickness of the sensitive emulsion from sample to sample and within a sample (was up to about 8 % from sample to sample for the older HD-810 and MD-55, but is claimed to be better than 2 % for EBT);

— variations in bulk sensitivity of the emulsion from batch to batch;

— dependence of the optical density on time and temperature;

— non-linearity in most film-densitometry systems, which requires calibration over the entire anticipated measurement range [81].

Former disadvantages such as rather high cost, low sensitivity, and amount of time required have been significantly improved with the introduction of the new EBT film which is about 10 times more sensitive and is 10 times less expensive. The latter was successfully used with a document scanner for dosimetry of $^{106}Ru + {}^{106}Rh$ eye applicators.[166]

Table D.1 — Radiochromic film types

Film type	Layer number	Description	Thickness μm
GAFCHROMIC HD-810	1	Surface [b]	0,75
	2	Active layer (emulsion) [g]	6,5 [a]
	3	Transparent polyester [c]	97
GAFCHROMIC MD-55	1	Transparent polyester [c]	67
	2	Active layer (emulsion) [g]	16 [a]
	3	Adhesive [d]	~ 20
	4	Transparent polyester [c]	25
	5	Adhesive [d]	~ 20
	6	Active layer (emulsion) [g]	16 [a]
	7	Transparent polyester [c]	67
GAFCHROMIC HS	1	Transparent polyester [c]	97
	2	Active layer (emulsion) [g]	38 [a]
	3	Transparent polyester [c]	100
GAFCHROMIC EBT	1	Transparent polyester [c]	97
	2	Active layer (EBT emulsion) [g]	17 [a]
	3	Interlayer [e]	6
	4	Active layer (EBT emulsion) [g]	17 [a]
	5	Transparent polyester [c]	97
GAFCHROMIC RTQA	1	Yellow polyester [c]	97
	2	Adhesive [d]	12
	3	Interlayer [e]	3
	4	Active layer (EBT emulsion) [g]	17 [a]
	5	White polyester [f]	97
GAFCHROMIC XR-R	1	Yellow polyester [c]	97
	2	Adhesive [d]	15
	3	Active layer (XR-R emulsion) [g]	18 [a]
	4	White polyester [f]	97

[a] The thickness of the active layer (emulsion) is adjusted from lot to lot to achieve design sensitivity and can vary by 10 % from the nominal thickness given in the table.

[b] The surface layer has a density of 1,2 g/cm^3 and is composed of 6,5 % H, 32,3 % C, 21,6 % N, 20,5 % O, 2,3 % Li and 16,8 % Cl.

[c] Transparent and yellow polyester have a density of 1,35 g/cm^3 and are composed of 4,2 % H, 62,5 % C and 33,3 % O.

[d] Adhesive has a density of ~ 1,2 g/cm^3 and is composed of 9,4 % H, 65,6 % C and 24,9 % O.

[e] Interlayer has a density of 1,2 g/cm^3 and is composed of 6,5 % H, 32,3 % C, 21,6 % N, 20,5 % O, 2,3 % Li and 16,8 % Cl.

[f] White polyester has a density of 1,6 g/cm^3 and is composed of 3,1 % H, 46,6 % C, 31,7 % O, 3,5 % S and 15,1 % Ba.

[g] Densities and compositions of emulsion, EBT emulsion and XR-R emulsion are given in Table D.2.

D.1.2 Plastic scintillator detector

Water-equivalent organic scintillators, long known as detectors in nuclear physics, have been applied as detector systems for dosimetry of high energy radiation beams by Flühs as well as independently by Beddar, *et al*. [97], [98], [99]. Plastic scintillator dosimetry systems fulfil most of the requirements of a beta radiation detector. Thus, Flühs, *et al*., developed in parallel plastic scintillator dosimeter systems also for clinical dosimetry in beta radiation brachytherapy [82], [83], [100], [101], [102]. The large dynamic range, over more than five orders of magnitude, allows for fast, direct reading, and almost energy-independent clinical dosimetry around high-dose-rate brachytherapy sources. The measurement of a full depth-dose distribution with a step size of 1 mm from the surface of high-dose-rate beta radiation sources down to the background of bremsstrahlung takes only a few minutes with a high spatial resolution of about 0,2 mm and a high precision and reproducibility of better than 2 %. Two- and three-dimensional distributions of absorbed dose to water can be determined by using a multi-channel photomultiplier and electrometer and thus enable dosimetric treatment planning, e.g. for ophthalmic brachytherapy sources [101]. Polyvinyltoluene-based plastic scintillators have useful properties for the relative dosimetry of beta radiation. They are approximately water-equivalent in density (1,032 g/cm^3) and electron density ($N_e = 336 \cdot 10^{27}$/m^3; water, $33 \cdot 10^{27}$/m^3). The collision mass-stopping powers of water and scintillator differ by less than 2 % between 10 keV and 5 MeV (see data in Reference [18]). For electron energies between 10 keV and 4 MeV, the mass-electronic-stopping power in polyvinyltoluene (PVT), the scintillator base material, and water does not differ by more than 1,5 %. All beta radiation sources used in brachytherapy, such as ^{106}Ru + ^{106}Rh, ^{90}Sr + ^{90}Y and ^{32}P, emit electrons in this energy range.

Detectors can be made small in size, typically 1 mm in diameter and 0,2 mm to 1 mm in height (volume $\leqslant$ 1 mm^3), thus providing a reasonable spatial resolution while retaining high sensitivity. The front of the scintillator covered by a 75 µm to 200 µm black glue for the light-tight mounting required allows the positioning of the sensitive volume very close to the source.

Plastic scintillators detect radiation by converting the deposited energy to short-wavelength light. The scintillation light signal is converted to visible light by a wavelength shifter dissolved in the scintillator base material and is then transmitted via (non-scintillating) plastic-fibre light guides to a photomultiplier tube for conversion into an electrical signal. Because the scintillator is connected via a photomultiplier and amplifier to a computer-controlled storage device (typically a multi-channel electrometer), data can be measured in real time and in small fractions of a second. Such a measuring system gives fast access to dosimetric data, especially when arrays of detectors, each with its own photomultiplier cathode, are used.

The scintillator light signal does not depend on the temperature between 15 °C and 25 °C, on normal variations of the atmospheric pressure, or on the direction of radiation incidence. With care, linearity of response can be maintained for dose rates varying by more than five orders of magnitude (0,1 mGy/min to 10 Gy/min).

Since electrons can also produce Čerenkov light in the optical fibre, it is necessary that this background be measured separately by a dual-channel system containing a second optical fibre with a dummy detector [82], [83], [97], [98], [103]. Both, the scintillation light-guide fibre and the background fibre are affixed in a light-tight borehole of the same detector head made of RW3[4)], a water-equivalent material developed for use in beta radiation dosimetry. The sensitivity of the two photomultipliers can be calibrated relative to each other with the Čerenkov signal produced by a beta radiation beam irradiating the scintillator light-guide fibre (not directly in front of the scintillator) and the "background fibre" at the corresponding position, respectively. This procedure allows one to obtain a relative calibration of a different optical length, a different light coupling to the cathode, etc., of the "scintillator" and the "background-fibre".

While much better suited for relative dosimetry, very thin plastic scintillators can be used for absolute dosimetry if calibrated appropriately together with a ^{90}S + ^{90}Y check source. For the absolute calibration in terms of absorbed dose to water, the detector is fixed in a probe structure that allows positioning the sensitive volume of the dosimeter with high precision and in a reproducible way in front of a calibrated ^{90}Sr + ^{90}Y source.

4) White polystyrene material containing 2 % by mass TiO_2.

The dimensions of the scintillator are an important determinant in the energy dependence of the response due to the volume effects described in 7.4 [78]. Thus, scintillator systems used to calibrate beta radiation fields shall be calibrated in reference beta radiation fields of the same type ion in which they are employed.

The relative standard uncertainty of the plastic scintillator detector for relative measurements is about $\pm$ 3 % (subject to current investigations at the PTB). In addition, it is necessary to take the standard uncertainty of the absolute calibration procedure into account.

Precautions of which users should be aware include, but are not limited to, the following.

— The use in fields where there is a significant variation of absorbed dose rate within the volume of the detector leads to errors in the estimation of dose rate at the reference point.

— Changes can occur in the sensitivity with time of the scintillator and/or its associated light guides due to radiation damage and of the light-collection system.

— Changes can occur in the background signal due to ambient light leakage.

D.1.3 Thermoluminescence dosimeters

Thermoluminescent dosimeters (TLD), the most commonly used dosimeters for relative and absolute measurements of absorbed dose from low-energy photon-radiation-emitting sources in brachytherapy [104], [105], [106] are sometimes also used for beta radiation dosimetry. These solid-state dosimeters, when irradiated, populate energy traps with charge carriers (electrons and holes) in numbers proportional to the radiation energy absorbed. When a TLD is heated in a readout device, the traps empty and light is emitted as a result of radiative recombination of charge carriers at a luminescent centre. A photomultiplier converts the light to a current, the integral of which is proportional to the absorbed dose.

Lithium fluoride, LiF (density 2,6 g/cm^3), is the most popular TLD material for brachytherapy dosimetry, because it is the most readily available and has radiation absorption characteristics not too far from that of water [18]. Both solid LiF and LiF powder have been used for measurements. The solid material available from commercial suppliers is typically in the form of rods 6 mm long and 1 mm in diameter, and 3 mm $\times$ 3 mm square wafers of thicknesses 0,1 mm, 0,3 mm or 0,9 mm, and cubes of dimensions 1 mm $\times$ 1 mm $\times$ 1 mm. It is also available in the form of TLD embedded in thin sheets of plastic. LiF in powder form can also be used. It can be prepared in large, pre-annealed batches, from which small, nominally identical samples can be made by using tiny containers like polyethylene capsules.

Thin (less than 25 mg/cm^2) thermoluminescence dosimeters of low-atomic-number materials such as LiF:Mg,Ti; LiF:Mg,Cu,P; $Li_2B_4O_7$:Cu; MgB_4O_7:Dy; or Al_2O_3:C may be used successfully without correction for detector thickness for the calibration of beta radiation fields for all but the lowest energies ($E_{max} < 200$ keV). Other TLDs, such as CaF_2:Dy and $CaSO_4$:Dy (Table D.2) may also be used.

Ultra-thin (about 4 mg/cm^2) thermoluminescence dosimeters (TLDs) of low-atomic-number materials such as LiF may be used successfully without correction for detector thickness for the calibration of beta radiation fields for all but the lowest energies ($E_{max} < 200$ keV) [33]. For the best results, these systems should be calibrated in reference beta radiation fields. However, adequate results can be obtained with absorbed-dose calibrations in high-energy photon beams under conditions of electronic equilibrium. It is possible to use thicker dosimeters without corrections for thickness if they are loaded with an opaque material to effectively limit the light emitted to only that to the dosimeter surface. If thicker dosimeters are used, then it is necessary that an independent means be used to determine the transmission function in the medium of interest in order to correct the dosimeter reading for volume-averaging effects (see 7.4).

It is necessary that each solid dosimeter detector have an individually established calibration coefficient (absorbed dose per unit readout). It is necessary that the dosimeter detectors be carefully identified throughout the calibration and measurement procedures. To be reused, it is necessary that the solid TLDs be annealed between exposures. This process for LiF:Mg,Ti consists of heating at 400 °C for 1 h, then at a lower temperature (about 80 °C) for a day, to empty and reset all traps. For other TLDs, it can be a much simpler treatment, e.g, at 240 °C for 10 min for LiF:Mg,Cu,P. A rapid cooling to room temperature is recommended for the annealing of all LiF-based TLDs [104]. It is necessary that a stable sensitivity factor be demonstrated for

each TLD used and to take care in handling the dosimeters, since physical damage, such as surface abrasions, can alter the calibration. It is necessary to keep reading conditions as reproducible as possible, and to periodically calibrate the reader/dosimeter system.

Usually TLD measurements are made in solid phantoms, where precise geometry can be maintained. Though nominally water-equivalent materials are used, at low energies the materials might not be truly equivalent and corrections, based on Monte Carlo calculations, for example, can be required. It is necessary to make corrections for any perturbing influence caused by the introduction of the TLDs into the phantom. Clever phantom designs insure that closer TLDs do not shield the distant ones. Also, if the dimensions of the TLDs are relatively large compared to the source-dosimeter distance, it is necessary to correct the volume-averaged signal to the value obtained at the dosimeter centre. Careful analysis of measured TLD data should lead to accuracy on the order of 3 % to 4 % for a single dose measurement, with improved precision resulting from multiple measurements.

TLDs combine sensitivity and near water equivalence with small dimensions. The thickness of the dosimeter used is decided from the energy of the beta radiation being measured. For the dosimetry of $^{90}Sr + ^{90}Y$, a beta-ray-source thickness of 1 mm does not pose any limitation and therefore, 1 mm $\times$ 1 mm $\times$ 1 mm cubes of LiF:Mg,Ti offer an acceptable dosimeter if the effective point of measurement can be properly accounted for. For very-low-energy beta-ray sources, it is not necessary to correct thin-film TLDs (less than or equal to 0,1 mm thick), for the thickness. Accurate correction can be made only with a detailed knowledge of the beta radiation spectrum incident on the detector. As an example, measurements in liquid water using a 0,5 mm $\times$ 1 mm $\times$ 1 mm half micro-cube verified the radial dose function for intravascular brachytherapy sources [107].

TLDs suffer from several disadvantages when used for the absolute dosimetry of beta radiation sources. Chief among these is the relatively large size necessary in at least one of the detector dimensions required for mechanical stability and suitable signal output. Most suitable for beta radiation source measurements are very thin (0,1 mm thick) dosimeters, which, however, are usually several millimetres on a side, and hence average the absorbed dose over an area in which the absorbed dose can vary considerably. Other precautions that should be kept in mind include, but are not restricted to, the following:

— variations in sensitivity between individual samples (unlike coated-film dosimeters, these can be accounted for by pre-irradiation and readout to get individual dosimeter-sensitivity corrections);

— supra-linearity of the dose-response function, which requires calibration over the entire anticipated measurement range;

— difficulty of use in water.

D.1.4 Diodes

P-type silicon diodes are widely used for relative dose measurements in external beam therapy. Their small sensitive volume as well the ability to use the detectors in water make them attractive for brachytherapy applications. They have been applied successfully for ophthalmic brachytherapy source measurements, both planar and concave [29], [85], [108]. Properly calibrated Si diodes have been used for absolute measurements as well. Si diodes are commercially available with active diameters of 0,6 mm and active thicknesses of 0,06 mm (for example the Scanditronix stereotactic field detector[5)]). The main disadvantage of diode detectors for brachytherapy measurements is the often rather thick coverings over the detectors, which preclude measurements at very close distances to the source. However, the effective point of measurement of commercially available stereotactic field detector is just (0,7 $\pm$ 0,15) mm (see Figure D.1) making it suitable for contact measurements. It is also necessary to consider the angular response of the diode.

5) The Scanditronix stereotactic field detector is an example of a suitable product available commercially. This information is given for the convenience of users of this International Standard and does not constitute an endorsement by ISO of this product.

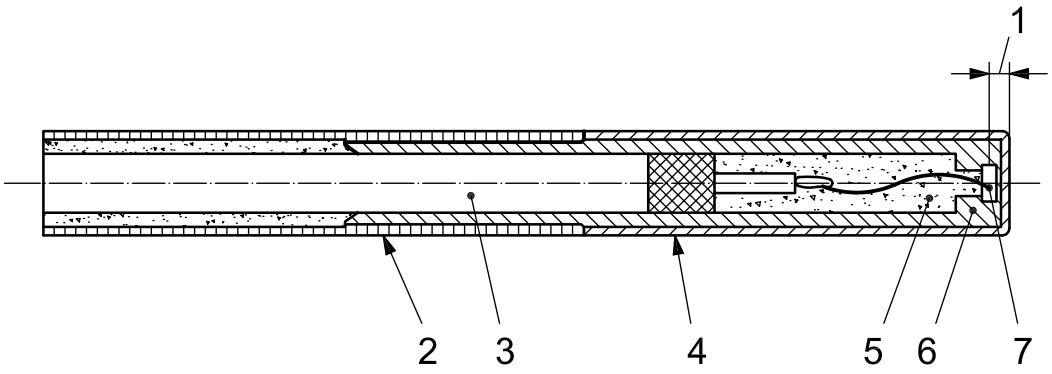

Key

1	effective measuring depth	5	epoxy
2	stem	6	inner shell
3	cable	7	chip
4	outer shell		

Figure D.1 — Scanditronix stereotactic diode

D.1.5 Well ionization chambers

Well chambers have been used for dosimetry and quality-assurance purposes to provide a measurement related to reference absorbed-dose rate to water, traceable to the primary standard for intravascular brachytherapy sources. Their characteristics are the subject of an IEC standard [86].

Well chambers provide a total absorbed-dose to water calibration for the sources in a length configuration. The calibration obtained can be divided by the number of individual sources to obtain an average output per source [109].

D.1.6 Other detectors

Other detectors that have been applied to the dosimetry of beta radiation brachytherapy sources are small-volume ion chambers [29], gel dosimeters [110], [111], diamond detectors [29], and alanine pellet dosimeters [29],[80]. Use of all these detectors is subject to the caveats discussed in 7.2. A good review of the relative merits of these various systems appears in the literature [21]. Of late, optically stimulated luminescence dosimeters based on Al_2O_3:C have been developed to the point that they are now also attractive for beta radiation dosimetry [112], [113].

The composition of typical detector materials is given in Table D.2.

Table D.2 — Composition of typical detector materials

Material	Density g/cm^3	Scaling factor relative to water η	Number of electrons per unit volume $10^{27}/m^3$	Elemental composition % mass fraction				
				H	C	N	O	Others
GAFCHROMIC emulsion	1,08	1,129	418	29,1	56,8	6,9	7,1	—
GAFCHROMIC EBT emulsion	1,1	1,123	423	28,4	56,9	5,7	5,7	1,7 Li; 1,5 Cl
GAFCHROMIC XR-R emulsion	1,75	1,376	823	57,4	28,5	6,6	6,1	0,7 Br; 0,7 Cs
Plastic scintillator (vinyltoluene)	1,032 [a]	0,956	336	8,5	91,5	—	—	—
Silicon	2,33	0,944	699	—	—	—	—	100 Si
Lithium fluoride	2,635	0,827	734	—	—	—	—	26,8 Li; 73,2 F
Calcium fluoride	3,18	0,944	932	—	—	—	—	48,7 F; 51,3 Ca
Calcium sulphate	2,96	0,974	890	—	—	—	47,0	23,6 S; 29,4 Ca
Lithium tetraborate	2,44	0,851	712	—	—	—	66,2	8,2 Li; 25,6 B
Magnesium tetraborate	2,53	0,870	747	—	—	—	62,4	24,1 B; 13,5 Mg
Polymer gel, “BANG-2”	1,03 [a]	0,990	342	10,6	5,7	1,4	81,7	0,6 Na
Alanine	1,424	0,957	462	7,9	40,4	15,7	35,9	—
Aluminium oxide	3,97	0,894	1172	—	—	—	47,1	52,9 Al
Carbon	2,265	0,862	681	—	100	—	—	—

[a] Nominal value; should be verified by the user.

NOTE See Reference [33].

D.2 Phantom materials

D.2.1 General

Table D.3 shows a selection of commonly used materials used as water-equivalent materials for phantom construction. Further information about each material is given in D.2.2 to D.2.7. Spectrographic examination of material is recommended if precise material quantification is necessary.

Table D.3 — Water-equivalent phantom materials

Material	Density [a] g/cm^3	Scaling factor relative to water η	Number of electrons per unit volume $10^{27}/m^3$	Elemental composition % mass fraction				
				H	C	N	O	Others
WT1 (Solid Water™)	1,046	0,957	335	8,0	67,2	2,4	19,9	0,1 Cl; 2,3 Ca
A150 plastic	1,12	0,968	370	10,1	77,7	3,5	5,2	1,7 F; 1,8 Ca
Polystyrene	1,05	0,938	340	7,7	92,3	—	—	—
RW3 polystyrene	1,045	0,998	338	13,9	83,3	—	1,1	2,0 Ti
D400 (carbon loaded polystyrene)	1,160	0,939	375	7,7	92,3	—	—	—
Polyethylene	0,92	0,997	323	14,4	85,6	—	—	—
Polyethylene terephthalate (PET)	1,40	0,919	439	4,2	62,5	—	33,3	—
Polymethyl methacrylate (PMMA)	1,18	0,949	387	8,0	60,0	—	32,0	—
ICRU tissue [b]	1,00	0,985	331	10,1	11,1	2,6	76,2	—
Water	0,998	—	334	11,2	—	—	88,8	—

[a] Except for water and ICRU tissue, these are nominal values and should be verified by the user.

[b] Included for informational purposes only since it doesn't exist as a material.

NOTE See Reference [33].

D.2.2 WT1

The “standard” material used for most in-phantom photon brachytherapy source measurements is “solid water”, also known generically as WT1 [31]. It is a red-brown epoxy resin with polyethylene and some calcium carbonate. Its hardness and ease of machining make it a good choice for phantom construction. There are problems, however, with batch uniformity and with obtaining information on the exact composition of the material. The density is very near that of water making it a good water-equivalent material for beta radiation.

D.2.3 A-150 tissue-equivalent plastic

This material, as its name indicates, is meant to be a tissue equivalent, and thus also has a fair water-equivalence. It is black, a mixture of polyethylene and nylon, with fillers of carbon and calcium fluoride. One advantage for high-dose-rate beta radiation applications is the fact that this material is electrically conductive, which alleviates concerns about charge trapping and resulting distortions in measurements. Although the material has a somewhat higher density than water, it exhibits good water-equivalence for electrons of all energies.

D.2.4 Polystyrene

More commonly available at one time than it is now, clear polystyrene is the best water-equivalent material for beta radiation in the energy range of interest in brachytherapy [114]. The density is near that of water and the stopping powers match those of water over the entire energy range of interest. It is becoming very difficult to find clear polystyrene now.

D.2.5 RW3

This white plastic consists of polystyrene with an addition of 2 % mass fraction TiO_2. It is a good water-equivalent material for beta radiation dosimetry.

D.2.6 Polyethylene terephthalate (PET)

This material is useful mainly because of its availability, the very wide range of foil thickness and the metal coatings that are available. The density is rather high; however, for beta radiation this non-equivalence can largely be accounted for (see 7.3). The metallized foils are commonly used as entrance windows in gas-filled beta radiation detectors. Foils with a thickness as small as 0,000 9 mm make this material extremely valuable in studying depth-dose profiles for weakly penetrating radiations. Sometimes referred to as polyester, it is marketed under the trade names of Mylar, Hostaphan, and many others.

D.2.7 Polymethyl methacrylate (PMMA)

This is the most commonly available clear plastic and is most useful as a bulk material when water-equivalence is not critical, such as to provide backscatter for beta radiation measurements. PMMA is also known by the trade names Lucite, Perspex and Plexiglas. It is very easy to machine with high precision, a quality that offsets its rather high density and electric insulator properties.

D.2.8 D400

This is a carbon-loaded polystyrene that combines electrical conduction with the superior water-equivalence of polystyrene. It has been recently used for collecting electrodes at the primary laboratories in the US and the Netherlands. It has the same atomic composition as polystyrene and is claimed to be precisely polystyrene-equivalent with respect to all types of radiation. It has an electrical resistivity in the range of 0,1 ohm-meter to 1 ohm-meter.

Annex E
(informative)

Monte Carlo calculations

E.1 Review of available codes

E.1.1 General

There are four families of general-purpose Monte Carlo codes commonly used for beta radiation dose calculations: EGS [115], [116], ETRAN/ITS/MCNP [46], [117], [118], [119], [120], PENELOPE [121] and GEANT4 [122]. A recent review of other codes relevant for beta radiation dosimetry, including a number of single-scattering codes, can be found in ICRU Report 56 [33].

Although some Monte Carlo codes are available free of charge, most are licensed software that it is necessary to purchase.

E.1.2 ETRAN, ITS, MCNP

ETRAN (Electron TRANsport) is an electron/photon Monte Carlo transport code maintained at the National Institute of Standards and Technology (NIST), Gaithersburg, Maryland, USA. ETRAN was developed by Berger and Seltzer [46], [123], [124]. It was originally developed for electron transport for up to 100 MeV, with the capability of simulating coupled electron-photon transport.

The ETRAN codes are also the basis for the Integrated TIGER Series (ITS), a system of general-purpose, application-oriented electron/photon transport codes developed by Halbleib, *et al*., [125] at the Sandia National Laboratories, Albuquerque, New Mexico, USA. The current version is ITS v. 3.0 [117]. ITS has several codes, each treating a different geometry:

— TIGER, for multiple-plane slabs;

— CYLTRAN, for geometries with a cylindrical symmetry;

— ACCEPT, which uses 3D combinatorial geometry.

The ETRAN code takes into account primary electrons, positrons or photons, and all secondary radiations, including knock-on electrons from electron-impact ionization events, electron bremsstrahlung, Compton electrons, photoelectrons, electron-positron pairs, annihilation radiation, K-shell characteristic X-radiation, and Auger electrons resulting from electron/photon ionization events. ETRAN capability extends over a wide range of electron energy between 1 keV and 1 GeV in any material. In ITS version 3.0, important changes were made that impacted the accuracy of electron transport of up to a few MeVs. The most important are the use of the revised collision-stopping powers [126], values for water about 2 % smaller than the previous values, improved bremsstrahlung production cross-sections and an improved method of calculating energy-loss straggling [46].

In the ETRAN code family, step path lengths are chosen on two levels. The first level is called the “major step,” where on average the kinetic energy of the electron is reduced by a constant factor of ~ 8,3 %, which is the standard choice [48]. The error associated with the use of a constant energy per step is estimated to be 1 % [122]. The second level is dividing the major step into equal lengths called “sub-steps”. By sampling the angular deflections at the end of each sub-step, the deviation of the mean deflection angle remains small. The net angular deflection from the combined effect of the elastic and inelastic collisions in a given sub-step is sampled from the Goudsmit-Saunderson multiple scattering distribution [127].

Monte Carlo N-Particle code, MCNP is a general-purpose, continuous-energy, generalized-geometry, time-dependent, coupled neutron/photon/electron Monte Carlo transport code, maintained at the Los Alamos National Laboratory, Los Alamos, New Mexico, USA [118], [119]. MCNP, originally developed for neutron transport simulations, has been extended to include electron transport using the algorithms of ITS 3.0. Because of its versatility and user-friendliness, MCNP probably is the most frequently used member of the ETRAN/ITS/MCNP code family today.

Two versions of the MCNP code, developed by different groups, currently exist. MCNP4C [118] is able to simulate the (coupled) transport of neutrons, photons and electrons, whereas MCNPX [119] can simulate a variety of additional particle types. The photon and electron physics in the present version of MCNPX (version 2.5) are identical to those in MCNP4C. Hence, in the following we denote both codes as MCNP. It is noted that the successor of MCNP4C, MCNP5 [120], has been released.

MCNP does not require any programming by the user. In MCNP, the user creates an ASCII input file that has a certain format including the problem geometry (using a variety of available surface types and/or macrobodies such as spheres, boxes and cylinders), the description of materials and selection of cross-section evaluation, the source description (spatial, energy, time, position and directional probability distributions), the type of answers or tallies (e.g. energy deposition) and any variance-reduction techniques used to improve efficiency (such as energy cutoff, cell importance). The simulation results are provided in ASCII output files. Graphical user interfaces, such as VISED [128] are available to generate input files and to visualize the output data. MCNP has internal checks for geometry errors and a plotting capability that provides the user with a tool to correct any geometry errors in the input file.

The MCNP electron library contains data for elements Z equal to 1 to 94. The data contain energies for tabulation, bremsstrahlung production cross-sections, bremsstrahlung energy distributions, X-radiation production probabilities, K-edge energies and fluorescent probabilities, electron-stopping powers and ranges, and parameters for the evaluation of the Goudsmit-Saunderson theory of angular deflections and the Landau-Leisegang theory of energy-loss fluctuations.

Several investigators have shown though that care should be taken with the electron transport in MCNP4C [129], [130], [131]. A systematic error is present in the default MCNP electron energy indexing algorithm. However, the user can choose to use the ITS electron energy indexing algorithm instead, which leads to correct results. An additional problem exists with MCNP4C when the geometry contains many boundaries, e.g. in the case of a voxelized phantom. MCNP4C requires the voxels in such a phantom to be modelled as separate material regions, even if they exist of the same material. It has been shown that in such cases the cumulative effect of many small boundary crossing artefacts can lead to significant errors in the calculated dose distribution [129], [131].

E.1.3 EGS

During the early 1960s, Nagel [132] wrote his Ph.D. thesis at the Rheinischen Friedrich-Wilhelms-Universität in Bonn on electron-photon Monte Carlo. His in-house developed Fortran code SHOWER was a very practical (freeware) tool for experimental physicists during the mid 1960s. Electrons and positrons could be simulated from 1 GeV down to 1,5 MeV, and photons were followed down to 0,25 MeV. The code was limited in geometry handling. From 1972 to 1978, Ford and Nelson from Stanford Linear Accelerator Center (SLAC) collaborated to revamp Nagel's program and make it more user friendly. In addition, special attention was given to allow easy future enhancements. The resulting EGS3 code (Electron Gamma Shower) was introduced in 1978 [133]. Nelson (SLAC) and Hirayama (National Laboratory for High Energy Physics, KEK) extended the flexibility of EGS in general and, in particular, for high-energy accelerators. Rogers and colleagues (National Research Council of Canada, NRC) extended the code to lower energies, i.e. down to 1 keV. These efforts were pooled together in 1985 and EGS4 was introduced [111], [134]. In 1990, PRESTA (Parameter Reduced Electron Stepping Algorithm) was introduced in EGS4 [135], [136], which included, amongst other items, an improved method for determining the electron step size. Other modifications and updates in photon and electron cross-sections and different geometrical packages (Cartesian DOSXYZ, and Cylindrical DOSRZ) have improved the code capabilities.

EGS4 uses the Molière multiple scattering theory, which is only valid for small scattering angles. In 2000, Kawrakow and Rogers released the EGSnrc code [116], [137], which uses an improved multiple scattering theory based on screened Rutherford elastic scattering, new elastic electron-scattering cross-sections involving relativistic and spin effects, and a new electron-step algorithm, the PRESTA-II algorithm. An important improvement of PRESTAII compared to PRESTA is the introduction of a single scattering model of electron transport, making it possible to reduce the electron-step length to very small values near material boundaries. These improvements are expected to increase the calculation accuracy of angular deflections for electrons, eliminate restrictions on the maximum and minimum electron path length in EGS4/PRESTA-I imposed by the Molière theory, and provide an exact boundary-crossing algorithm by using single elastic collisions of electrons.

In EGS, it is necessary that users program their user code in a macro Fortran code called Mortran. Obviously, it is necessary to program only the geometry, source input and tallying. In a pre-compilation step, the user code is then connected to the EGS core.

From a recent benchmark applied to EGSnrc [138], it can be concluded that very accurate modelling of electron transport is possible with this code. Several authors have used EGS4 and EGSnrc to characterize beta radiation brachytherapy source dosimetry [48], [57], [139], [140]. Comparisons among EGSnrc, EGS and MCNP4 for IVB application are discussed by Wang and Li [63].

E.1.4 PENELOPE

PENELOPE (PENetration and Energy LOss of Positrons and Electrons) was developed at Universitat de Barcelona and Institut de Tècniques Energètiques, Universitat Politècnica de Catalunya in Barcelona, Spain, and Universidad Nacional de Córdoba, Argentina [121], [141]. It was first released in 1996. Initially, it was devised to simulate the penetration and energy loss of positrons and electrons in matter. Photons were introduced later. The code simulates the coupled transport of electrons, positrons and photons with energies between a few hundred electron volts and 1 GeV in arbitrary materials. PENELOPE is capable of handling complex geometries and static electromagnetic fields.

Large efforts were made to make the simulation of electron transport as accurate as possible. Especially in the low-energy region, the electron transport algorithms are considered to be very sophisticated. Ideas introduced in PENELOPE have been implemented in EGSnrc and *vice versa*. So it can be expected that these codes provide rather similar results. In PENELOPE, a mixed scheme of single and multiple scattering is used, comparable to EGSnrc. The multiple scattering algorithms are based on the Goudsmit-Saunderson theory. In the PENELOPE implementation of multiple scattering, the angular deflection and the lateral displacement for each electron step are accounted for using the so-called random hinge method, which is a simple and fast method for obtaining an accurate geometric representation of the electron track.

It is necessary that the application be programmed by the user in Fortran, although several user codes are available in the system.

A benchmark of PENELOPE against experiments has recently been published by Sempau, *et al.*, [142] showing that PENELOPE yields a consistent description of electron transport processes in the energy range from a few thousand electron volts up to about 1 GeV.

E.1.5 GEANT/GATE

The first version of GEANT (GEometry ANd Tracking) was written in 1974 as a bare framework, which initially emphasized tracking of a few particles per event through relatively simple detectors. The code was developed as a simulation tool for high-energy physics experiments. From 1993 to 1998, the FORTRAN-based GEANT3 simulation program was entirely redesigned as an object-oriented program written in C++, designated GEANT4 [122]. This code is a collaboration of many international research groups under supervision of CERN (European Organization for Nuclear Research; in French: Conseil Européen pour la Recherche Nucléaire).

GEANT4 is a very versatile code, useful for many different types of particle over a wide range of energies and capable of handling complex geometries, electromagnetic fields, (electronic) detector responses, etc., and time-dependent (4D) modelling of, for example, decaying particles and/or moving objects. A variety of visualization tools is provided, as well as connectivity to data-analysis software and computer-aided design

(CAD) programs (for geometry input). It is necessary that the user provide a set of C++ objects that are built upon the Monte Carlo core of the program in an object-oriented approach. Although GEANT was originally developed for high-energy physics, GEANT4 includes a low-energy electromagnetic physics package [122]. Very recently, an implementation of the PENELOPE electromagnetic physics has also been added to the code.

GEANT4 has recently found use in a variety of medical physics applications [143], [144]. A benchmark of GEANT4 electron and photon transport against other Monte Carlo codes and measurements has recently been published by Carrier, *et al*. [145]. This study shows good agreement for photons and fair agreement for electrons, although some non-negligible differences, for example, with EGSnrc, were found. A recent application of GEANT4 to calculate the dose distribution about an intravascular beta radiation source similarly shows non-negligible differences between GEANT4 and PENELOPE [75]. Although GEANT4 has not yet been validated for medical physics applications to the same extent as, for example, EGS and MCNP, the ongoing development and improvement of the code (new versions are released on a regular basis) make it likely that the role of GEANT4 in medical physics will become more important in the near future.

In this context, it is interesting to note that the OpenGATE collaboration has recently released the first version of GATE (GEANT4 Application for Tomographic Emission), a modular, scripted, GEANT4-based Monte Carlo code, which, in contrast with GEANT4 itself, does not require the user to be familiar with C++ [146]. Although this code was developed primarily for nuclear medicine applications (modelling of PET and SPECT scanners), extensions into other domains such as radiotherapy and dosimetry are currently being developed.

E.2 Modelling of electron transport

The physical processes being modelled when simulating the transport of electrons through matter are elastic scattering by (screened) atomic nuclei, inelastic collisions with atomic electrons causing either excitation or ionization, Bremsstrahlung production and the emission of X-radiation and Auger electrons following electron-impact ionization. Nuclear processes that occur only at high electron energies are often neglected. Positrons are sometimes simply modelled as electrons with the addition that annihilation photons are created when the particle comes to rest. More elaborate models use separate positron cross-section tables and include rare positron decay processes, such as in-flight annihilation and three-photon annihilation.

An important difference between the Monte Carlo modelling of the transport of charged particles, such as electrons, and uncharged particles, such as photons, lies in the fact that uncharged particles undergo a relatively small number of discrete interactions per particle track, whereas charged particles undergo a very large number of Coulomb interactions with the electrons and atomic nuclei in the material along their path.

In a Monte Carlo simulation of, for example, photon transport, the distance to the next photon interaction is sampled using the appropriate attenuation coefficient and the type of interaction is sampled from the appropriate relative probabilities. The history of each photon is continued from interaction to interaction until the photon is either absorbed or escapes the problem boundary, or its energy falls below a chosen cut-off energy at which the remaining energy of the photon is locally deposited [50].

It is possible to adopt a similar approach for electrons. Monte Carlo codes in which this is done are commonly referred to as single-scattering codes. However, for electrons with an initial energy above, say, 100 keV, simulating each individual Coulomb interaction is computationally very expensive. In addition, whereas rather complete and accurate cross-sections are available, a single-scattering treatment requires more detailed information than is generally known on the differential electron-atom inelastic-scattering cross-sections [47]. For these reasons, single-scattering models are not normally applied in general-purpose Monte Carlo codes. Instead, a so-called condensed-history approach is usually applied. In such a model, each electron track is subdivided into a series of track segments, usually called “steps”. Instead of modelling the individual elastic and inelastic collisions along each step, a so-called multiple-scattering algorithm is used to sample the net (cumulative) energy loss and angular deflection once per step only. A detailed discussion of the condensed-history Monte Carlo technique, including a rather complete overview of the various multiple-scattering theories, can be found in the classic work by Berger [49], which is still remarkably up-to-date. Some important aspects of condensed-history electron transport modelling are briefly discussed in Clause E.4, including a discussion of potential problems and pitfalls.

E.3 Important considerations in Monte Carlo beta radiation dose simulations

In any form of radiotherapy, to minimize the overall uncertainty in the dose delivered to the patient, it is crucial to know with a sufficiently low uncertainty the dose distribution delivered by the radiation source to water. In cases where Monte Carlo methods are applied to determine this dose distribution, it is very important to realize that, similar to a measurement, the uncertainty in the result of any Monte Carlo simulation is comprised of several components of uncertainty, which can be classified into two categories: components of uncertainty evaluated by statistical methods (type A evaluation) and components of uncertainty evaluated by other than statistical means (type B evaluation). Therefore, when performing a Monte Carlo dose calculation, it is necessary to consider and quantify both categories of uncertainty components. Since the means to do so are very different for the two categories, they are discussed separately in the following paragraphs.

The result of any Monte Carlo simulation represents the mean of the contributions from a large number of histories. This mean is associated with a standard deviation (determined by a type A evaluation) that depends on the number of histories, N, and is approximately proportional to $1/\sqrt{N}$. The number of histories should, therefore, be chosen large enough to decrease this uncertainty to a sufficiently low level. It is convenient to define a figure of merit, FOM, equal to $1/\sigma^2 t$ [147] where σ is the standard deviation and t is the computation time. A more efficient run has a larger FOM because less computer run time is required to reach a given value of σ. The FOM is expected to stay constant with N because σ^2 is proportional to $1/N$ and t is proportional to N.

It is important to realize that the number of histories, in itself, is not at all indicative of the quality of the result. First, the FOM and, therefore, the number of histories required to decrease the standard deviation to a given level, can be very different for different problems. Second, adequate application of variance-reduction techniques can dramatically increase the FOM (although it is necessary to take care that this does not introduce systematic errors as is discussed further below).

Fortunately, many codes provide an estimate of the standard deviation, σ, together with the mean of the quantity of interest. Of course, this estimate of σ should always be reported as a part of the result. However, it is important to realize that this number is only an estimate of the standard deviation. It is quite possible for this estimate to be significantly too low at a given number of N, a situation called false convergence. One can experience, in such cases, that the estimate of σ suddenly rises when additional histories are being run. For this reason, some codes provide a number of checks to assess the reliability of the estimated standard deviation. First of all, the estimate of the relative standard deviation should be sufficiently low for it to be reliable (e.g. below 5 % or 10 %, depending on the type of scoring method). Furthermore, it is, for example, possible to monitor whether σ indeed decreases inversely proportional to $\sqrt{N}$, in other words, whether the FOM remains constant with N. A sudden sharp decrease in the FOM indicates that a rarely sampled radiation path has significantly affected the tally mean and standard deviation. In that case, the user should redefine the model to sample that rare path more frequently (e.g. using variance-reduction methods), or increase N to a point where the rare path has been sampled sufficiently often. Discussions of these, and several other means to check the quality of the end result can, for example, be found in Reference [147].

Besides the standard deviation associated with the mean of the quantity of interest, all other factors that can lead to significant additional components of uncertainty should be assessed and quantified. These components of uncertainty are, in most cases, determined via a type B evaluation. With the computer power available today, it is often possible, not to say tempting, to decrease the estimated relative standard deviation in Monte Carlo dose calculations to a very low level, e.g. below 1 %. In such cases, it is very well possible that the standard deviation, σ, is a very poor indicator of the quality of the result as the overall uncertainty is, in fact, dominated by other components of the uncertainty. A careful assessment of such other components of uncertainty is, therefore, of utmost importance. They can be introduced at the level of the interaction data libraries, the code and the modelling of the problem, topics that are discussed one by one in the following paragraphs.

The accuracy of any radiation-transport calculation depends critically on the accuracy of the input data, of which the radiation interaction data form an important part. Fortunately, the ongoing evaluation of interaction data libraries is expected to lead to a gradual decrease of the associated uncertainties with time. The uncertainty in current compilations of electron interaction data varies depending on the energy range and element as can be illustrated by the estimated uncertainties stated in the ICRU Report 37 [126]. The uncertainties in collision-stopping powers are estimated to be 1 % to 2 % for electrons with energies above 100 keV. Between 10 keV and 100 keV, they are estimated to be 2 % to 3 % for low-Z materials and 5 % to 10 % for high-Z materials. The uncertainties of radiative-stopping powers are estimated to be 5 % below

2 MeV, 2 % to 5 % between 2 MeV and 50 MeV and 2 % above 50 MeV. These uncertainties are considered to be approximately at the level of two standard deviations and of type B [148].

For current compilations of photon interaction data, the estimated uncertainty in the total attenuation coefficient of low-Z materials equals about 5 % between 1 keV and 5 keV, about 2 % between 5 keV and ~ 20 keV, about 1 % for ~ 20 keV to ~ 10 MeV, above which it falls to about 0,5 % at ~ 30 MeV [148], [149]. Although there are no clear statements on how to interpret these uncertainties, it seems reasonable to assume that they correspond to a confidence limit of 95 % (approximately two standard deviations) and are of type B [148].

Although the uncertainties in the cross-sections give rise to uncertainties in the end result of any calculation, it is necessary to note that the relationship between these uncertainties is not simple. It is, for example, possible for errors to (partly) cancel each other out in a simulation involving many particles of different energies moving along different paths. In this context, it is worthwhile to note that, for example, measured dose distributions from electron beams in water are very well reproduced by Monte Carlo results obtained with recent codes and cross-section libraries [150].

Components of uncertainty can also arise at the level of the code itself. Potential sources of uncertainty may include, but are not limited to, limitations of the mathematical models used to simulate the radiation transport physics (see, for example, the discussion on possible artefacts in electron transport simulations in Clause E.4), the quality of the representation of the radiation interaction data and the sampling thereof (including e.g. interpolation schemes), the quality of the random number generator, coding errors (bugs), etc. In general, it can be said that the ongoing validation and continuous improvement of codes (especially the well-known general-purpose codes) tends to decrease these uncertainties. However, it is necessary to note that each new release of a code can contain new errors and bugs. Furthermore, the use of these codes in different and/or novel areas of application can reveal previously unknown shortcomings. Therefore, there remains the necessity to benchmark Monte Carlo codes and particular code versions carefully, and to develop, maintain and improve appropriate benchmarks for each area of application.

A third, rather common, and often important class of uncertainty components, is found in the actual modelling of the problem by the user. Very often, not all parameters of the source, the problem geometry and the materials are known exactly. For example, there can exist uncertainties in the angular and energy distributions of the radiation emitted by the source. If the source is a radioactive source, the angular distribution is known to be isotropic, but uncertainties can arise from non-uniformities in the spatial distribution of the radioactivity and/or from contaminant radionuclides that can be present in any real source. Similarly, there can exist uncertainties in the dimensions of the source and problem geometry. The same applies to the chemical compositions and mass densities of the materials in the problem. Manufacturing tolerances in the dimensions and material properties of the source capsule, for example, can lead to significant uncertainties if self-absorption of the emitted radiation in the capsule is important, as is often the case for beta radiation sources. It is, therefore, important that source manufacturers provide complete and accurate data regarding the construction of their sources, including tolerances on the source dimensions and material properties.

In addition to uncertainties stemming from the use of ideal geometry and compositions, uncertainties also arise when the user has the ability to modify or influence the modelling of the radiation interaction physics. A common issue in Monte Carlo radiation-transport simulations is the proper setting of energy (or other) cut-offs for particle transport and/or secondary particle production. In case of electron transport simulations, for example, using a higher cut-off energy can greatly increase the speed of a simulation, but this can influence the results unless charged-particle equilibrium (CPE) can be assumed for electrons with energies below the cut-off energy. Another general issue is the use of variance-reduction techniques, which can also speed up a problem but which tend to modify the modelling of the transport physics and can, therefore, introduce a bias in the results if not used cautiously. A physics modelling issue of particular interest for clinical beta radiation dose simulations is the proper setting of the various parameters required by the condensed-history electron transport algorithms, such as those related to the electron (sub)step size. Some background information on the condensed-history approach is provided in Clause E.4, including a discussion of potential problems and pitfalls.

Another interesting issue, especially in cases where the dose gradients are steep, is the choice of the voxel size when a grid (or mesh) of scoring voxels is used to track the energy deposited by particles. On one hand, the voxel size influences the standard deviation in the calculated dose; in very small voxels, relatively few energy deposition events are scored, resulting in a larger standard deviation. On the other hand, when the

voxels are very big, large dose variations can occur over the voxel volume. In these circumstances, it becomes difficult to define the “effective point of measurement” (see 7.4), since only the average dose in the voxel is known. Also, it becomes difficult to derive the results at intermediate positions because of interpolation problems. For these reasons, the voxels should be kept small enough that the dose can be considered reasonably constant over the voxel volume. For typical clinical beta radiation sources, the dose gradients can be of the order of 10 % per 0,1 mm, which means that the voxels should have dimensions of the same order of magnitude.

It is clear from the above discussion that the user carries a large part of the responsibility for obtaining accurate results. Of course, the user should know the code well. The manual and other documentation provided with the code, as well as the scientific literature, can be considered indispensable in this respect. The proper installation and operation of the code and data libraries can be verified via benchmarks. Furthermore, the user can try to reproduce the results of published work in the same or similar field, which can also be a good exercise to become more familiar with the code. The user should model the problem very meticulously, defining the geometry and materials accurately, using proper energy cut-offs and other transport parameters, making sure to simulate all relevant particle types, cautiously using variance-reduction, avoiding boundary-crossing and/or step-size artefacts, etc.

The user should also thoroughly assess the uncertainty associated with the result, including not only the standard deviation that many codes provide automatically with the calculated mean, but also all other relevant components of uncertainty as discussed above. Fortunately, many components of uncertainty can be estimated in a relatively straightforward way. For example, the uncertainty due to dimensional manufacturing tolerances can be assessed by means of a sensitivity analysis in which the relevant dimensions are varied between the minimum and maximum values specified on the technical drawings. Similarly, the influence of uncertainties in materials properties, source emission properties, etc., can be evaluated. In the case of variance-reduction techniques, one can vary one or more of the associated parameters to investigate whether there are indications of bias.

E.4 Condensed-history electron transport simulation

For the reasons given in Clause E.2, a so-called condensed-history approach is often used to model the transport of charged particles such as electrons through matter. In such a model, each electron track is subdivided into a series of track segments, usually called “steps”. Instead of modelling the individual elastic and inelastic collisions along each step, the net (cumulative) energy loss and angular deflection are sampled only once per step. The sampling of angular deflection may be based on a so-called multiple-scattering formalism. One example is the implementation, in EGS4, of the theory by Molière [151]. The Molière distribution is a universal function of a scaled angular variable, which makes it relatively easy to sample the angular deflection for arbitrary step lengths during a run. A disadvantage of this theory is that it is based on a small-angle approximation, so large-angle deflections are modelled less accurately. Another multiple-scattering theory, the Goudsmit-Saunderson formalism [126], is valid for all scattering angles. However, sampling the angular deflection for arbitrary step lengths during a run is less straightforward, so codes based on this theory, such as ETRAN, ITS and MCNP, usually sample the deflection angle from stored multiple-scattering distributions that have been calculated for a pre-selected set of path lengths during the initiation phase of the run [152].

The sampling of electron energy loss may be done in different ways. A distinction is commonly made between so-called class I and class II algorithms [49], [53], [153]; see Figure E.1.

In a class I code, the primary electron is not directly affected by the generation of a secondary electron. Instead, energy straggling (i.e., the fluctuation in electron energy due to differences in the energy lost by different electrons of equal initial energy traversing the same path length) due to the creation of secondary electrons is taken into account explicitly in the algorithm used to sample the energy loss for each electron step. Examples of such codes are ETRAN and MCNP, in which the energy loss is sampled from the Landau straggling distribution [154]. An advantage of this approach is that energy straggling is always modelled accurately, even if a high-energy threshold for knock-on production is applied. This can greatly speed up a simulation if the transport of low-energy secondary electrons is not important. A disadvantage of the class I approach is the possibility for negative energy loss events in small voxels. Such events can occur if the energy carried out of a voxel by a secondary electron created within it is larger than the amount of energy deposited in the voxel by the primary (and secondary) electron.

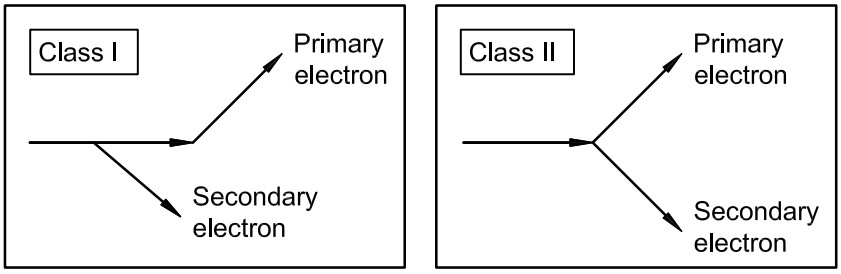

Figure E.1 — Sampling of electron energy loss based on class I and II algorithms

In a class II code such as EGS, the energy loss and angular deflection of the primary electron are directly affected by the generation of the secondary electron. The main advantage of this approach is that the creation of knock-on electrons is simulated in a way that is analogous to reality. This can be important in some cases. For example, when simulating the passage of electrons through a thin foil, the energy of the small fraction of electrons that have been scattered to large angles by a knock-on collision is much lower than their initial energy, as the remainder has been transferred to the secondary electron. A disadvantage of the class II approach is that the accuracy of the simulation of energy straggling depends on the cut-off energy for knock-on production. Since the number of knock-ons being simulated increases quickly when this cut-off energy is decreased, long computation times can be required in cases where energy straggling due to low-energy secondary-electron creation is important.

It is noted that the same distinction between class I and class II algorithms can be applied to the creation of Bremsstrahlung photons. However, most codes, including EGS, ETRAN and MCNP, use a class II algorithm for sampling radiative energy losses.

Some codes allow the user to switch off the sampling of energy loss and to use instead the expectation value of the energy loss per unit path length (i.e., the stopping power) to calculate the energy loss per electron step. This is called the continuously slowing-down-approximation (CSDA). In cases where the effect of energy straggling is not important, for example because it is small compared to the influence of path-length straggling (i.e., the fluctuation in electron energy due to differences in the total path length travelled by different electrons of equal initial energy traversing the same thickness of material), a simulation can be speeded up greatly by using the CSDA.

An important parameter in any condensed-history model is the electron-step size. On one hand, it is necessary that the step size be large enough so that a sufficiently large number of Coulomb interactions occur within each step for the applied multiple-scattering- and energy-loss-models to remain valid. On the other hand, it is necessary that the step size be small enough so that any errors due to the approximation of the curved electron track by a series of straight line segments remain negligible. In addition, it is necessary that the fractional energy loss per step remain small since multiple-scattering algorithms are usually based on the assumption that the electron energy remains constant during a step.

Some Monte Carlo codes apply a path-length correction to each simulated (straight) electron step to correct for the difference with the corresponding (curved) segment of the “true” electron track. Similarly, one may apply a correction for the lateral displacement that occurs during each electron step. EGS4 and EGSnrc, for example, offer such corrections through the PRESTA (Parameter Reduced Electron Stepping Algorithm [136] and PRESTAII [155] algorithms, respectively. Such algorithms allow the use of fewer, larger electron steps, increasing the speed of the simulation without compromising the accuracy of a simulation.

With any condensed-history approach, one can encounter problems in very small material regions. When the electron-step size becomes comparable to or larger than one or more of the dimensions of the region of interest (e.g. a small, gas-filled ionization chamber), the electron tracks within the region of interest are no longer accurately modelled and so-called step-size artefacts can occur. In such cases, one can try to solve the problem by reducing the electron-step size, as is indeed possible with some codes. Since reducing the step size slows down the calculation, it is preferable to reduce the step size only in the region(s) where the artefacts can be expected. In any case, however, it is necessary to be cautious to not reduce the electron-step size below the point where the underlying multiple-scattering theory ceases to be valid. As an example, in

MCNP, the electron tracks are subdivided into so-called major steps with pre-selected path lengths corresponding to an average energy loss of ~ 8,3 % [118]. These steps are further subdivided into an integer number of sub-steps. The energy loss is sampled at the level of the major steps, the length of which cannot be changed by the user. Angular deflections are sampled for each sub-step to increase the geometric accuracy of the simulated electron track. The user can adjust the number of sub-steps per major step, to increase the accuracy of the simulation in thin-material regions. An average of at least 10 sub-steps per electron track crossing a material region is recommended [118].

Yet another problem lies in the crossing of material boundaries, as the applicability of the multiple-scattering theories commonly used in Monte Carlo codes is limited to electron steps that occur within a single material. In some codes, an electron step crossing a material boundary is simply terminated at the boundary and a new step is begun at the same point. To improve the accuracy of the simulation in geometries involving many boundaries, some of the codes that use pre-selected step lengths apply a correction to the sampled energy loss and angular deflection for the interrupted step, to account for the fact that the length of this step is less than the length anticipated at the beginning of the step [51].

If the code uses arbitrary step lengths, one can gradually reduce the step length when an electron approaches a boundary. (Of course, for the electron to be able to cross the boundary eventually, it is necessary to halt the reduction of the step length at some finite minimum value that can, for example, be based on the minimum path length constraints of the multiple-scattering algorithm being used.) After the boundary has been crossed, the step size is again gradually increased as the electron moves away from the boundary. In this way, the number of interrupted steps as a fraction of the total number of steps can be minimized, improving the accuracy of the simulation at the expense of an increase in computing time. It is necessary to note that this approach may also be used to avoid step-size artefacts in geometries involving very small material regions. This type of boundary-crossing algorithm has, for example, been implemented in the PRESTA algorithm. It has been shown, however, that PRESTA still might not be adequate when simulating the dose deposited in a small air cavity or in the neighbourhood of high-Z interfaces. This leads to the introduction of PRESTA-II [155], which allows the user to revert to a single-scattering model in the close neighbourhood of boundaries, thereby reducing the minimum path length to very small values. This appears to resolve the problems observed in the above-described circumstances. Another interesting solution to the boundary-crossing problem is provided by the random-hinge method implemented in PENELOPE. It is claimed that this algorithm, although it handles interface crossing in a relatively simple (and therefore fast) way, gives rather accurate results [121].

Annex F
(informative)

Treatment planning

F.1 Treatment planning for ophthalmic brachytherapy

F.1.1 General

Treatment planning of ophthalmic malignancies can be based on the general principles employed in radiation therapy. ICRU Reports 50 [156] and 62 [157] define the standard volumes for external photon-beam therapy, most of which can be applied for any case of radiation therapy. In intraocular malignancies, the gross tumour volume (GTV) is the tumour observed, documented and photographed by the ophthalmologist using direct and indirect ophthalmoscopy, followed by ultrasound, fluorescence angiography, computed tomography (CT) or magnetic resonance imaging (MRI). An extensive review of these techniques is given by Chiu-Tsao [158]. The fundus photographs taken during ophthalmoscopy can give a good estimate of the tumour basal diameter if the tumour is located posteriorly by comparison with the diameter of the optic disc, since the latter is usually close to 1,5 mm [158]. If the tumour is located anteriorly, it is not easy to determine the dimensions. Ultrasound A-scans and B-scans are widely used for tumour visualization and measurements. The ultrasound A-scan is a one-dimensional scan that identifies the acoustic interfaces between different tissue layers. A series of ultrasound A-scans can accurately measure the thickness of the tumour (apical height), while ultrasound B-scans, even though less precise, can produce two-dimensional images of the tumour in various planes and are widely used for this purpose. The expected introduction of 3D ultrasound scanners can provide a new way of imaging intraocular malignancies. CT produces high-resolution images of the tumour and its surroundings within the eye, and demonstrates possible invasion outside the globe as well. High-quality 3D images can be reconstructed from axial or volumetric scans of the latest generation multi-slice CT scanners, which have sub-millimetre slice thicknesses. MRI imaging delivers comparable high-quality images. Using CT and MRI the physician can evaluate the applicability of eye-applicator therapy in each particular case, and precisely measure the tumour dimensions, as well as the distances to critical organs. The CT and MRI images can be imported into treatment planning systems for 3D planning.

For the clinical target volume (CTV), certain authors recommend the addition of a margin of about 1 mm in all lateral directions [9], [18], but not to the tumour apex, defining the CTV's thickness as the apical thickness of the GTV with an addition of 1 mm for the sclera. Chiu-Tsao [158] suggests using a 2 mm to 3 mm lateral margin through the selection of an applicator which would be 4 mm to 6 mm larger than the largest basal tumour diameter. With regards to the tumour thickness, the Collaborative Ocular Melanoma Study (COMS) [158] uses the apical height as the prescription point for tumours with thicknesses over 5 mm from the interior sclera similar to the approach by Pötter and Van Limbergen [9], [18]. On the other hand, COMS prescribes to 5 mm if the tumour height is under this number. Similar principles for $^{106}Ru + {}^{106}Rh$ applicators are used in some institutions for uveal melanomas as well as retinoblastomas. Effectively that means not only adding a margin to the tumour apical height but also increasing the lateral coverage in all directions, because all parts of the tumour will be covered by a higher isodose surface. The planning target volume (PTV) includes additional margins for placement uncertainties.

Treatment planning decisions should include doses to organs at risk or critical organs that, in case of the eye, are the optic nerve and optic disk, macula, lens, retina and sclera. The scleral dose is always higher than doses to other parts of the eye because it is adjacent to the ophthalmic brachytherapy source. Even though the sclera can tolerate relatively high doses [9], [159], it should be closely monitored. The dose to the sclera is the limiting factor in the use of $^{106}Ru + {}^{106}Rh$ applicators for treatment of tumours higher than 5 mm to 6 mm, because the rapid dose fall-off would result in an unacceptable scleral dose for a larger tumour height.

Ideally, the treatment planning of episcleral eye applicators should employ the standard radiation therapy principle of covering the PTV by the minimum prescribed dose (MPD) in the most conformal way possible. While the MPD deals with the local control of the tumour, the conformality helps to keep the doses to the

critical structures of the eye at an acceptable level. Due to the rapid dose fall-off, $^{106}Ru + ^{106}Rh$ eye applicators offer more conformal dose distributions than eye applicators utilizing other nuclides, such as ^{125}I; but the treatment planning is, accordingly, more complex. In clinical practice, the dose is usually prescribed to the tumour apex for larger tumours (over 5 mm apical height from the inner sclera) or to some point above the tumour apex for smaller tumours. Some institutions prescribe the dose to the tumour apex, simultaneously adding a constraint of a certain minimal dose to the centre of the tumour base, while other institutions use the tumour base as the main prescription point, accepting the resulting dose at the tumour apex. Therefore, the MPD covering the tumour is a direct result of the way in which the dose prescription is implemented.

The local control rate in radiation therapy strongly depends on delivering a certain minimal dose to the tumour. Messmer, *et al*., [160] report that a 20 % decrease in the external beam radiation dose used for primary treatment of retinoblastoma results in an increase in local failures observed within 26 months after radiation therapy from 22 % to 49 %. On the other hand Hermann, *et al*., [161] conclude that for melanomas treated by ophthalmic brachytherapy sources there are no significant differences in the range of 100 Gy to 160 Gy.

Until May 2002, $^{106}Ru + ^{106}Rh$ eye applicators were delivered by the only manufacturer (BEBIG) with the absolute absorbed dose rate calibration based on the primary standard of the national laboratory of the former German Democratic Republic. The measurements were carried out with a 2 mm diameter by 2 mm thick plastic scintillator and the stated uncertainty was $\pm$ 30 %. A number of authors [108], [162], [163], [164] found differences with the manufacturer's stated values reaching up to 110 % on the central axis for the smallest source types. In addition, the off-axis dose distributions showed significant asymmetries of 20 % to 50 % [108], [163], [164], [165], which result in clinically significant hot or cold spots in the tumour coverage. The examination of these discrepancies showed the decisive importance of adequate detector parameters in connection with a resolution-dependent calibration transfer from a primary standard to the points of interest in the near-field of concave sources.

In May 2002, BEBIG started delivering the applicators with calibrations traceable to the U.S. National Institute of Standards and Technology (NIST) with dosimetric data measured using a 1 mm diameter by 0,5 mm thick plastic scintillator. The stated uncertainty has changed to $\pm$ 20 %. A number of eye applicators tested in 2004 to 2006 [166] using radiochromic film demonstrated homogenous dose distributions in the planes perpendicular to the central axis of the applicator, as well as good agreement with the manufacturer’s data. Simultaneously with changing the dosimetry, BEBIG published recommendations suggesting changes to the prescribed doses in the form of multiplication factors based on ratios of the former to the new NIST-based dosimetry.

It is recommended here to understand clearly the original source of the prescription protocol prior to applying any changes, because certain institutions that can have been sources of the original prescription protocols can have based them on precise in-house dosimetry, so these do not require any change. On the other hand, even institutions that used the dosimetric data supplied by BEBIG prior to 2002 should approach this issue with great care due to the large uncertainty found in the old data. This uncertainty can be the reason for the conclusion by Hermann, *et al*., [161] that it is not yet clear what the optimal prescription doses for $^{106}Ru + ^{106}Rh$ eye applicators are, because a comparison of various studies showed that increasing apical doses did not affect treatment outcomes. It is the recommendation of this International Standard to base treatment decisions on precise dosimetric data, which should be either measured in-house as part of the eye-applicator acceptance and commissioning procedure or supplied by the manufacturer, but verified in-house (see 11.1). The treatment outcomes, combined with accurate dosimetry, help to refine existing prescription protocols and create new ones for situations in which the radiation treatment is combined with other techniques like transpupillary thermotherapy. This International Standard is not recommending specific prescription doses, because they depend on each particular case in the sense of the exact tumour location, dimensions, proximity to critical structures, tumour stage and other relevant factors. Proper delivery of the treatment, including the prescription and definitions of the CTV and PTV in each particular case, therefore, remains the responsibility of the radiation oncologist, while accurate dosimetry is the responsibility of the medical physicist of the institution.

It should be mentioned prior to discussing treatment planning options that at present there are no commercially available treatment planning programs for ophthalmic brachytherapy sources. All treatment planning in the various institutions uses either in-house written programs or manual calculations.

F.1.2 One-dimensional and two-dimensional treatment planning

In many institutions, treatment planning is still based on fundus photographs and two-dimensional ultrasound due either to existing treatment paradigms or to the higher cost involved in CT and MRI. Another factor is the inability of most of the eye-applicator treatment-planning software to deal with large 3D data sets produced by CT and MRI. In these situations, the treatment planning is usually based on the depth-dose curve only (dose distribution along the central axis of the applicator starting at the applicator's surface). The centre of the applicator is assumed to be at the centre of the tumour base, tightly attached to the outer sclera. One-dimensional treatment planning consists only of a calculation of the time necessary to keep the applicator attached to the eye in order to deliver the dose to the prescription point (apex or other point), to the centre of the tumour base (inner scleral surface) and to the outer scleral surface, which is assumed to be 1 mm from the inner sclera. The latter dose is used either to confirm that the sclera is not being overdosed or, sometimes, as the prescription point.

$^{106}Ru + {}^{106}Rh$ eye applicators can demonstrate off-axis dose asymmetries as mentioned above. Two-dimensional treatment planning provides a method of accounting for the dose inhomogeneity in order not to underdose the tumour in case of cold spots or not to overdose critical structures in the case of hot spots. This method [108],[166] can reduce a 3D set of dosimetric data to a 2D set. The 3D data set usually consists of dose distributions in planes perpendicular to the central axis of the applicator. For each plane, it is possible to calculate the minimum and maximum doses for each radial distance from the central axis of the applicator. The resulting data can be arranged in the plane that includes the central axis of the applicator in the form of minimal and maximal isodose lines. These can be superimposed on the 2D ultrasound image of the tumour for verification of the coverage and doses to the points of interest. While the treatment duration is still calculated the same way as in the one-dimensional technique, the two-dimensional method enables selection of the optimal applicator based on tumour coverage by the minimal prescribed dose, as well as modification of the prescription to avoid overdosing the structures at risk. A 2D software program incorporating this algorithm has been written at Memorial Sloan-Kettering Cancer Center [108].

F.1.3 Three-dimensional treatment planning

The availability of 3D anatomical data from CT or MRI, combined with appropriate software, permits full 3D treatment planning based on the PTV and dose-volume histograms (DVH). A commercially available vizualization program (not intended for treatment planning) called the "Plaque Simulator"[6)] has been developed by Astrahan [167], which, while not really 3D for representing the tumour since the tumour is only modelled from reference data, can be used to visualize the dose to the tumour and organs at risk in 3D. In the case of $^{106}Ru + {}^{106}Rh$ applicators, the program uses a "patch source" model for calculating the dose at any point. The patch source is a macroscopic disk area of the applicator and the active area of the applicator is approximated by 300 to 1 000 overlapping patches [167]. Dose calculations are then done using dose superpositioning as is done in AAPM TG 43 [22] and AAPM TG 60 [24]. The model uses as input the data provided by BEBIG in the form of plastic scintillator measurements at 33 points 1 mm from the surface of the applicator as well as at the depth dose profile.

F.1.4 Selection and placement of the eye applicators

Due to the steep lateral dose fall-off, the correct applicator placement, including sufficient safety margins, significantly contributes to therapy success. A deviation of 1 mm in the edge region, for instance, decreases the dose applied by a $^{106}Ru + {}^{106}Rh$ applicator at the edge of the tumour base by more than 50 %. For the applicator positioning, it is necessary to take into account that fact that, for most ophthalmic brachytherapy sources, the diameter of the "active area" (area overlaid with radioactive material) is 1,5 mm smaller than the total applicator diameter. Therefore, the selection of the applicator should insure full coverage of the PTV and include an additional margin due to the significantly reduced dose at the edges of the applicator. A 2D or 3D treatment-planning system based on actual dosimetry enables testing of the coverage of the tumour by the applicators owned by the institution and selection of the optimal one.

6) This is an example of a suitable product available commercially. This information is given for the convenience of users of this International Standard and does not constitute an endorsement by ISO of this product.

Applicator displacement perpendicular to the eye surface can be caused by insufficient fixing of the applicator on the sclera or by the development of a haematoma between applicator and sclera post-surgery. The displacement causes an underdosage at the tumour apex with a typical value of 20 % to 30 %/mm for $^{106}Ru + {}^{106}Rh$ applicators.

Dummy applicators, which are an exact replica of the actual applicator, are used to facilitate the placement of the applicator in the operating room [158], [168]. First, the ophthalmologist places a dummy applicator in the exact position covering the tumour. Then he places sutures through the suture lugs of the dummy applicator and the sclera, removes the dummy applicator and sutures the actual applicator in place. The distance from the detectable tumour to the dummy edge should be verified. This procedure enables the team to use as much time as needed for adjusting the position of the applicator, or even change the applicator type being used, without being exposed to unnecessary radiation. In pre-planning, to aid in placement of the applicator, one can check distances measured on the retinal diagram to fix the applicator on the sclera, during the application.

One can check the applicator position after the placement using MRI [158] or ultrasound. CT cannot be used for this purpose due to artefacts caused by the metal of the applicator. If the actual position does not provide proper tumour coverage, it should be adjusted; and if the position is reasonable, the dosimetric calculations can be rechecked and the prescription and/or duration of the treatment modified accordingly.

F.1.5 Multi-segmental sequential irradiation with ophthalmic brachytherapy sources

A multi-segmental, sequential irradiation is applied in all cases when the target size (tumour dimensions including the safety margins) exceed the size of the largest available applicator. It is also considered in cases where the tumour shape is elongated in one dimension. Here a multi-segmental irradiation with smaller sized applicators can spare more of the surrounding tissue. A multi-segmental, sequential irradiation is performed under the condition that, in general, the dose to the sclera in the overlapping area of two or more applicators does not exceed the permissible maximum.

F.1.6 Shielding

Partial shielding of the radiation field of standard $^{90}Sr + {}^{90}Y$ ophthalmic brachytherapy sources is utilized in order to spare the tissue surrounding the small sized target volumes on the conjunctiva. A Pb or other acceptable high-Z material shield with a thickness of 0,5 mm to 1 mm between the radioactive applicator surface and the tissue is used as shielding material. The dose (rate) of $^{90}Sr + {}^{90}Y$ underneath a 1 mm Pb shielding, for instance, is reduced by approximately four orders of magnitude. The lateral dose distribution shows a typical exponential dose fall off from the unshielded to the shielded area. The stochastic health risk of the Pb induced bremsstrahlung is negligible compared to the avoidance of deterministic damage of non-malignant tissue in the full radiation field.

F.2 Treatment planning for intravascular brachytherapy

F.2.1 General

In the special case of intravascular brachytherapy, time for treatment planning is limited due to the very invasive character of the entire intervention. Furthermore, imaging modalities combining angiography and intravascular ultrasound are not available in most of the centres. Therefore, a level approach, as already proposed for external beam therapy reporting [156], [157], and recently adapted for intravascular brachytherapy treatment planning [20], is appropriate.

Basic treatment planning (level 1) is based only on the intervention length (IL) plus safety margins and the reference lumen diameter (RLD) [169]. Dose is prescribed to a specific point relative to the source axis or the vessel lumen diameter. Dose reporting is limited to points at the vessel lumen surface (reference lumen dose point) and at the reference depth into the vessel wall (reference depth dose point) at the representative central plane including minimal and maximal variations in case of non-centred devices. The calculation of these doses is possible using a reference absorbed-dose rate and a description of the radial dose profile at the central plane of the sources used. The choice of the adequate active source length in order to encompass the

entire target length is based on a longitudinal dose profile. For simplification of the treatment-planning process, the respective devices are characterized with a reference isodose length (RIL), which is defined as the length of the source over which the dose rate is greater than 90 % of the reference absorbed-dose rate. In summary, the dosimetric data for basic treatment planning are reduced to values for the reference absorbed-dose rate, the radial dose profile at the central plane and the reference isodose length (RIL). These data are related to an entire source arrangement including each seed of a complete source train or any dwell position of a stepping source.

Advanced treatment planning (level 2) includes dose calculation with respect to anatomical and pathological structures in the vessel wall not limited to the central plane. In developmental treatment planning (level 3), the calculation of dose-volume histograms for vessel-wall structures is included in the treatment-planning process or at least in the retrospective analysis of the actual treatment. In these cases, it is necessary that the calculation be based on a full 3D dose distribution. In contrast to the information provided for level 1 treatment planning, these source data are related to each single seed or to a small wire segment of the entire source. Using this concept, the dose calculation is more flexible to describe the dose distribution for curved sources. Furthermore, the use of small segments avoids problems related to the existing AAPM TG 43 and AAPM TG 60 formalism as outlined in 7.3.

The radial dose profile, $R(r)$, in combination with the reference absorbed dose rate, is the basis for calculating the treatment time and the dose to specific points in the central plane in a level 1 treatment planning approach.

F.2.2 Longitudinal dose profile — Reference isodose length (level 1)

The knowledge of a longitudinal dose profile is necessary to determine the reference isodose length (RIL), which is the main parameter for the choice of the respective device after determination of the intervention length and safety margins.

The exact value of the RIL is given by $H(r',z)$, where r' is the distance from the source axis to the location of the reference depth dose point, i.e. the vessel radius plus reference depth. The RIL is then the length where $H(r',z)$ is greater than or equal to 0,9. Therefore, it is necessary to give $H(r,z)$ for several distances, r, of clinical interest. However, the difference of the RIL for distances at clinical interest are small in case of beta radiation sources used for intracoronary brachytherapy [169]. In order to establish common rules for treatment planning, the determined RIL values can be applied as follows.

Vessels treated in intracoronary brachytherapy are generally between 2,0 mm to 4,0 mm in diameter. Using a reference depth of 1 mm into the vessel wall, the radial distances from the source axis of 2,0 mm to 3,0 mm are then important when applying the RIL concept. For daily clinical practice, approximate values for the RIL can be used that should be as close as possible to the determined values. Therefore, it is proposed to use a RIL of 36 mm for the 20 mm Guidant source wire stepping over 40 mm and 35 mm for the Novoste 40 mm seed train. These values are a compromise between calculated and measured values for 2 mm and 3 mm radial distances. For beta radiation sources, the difference between ASL and RIL are found to be similar also for longer ASL. This can be related to the short range of the beta radiation resulting in a saturation effect when using source lengths longer than the maximum electron range of the emitted source spectra.

EXAMPLE A RIL of 56 mm can be used for three dwell positions using the Guidant system and 55 mm for the 60 mm Novoste source train.

As already discussed in the general aspects, this value is related to the entire source arrangement for level 1 data or to a single seed or a wire segment in case of levels 2 and 3 data, applying the AAPM TG 43/AAPM TG 60 formalism.

In order to take into account the non-uniformity of some sources, e.g. for seed trains and seed ribbons, it is suggested to define the reference absorbed-dose rate of the entire source arrangement at the reference distance as the mean value along the central seeds. For an even number of seeds, the central two elements should be used, and for an odd number, the central three elements should be used.

Bibliography

[1] QUAST, U., BÖHM, J., AND KAULICH, T.W., Clinical beta radiation dosimetry for brachytherapy in terms of absorbed dose to water, *Cardiovasc. Radiat. Med.*, **3,** pp. 209-212 (2002)

NOTE This is also an ISO new work item proposal for an International Standard.

[2] QUAST, U., BÖHM, J., AND KAULICH, T.W., The need of international standardization in clinical beta dosimetry for brachytherapy, Proc. Intern. Symp. on Standards and Codes of Practice in medical Radiation Dosimetry, IAEA-CN-96-73, International Atomic Energy Agency, Vienna (2003)

[3] QUAST, U., Standardization and harmonisation in clinical dosimetry in terms of absorbed dose to water as the measurand for beta radiation brachytherapy, Editorial, *Jour. Med. Phys.*, **31**, pp. 59-60 (2006)

[4] LOMMATSCH, P.K., Experiences in the treatment of malignant melanoma of the choriod with $^{106}Ru + ^{106}Rh$ beta-ray applicators, *Trans. Ophthalmol. Soc. UK*, **93**, pp. 119-132, (1973)

[5] LOMMATSCH, P.K., Results after beta-irradiation ($^{106}Ru/^{106}Rh$) of the choroidal melanomas: 20 years experience., *Br. J. Ophthalmol.*, **79**, pp. 844-851 (1986)

[6] SHIELDS, C.L., SHIELDS, J.A., *et al.*, Applicator radiotherapy for uveal melanoma: Long-term visual outcome in 1106 consecutive patients., *Arch. Ophthalmol.*, **118**, pp. 1210-1228 (2000)

[7] SEREGARD, S., Long-term survival after ruthenium applicator radiotherapy for uveal melanoma. A meta-analysis of studies including 1066 patients, *Acta Ophthalmol. Scand.*, **77**, pp. 414-417 (2000)

[8] LOMMATSCH, P.K., WERSCHNIK, C., AND SCHUSTER, E., Long-term follow-up of Ru-106/Rh-106 brachytherapy for posterior uveal melanoma, *Graefers Arch. Clin. Axp. Ophthalmol.*, **238**, pp. 129-137 (2000)

[9] PÖTTER, R. AND VAN LIMBERGEN, E., Uveal Melanoma, in The GEC ESTRO Handbook of Brachytherapy, Eds. GERBAULET, A., PÖTTER, R., MAZERON, J.J., MEERTENS, H. AND VAN LIMBERGEN, E. (Brussels, Belgium, ESTRO), pp.591-610 (2002)

[10] VAN GINDERDEUREN, R., VAN LIMBERGEN, AND E., SPILEERS, W., 18 years' experience with high dose rate strontium-90 brachytherapy of small to medium sized posterior uveal melanoma, *Br. J. Ophthalmol.*, **89**, pp. 1306-1310 (2005)

[11] FLÜHS, D., ANASTASSIOU, G., WENING, J., SAUERWEIN, W., AND BORNFELD, N., The design and the dosimetry of bi-nuclide radioactive ophthalmic applicators, *Med. Phys.*, **31**, pp. 1481-1488 (2004)

[12] DELANEY, T.F., CHEN, G.T., MAUCERI, T.C., MUNRO III, J.J., HORNICEK, F.J., PEDLOW, F.X., AND SUIT, H.D., Intraoperative dural irradiation by customized ^{192}Iridium and ^{90}Yttrium brachytherapy plaques, *Int. J. Radiat. Oncol. Biol. Phys.*, **57**, pp. 239-245 (2005)

[13] QUAST, U., Definition and determinants of the relevant parameters of vascular brachytherapy, in Vascular Brachytherapy: New perspectives, Ed. LEVENDAG, P.C., Remedica Publishing, London, pp. 51-74 (1999)

[14] WAKSMAN, R. (Ed.), Vascular Brachytherapy, Third Edition, Armonk, NY, Futura (2002)

[15] BALTER, S., CHAN, R.C., AND SHOPE, JR., T. B. (Eds.), Intravascular Brachytherapy/ Fluoroscopically Guided Interventions, Medical Physics Monograph No. 28 (AAPM 2002 Summer School Proceedings), Medical Physics Publishing, Madison, WI, pp. 373-422 (2002)

[16] NuDat2 - Decay Radiation database, Evaluated Nuclear Structure Data File, National Nuclear Data Center, Brookhaven National Laboratory, www.nndc.bnl.gov (2005 August 5)

[17] IAEA Safety Standards Series No. TS-R-1. Regulations for the Safe Transport of Radioactive Material, 2005 Edition. International Atomic Energy Agency (2005)

[18] ICRU Report 72, Dosimetry of beta rays and low-energy photons for brachytherapy with sealed sources

[19] DGMP-Report No. 16, QUAST, U., KAULICH, T.W., AND FLÜHS, D. (Eds.): Guideline for Medical Physical Aspects of Intravascular Brachytherapy. www.dgmp.de (pdf-file). Deutsche Gesellschaft für Medizinische Physik, Cologne, (2001)

[20] EVA GEC ESTRO Recommendations: PÖTTER, R., VAN LIMBERGEN, E., DRIES, W., *et al*. (Eds.): Recording, reporting, quality assurance, education, and training in endovascular brachytherapy. Recommendations of the Endovascular GEC-ESTRO Working Group EVA GEC-ESTRO. *Radioth. Oncol*. **59,** pp. 339-360 (2001)

[21] IAEA TECDOC-1274. Calibration of photon and beta ray sources used in brachytherapy. Guidelines on standardized procedures at Secondary Standards Dosimetry Laboratories (SSDLs) and hospitals. International Atomic Energy Agency (2002)

[22] AAPM TG 60 Report. Intravascular Brachytherapy Physics. NATH, R., AMOLS, H., COFFEY, C., *et al*., Report of the AAPM Radiation Therapy Committee Task Group No. 60. *Med. Phys*., **26,** pp. 19-152 (1999)

[23] QUAST, U., Reporting vascular brachytherapy - Proposal for a revision of the AAPM TG 60 report, Editorial. Cardiovasc. *Radiat. Med*., **1**, pp. 378-381 (1999)

[24] AAPM TG 43 Report, Dosimetry of Interstitial Brachytherapy Sources. NATH, R., ANDERSON, L.L., AND LUXTON, G., eds.: Recommendations of the AAPM Radiation Therapy Committee Task Group No. 43. *Med. Phys*., **22,** pp. 209-234 (1995)

[25] MOURTADA, F.M., SOARES, C.G. AND HORTON, J.H., A segmented ^{32}P source Monte Carlo model to derive AAPM TG-43/60 dosimetric parameters for intravascular brachytherapy, *Med. Phys*., **31**, pp. 602-608 (2004)

[26] SCHAART, D.R., CLARIJS, M.C. AND BOS, A.J.J., On the applicability of the AAPM TG-60/TG-43 dose calculation formalism to intravascular line sources: Proposal for an adapted formalism, *Med. Phys*., **28**, pp. 638-653 (2001)

[27] CHIU-TSAO, S.-T., SCHAART, D.R., SOARES, C.G. AND NATH, R., Dose calculation formalisms and consensus dosimetry parameters for intravascular brachytherapy dosimetry: Recommendations of the AAPM Therapy Physics Committee Task Group No. 149, *Med. Phys*., **34**, pp. 4126-4157 (2007)

[28] KOLLAARD, R.P., DRIES, W.J.F., VAN KLEFFENS, H.J., AALBERS, A.H.L., VAN DER MAREL, J., MARIJNISSEN, J.P.A., PIESSENS, M., SCHAART, D.R. AND DE VROOME, H., Quality control of sealed brachytherapy sources in brachytherapy, NCS Report 14, Netherlands Commission on Radiation Dosimetry (2004)

[29] SOARES, C.G., Calibration of ophthalmic applicators at NIST: a revised approach, *Med. Phys*., **18,** pp. 787-793 (1991)

[30] SOARES, C.G., VYNCKIER, S., JÄRVINNEN, H., CROSS, W.G., SIPILÄ, P., FLÜHS, D., SCHAEKEN, B, AND MOURTADA, F.A., Dosimetry of beta-ray ophthalmic applicators: Comparison of different measurement methods, *Med. Phys.*, **28**, pp. 1373-1384 (2001)

[31] ICRU Report 44, Tissue substitutes in radiation dosimetry and measurement

[32] CROSS, W.G., Variation of beta dose attenuation in different media, *Phys. Med. Biol*., **13**, pp. 611-618 (1968)

[33] ICRU Report 56, Dosimetry of external beta rays for radiation protection

[34] SCHAART, D.R., The scaling method applied to beta line sources with a finite diameter, *Med. Phys*., **29**, pp. 2682-2686 (2002)

[35] ICRU Report 35, Radiation Dosimetry: Electron Beams with Energies Between 1 and 50 MeV

[36] TABATA, T., ANDREO, P., SHINODA, K. AND ITO, R., Depth profiles of charge deposition by electrons in elemental absorbers: Monte Carlo results, experimental benchmarks and derived parameters, *Nucl. Instrum. Methods Phys. Res*., **B 95**, pp. 289-299 (1995)

[37] TABATA, T., ANDREO, P., SHINODA, K. AND ITO, R., Range distributions and projected ranges of 0.1- to 100-MeV electrons in elemental absorbers, *Nucl. Instrum. Methods Phys. Res*., **B 108**, pp. 11-17 (1996)

[38] BAMBYNEK, M., HIGERS, G., KRUMREY, M., Bestimmung der räumlichen Variation des Ansprechvermögens von Plastikszintillator-Detektoren.Tagungsband der 35. Jahrestagung der Deutschen Gesellschaft für Medizinische Physik (DGMP), Leipzig, (2004)

[39] LOEVINGER, R. AND BERMAN, M., A schema for absorbed dose calculations for biologically distributed radionuclides, MIRD Pamphlet No. 1, *J. Nucl. Med*., pp.7-14 (1968)

[40] CROSS, W. G., Tables of beta dose distribution, Report AECL 2793 (1967)

[41] CROSS, W.G., The distribution of absorbed energy from a point beta source, *Can. Journ. Phys*., **45,** pp. 2021-2040 (1967)

[42] SPENCER, L.V., Energy dissipation by fast electrons, Monograph 1, NBS (National Bureau of Standards, Washington D.C.) (1959)

[43] BERGER, M.J., Distribution of absorbed dose around point sources of electrons and beta particles in water and other media. MIRD Pamphlet 7, *J. Nuc. Med*., **12,** Suppl. 5, pp. 5-24 (1971)

[44] BERGER, M.J., Improved point kernels for electron and beta-ray dosimetry, NBS Report NBSIR 73-107. Gaithersburg, MD, National Bureau of Standards (1973)

[45] SIMPKIN, D.J. AND MACKIE, T.R., EGS4 Monte Carlo determination of the beta dose kernel in water, *Med. Phys*., **17,** pp. 179-186 (1990)

[46] SELTZER, S.M., Electron-photon Monte Carlo calculations: The ETRAN code, Int. J. Radiat. App. Instrum., Part A, *App. Rad. Isot.,* **42,** pp. 917-941 (1991)

[47] SELTZER, S.M., Monte Carlo Modeling for Intravascular Brachytherapy Sources, in Intravascular Brachytherapy/ Fluoroscopically Guided Interventions, Eds. BALTER, S., CHAN, R.C., SHOPE, JR., T. B. Medical Physics Monograph No. 28 (AAPM 2002 Summer School Proceedings), Medical Physics Publishing, Madison, WI, pp. 373-422 (2002)

[48] CROSS, W.G., HOKKANEN, J., JÄRVINNEN, H., MOURTADA, F., SIPLILÄ, P., SOARES, C.G., AND VYNCKIER, S., Calculation of beta-ray dose distributions from ophthalmic applicators and comparison with measurements in a model eye, *Med. Phys*., **28,7**, pp. 1385-1396 (2001)

[49] BERGER, M.J., Monte Carlo Calculation of the Penetration and Diffusion of Fast Charged Particles. in Methods in Computational Physics. B. Alder, S. Fernbach and M. Rotenberg. New York, Plenum Press, Vol. **1**, pp.135-215 (1963)

[50] TURNER, J.E., WRIGHT, H.A., *et al.*, A Monte Carlo primer for health physicists, *Health Phys.*, **48,** pp. 717-33 (1985)

[51] JENKINS, T.M., NELSON, W.R., *et al.*, Monte Carlo Transport for Electrons and Photons. New York, Plenum Press. (1988)

[52] ROGERS, D.W.O. AND BIELAJEW, A.F., Monte Carlo techniques for electron and photon transport for radiation dosimetry. in The Dosimetry of Ionizing Radiation. K. T. Kase, B. E. Bjarngard and F. H. Attix. New York, Academic Press, Vol. **3**, pp. 427-539 (1990)

[53] ANDREO, P., Monte Carlo techniques in medical radiation physics, *Phys. Med. Biol.*, **36**, pp. 861-920 (1991)

[54] BIELAJEW, A.F., Some Random Thoughts on Monte Carlo Electron and Photon Transport," in Advanced Monte Carlo for Radiation Physics, Particle Transport Simulation and Applications, Proceedings of the Monte Carlo 2000 Conference, Lisbon, 23-26 October 2000. Eds. A. KLING, F. BARÃO, M. NAKAGAWA, L. Távora and P. Vaz. Berlin, Springer, pp. 1-6. (2001)

[55] MOURTADA, F.A., SOARES, C.G., SELTZER, S.M., AND LOTT, S.H., Dosimetry characterization of ^{32}P catheter-based vascular brachytherapy source wire, *Med. Phys.*, **27**, pp. 1770-1776 (2000)

[56] SOARES, C.G., HALPERN, D.G., AND WANG, C.-K., Calibration and characterization of beta-particle emitting sources for intravascular brachytherapy. *Med. Phys.*, **25**, pp. 339-346 (1998)

[57] WANG, R. AND LI, X.A., A Monte Carlo calculation of dosimetric parameters of ^{90}Sr/^{90}Y and ^{192}Ir SS sources for intravascular brachytherapy, *Med. Phys.*, **27,** pp. 2528-2535 (2000)

[58] WANG, R. AND LI, X.A., Monte Carlo characterization of a ^{32}P source for intravascular brachytherapy. *Med. Phys.*, **28**, pp. 1776-1785 (2001)

[59] MOURTADA, F.A., SOARES, C.G., SELTZER, S.M., BERGSTROM, P.M. JR., FERNANDEZ-VAREA, J.M., ASENJO, J., AND LOTT, S.H., Dosimetry Characterization for ^{32}P Source Wire Used for Intravascular Brachytherapy with Automated Stepping, *Med. Phys.*, **30**, pp. 959-971 (2003)

[60] YE, S.J., LI, X.A., ZIMMER, J.R., CHU, J.C. AND CHOI, C.K., Dosimetric perturbations of linear array of beta-emitter seeds and metallic stent in intravascular brachytherapy, *Med. Phys*. **27**, pp. 374-380 (2000)

[61] BOHM, T.D., MOURTADA, F.A., AND DAS, R.K., Dose rate table for a ^{32}P intravascular brachytherapy source from Monte Carlo calculations, *Med. Phys.*, **28**, pp. 1770-1775 (2001)

[62] PATEL, N.S., CHIU-TSAO, S.-T., FAN, P., AHUNBAY, E., RAVI, K., SHERMAN, W., QUON, H., PISCH, J., TSAO, H.-S., AND HARRISON, L.B., Treatment planning dosimetric parameters for a ^{90}Y coil source used in intravascular brachytherapy, *Cardiovasc. Radiat. Med.*, **2**, pp. 83-92 (2001)

[63] WANG, R. AND LI, X.A., Monte Carlo dose calculations of beta-emitting sources for intravascular brachytherapy: a comparison between EGS4, EGSnrc, and MCNP, *Med. Phys.*, **28**, pp. 134-141 (2001)

[64] ASENJO, J., FERNÁNDEZ-VAREA, J.M., AND SÁNCHEZ-REYES, A., Characterization of a high-dose-rate ^{90}Sr-^{90}Y source for intravascular brachytherapy by using the Monte Carlo code PENELOPE, *Phys. Med. Biol.*, **47**, pp. 697-711 (2002)

[65] CLARIJS, M.C., BOS, A.J.J. AND SCHAART, D.R., Modelling of a ^{188}W/^{188}Re beta line source for coronary brachytherapy by means of EGS4 Monte Carlo simulations, *Phys. Med. Biol.*, **45**, pp. 1319-1334 (2000)

[66] LI, X.A., WANG, R., YU, C. AND SUNTHARALINGAM, M., Beta versus gamma for catheter-based intravascular brachytherapy: dosimetric perspectives in the presence of metallic stents and calcified plaques, *Int. J. Radiat. Oncol. Biol. Phys*., **46**, pp. 1043-1049 (2000)

[67] FAN, P., CHIU-TSAO, S.T., PATEL, N.S., SHIH, A., RAVI, K., SHERMAN, W., TSAO, H.-S., PISCH, J. AND HARRISON, L., Effect of stent on radiation dosimetry in an in-stent restenosis model, *Cardiovasc Radiat Med.*, **2**, pp. 18-25 (2000)

[68] LI, X.A., Dosimetric effect of contrast media for catheter-based intravascular brachytherapy, *Med. Phys*., **28**, pp. 757-763 (2001)

[69] SEHGAL, V., LI, Z., PALTA, J.R. AND BOLCH, W.E., Dosimetric effect of source centering and residual plaque for beta-emitting catheter based intravascular brachytherapy sources, *Med. Phys*., **28**, pp. 2162-2171 (2001)

[70] NATH, R. AND YUE, N., Shielding effects of metallic encapsulations and radiographic contrast agents for catheter-based intravascular brachytherapy, *Cardiovasc. Radiat. Dosim*., **2**, pp. 93-103 (2001)

[71] WANG, R. AND LI, X.A., Dosimetric comparison of two 90Sr/90Y sources for intravascular brachytherapy: an EGSnrc Monte Carlo calculation, *Phys. Med. Biol*., **47**, pp. 4259-4269 (2002)

[72] SCHAART, D.R., BOS, A.J.J., WINKELMAN, A.J.M. AND CLARIJS, M.C., The radial depth-dose distribution of a 188W/188Re beta line source measured with novel, ultra-thin TLDs in a PMMA phantom: Comparison with Monte Carlo simulations, *Phys. Med. Biol*., **47**, pp. 3605-3627 (2002)

[73] YE, S.J., PARSAI, E.I. AND FELDMEIER, J.J., Dosimetric characteristics of a linear array of β or γ-emitting seeds in intravascular irradiation: Monte Carlo studies for the AAPM TG-43/60 formalism, *Med. Phys*., **30**, 403-414 (2003)

[74] LI, X.A., SUNTHARALINGAM, M. AND YU, C., Dosimetry of source stepping for intravascular brachytherapy, *Cardiovasc. Rad. Med*., **2**, pp. 165-172 (2001)

[75] TORRES, J., BUADES, M.J., ALMANSA, J.F., GUERRERO, R. AND LALLENA, A.M., Dosimetry characterization of 32P intravascular brachytherapy source wires using PENELOPE and GEANT4, *Med. Phys*., **31**, pp. 296-304 (2004)

[76] IEC/TR 60788:2004, *Medical electrical equipment — Glossary of defined terms*

[77] SELBACH, H.-J. AND SOARES, C.G., New developments on primary standards for brachytherapy at NIST (US) and PTB (Germany), in Standards and Codes of Practice in Medical Radiation Dosimetry, Proceedings of an International Symposium, Vienna, 25-28 November 2002, International Atomic Energy Agency, Vienna, pp. 101-110 (2003)

[78] BAMBYNEK, M., *et al*., Development of a multi-electrode extrapolation chamber as a prototype of a primary standard for the realization of the quantity of the absorbed dose to water for beta radiation brachytherapy sources, *Nucl. Inst. Meth*., **A 492**, pp. 264-275 (2002)

[79] BIPM, The BIPM key comparison database, Appendix C, Calibration and measurement capabilities of national metrology institutes, http//kcdb.bipm.org/ (2005)

[80] BASS, G.A. AND PALMER, M.J., The development of a calibration service for ophthalmic applicators at NPL, Consultative Committee for Ionizing Radiation, Report CCRI(I)/05-21 (2005)

[81] AAPM TG 55 Report. Radiochromic film dosimetry. NIROOMAND-RAD, A., *et al*., eds.: Recommendations of AAPM Radiation Therapy Committee Task Group No. 55, *Med Phys.,* **25,** pp. 2093-2115 (1998)

[82] FLÜHS, D., HEINTZ, M., INDENKÄMPEN, F., WIECZOREK, C., KOLANOSKI, H. AND QUAST, U., Direct reading measurement of absorbed dose with plastic scintillators - The general concept and applications to ophthalmic dosimetry, *Med. Phys*., **23,** pp. 427-434 (1996)

[83] BAMBYNEK, M., FLÜHS, D., QUAST, U., *et al*., A high-precision, high-resolution and fast dosimetry system for beta sources applied in cardiovascular brachytherapy, *Med. Phys*., **27**, pp. 662-667 (2000)

[84] HARRIS, S.M., DEWERD, L.A., MICKA, J.A., Experimental determination of the radial dose function of ^{90}Sr/^{90}Y IVBT sources, *Med. Phys*., **33**, pp. 3225-3233 (2006)

[85] LAX, I., Dosimetry of ^{106}Ru eye applicators with a p-type silicon detector, *Phys. Med. Biol*., **36**, pp. 963-972 (1991)

[86] IEC 62427-1, *Medical electrical equipment — Dosimetric instruments as used in brachytherapy — Part 1: Instruments based on well-type ionization chambers* 7)

[87] QUAST, U., WEICHERT, F., KRAUSHAAR, A., SPILLES, P., A virtual 3D IVUS vessel model for intracoronary brachytherapy planning: visualization of the 3D vessel orientation and 3D vessel wall architecture by automated segmentation and 3D reconstruction, *Med. Phys*., **30**,9, pp. 2530-2533 (2003)

[88] KAULICH, T.W., ZURHEIDE, J., HAUG, T., NÜSSLIN, F., BAMBERG, M. Clinical quality assurance for ^{106}Ru ophthalmic applicators, *Radioth. Oncol*., **76**, pp 86-92 (2005)

[89] ISO 9978:1992, *Radiation protection — Sealed radioactive sources — Leakage test methods*

[90] BÖHM, J., The National Primary Standard of the PTB for Realizing the Unit of the Absorbed Dose Rate to Tissue for Beta Radiation, Report PTB Dos 13 (Physikalisch-Technische Bundesanstalt, Braunsschweig) (1986)

[91] VAN DER MAREL, J. AND VAN DIJK, E., Development of a Dutch primary standard for beta emitting brachytherapy sources, in Standards and Codes of Practice in Medical Radiation Dosimetry, Proceedings of an International Symposium, Vienna, 25-28 November 2002, International Atomic Energy Agency, Vienna, pp. 93-100 (2003)

[92] MCLAUGHLIN, W.L., CHEN, Y.-D., SOARES, C.G., MILLER, A., VAN DYK, G., AND LEWIS, D.F., Sensitometry of the response of a new radiochromic film dosimeter to gamma radiation and electron beams, *Nucl. Instrum. Meth*. *Phys. Res*., **A302**, pp. 165-176 (1991)

[93] DEMPSEY, J.F., LOW, D.A., MUTIC, S., MARKMAN, J., KIROV, A.S., NUSSBAUM, G.H. AND WILLIAMSON, J.F., Validation of a precision radiochromic film dosimetry system for quantitative two-dimensional imaging of acute exposure dose distributions, *Med. Phys*., **27**, pp. 2462-2475 (2000)

[94] SOARES, C.G. AND MCLAUGHLIN, W.L., Measurement of radial dose distributions around small beta particle emitters using high resolution radiochromic foil dosimeter, *Radiat. Prot. Dosim*., **47,** pp. 367-372 (1993)

[95] RICHTER, S., TRICHTER, F., SABBAS, A., LOVELOCK, D., KULIDZHANOV, AND F., NORI, D., Evaluation of GafChromic EBT film for IMRT QA using two different scanners, *Med. Phys*., **32**, p. 2167 (2005)

[96] TRICHTER, F., AND TRICHTER, S., CORVUS IMRT film dosimetry using novel GafChromic EBT film, *Med. Phys*., **32**, p. 2167 (2005)

[97] BEDDAR, A.S., MACKIE, T.R. AND ATTIX, F.H., Water-equivalent plastic scintillator detectors for high-energy beam dosimetry: I. Physical characteristics and theoretical considerations, *Phys. Med. Biol*., **37**, pp. 1883-1900 (1992)

7) Under preparation.

[98] BEDDAR, A.S., MACKIE, T.R. AND ATTIX, F.H., Water-equivalent plastic scintillator detectors for high-energy beam dosimetry: II. Properties and measurements, *Phys. Med. Biol.*, **37**, pp. 1901-1913 (1992)

[99] FLÜHS, D., Aufbau und Einsatz eines Szintillationsdetektorsystems zur Messung von Dosisverteilungen an einer ^{60}Co-Teletherapieanlage. Physics-Diploma Work. Dortmund University, Germany (1989)

[100] KIROV, A.S., HURLBUT, C., DEMPSEY, J.F., SHRINIVAS, S.B., EPSTEIN, J.W., BINNS, W.R., DOWKONTT, P.F. AND WILLIAMSON, J.F., Towards two-dimensional brachytherapy dosimetry using plastic scintillator: New highly efficient water equivalent plastic scintillator materials, *Med. Phys.*, **26,** pp.1515-1523 (1999)

[101] FLÜHS, D., QUAST, U., KOLANSKI, H., AND HEINTZ, M., Dosimetric treatment planning – fast 2D/3D dosimetry. In: HOUNSELL, A.R., WILKINSON, J.M., WILLIAMS, P.C., Eds.: XITH Proceedings International Conference on the use of computers in radiation therapy, Manchester, UK., pp. 38-39 (1994)

[102] QUAST, U., FLÜHS, D., AND KOLANOSKI, H., Clinical dosimetry with plastic scintillators – almost energy independent, direct absorbed dose reading with high resolution. In: IAEA-seminar on radiation dosimetry, Rio de Janeiro. IAEA-TECDOC-896, pp. 165-169 (1996)

[103] BEDDAR, A. S., MACKIE, T.R. AND ATTIX, F.H., Cerenkov light generated in optical fibers and other light pipes irradiated by electron beams, *Phys. Med. Biol.*, **37**, pp. 925-935 (1992)

[104] MCKEEVER, S.W.S., MOSCOVITCH, M., AND TOWNSEND, P.D., Thermoluminescence Dosimetry Materials: Properties and Uses (Nuclear Technology Publishing, Ashford, Kent) (1995)

[105] ICWG: Interstitial Collaborative Working Group. Interstitial Brachytherapy: Physical, Biological and Clinical Considerations (Raven Press, New York) (1990)

[106] WILLIAMSON, J. AND MEIGOONI, A. Quantitative dosimetry methods in brachytherapy, In: WILLIAMSON, J., THOMADSEN, B. AND NATH, R., eds. Brachytherapy Physics (Medical Physics Publ. Corp., Madison, Wisconsin, USA), pp. 87-134 (1995)

[107] HOLMES, S.H., DEWERD, L.A., AND MICKA, J.A. Experimental determination of the radial dose function of ^{90}Sr/Y IVBT sources, *Med. Phys.*, **33**, pp. 3225-3233 (2006)

[108] TRICHTER, S., COHEN, G.N., LOSASSO, T., MCCORMICK, B., ABRAMSON, D., ZAIDER, M., AND AMOLS, H., Treatment planning for Ru-106 eye plaques: pitfalls and remedies, Proceedings of the 88th Scientific Assembly and Annual Meeting of the RSNA, (2002)

[109] DEWERD, L.A., MICKA, J.A., HOLMES, S.H., AND BOHM, T.D., Calibration of multiple LDR brachytherapy sources, *Med. Phys.*, **33**, pp. 3804-3813 (2006)

[110] MARYANSKI, M., IBBOTT, G., EASTMAN, P., SCHULZ, R., AND GORE, J., Radiation therapy dosimetry using magnetic resonance imaging of polymer gels, *Med. Phys*. 23, pp. 699-705 (1996)

[111] CHAN, M.F., FUNG, A.Y., HU, Y.C., CHUI, C.S., AMOLS, H., ZAIDER, M., AND ABRAMSON, D., The measurement of three dimensional dose distributions of a ruthenium-106 ophthalmological applicator using magnetic resonance imaging of BANG oilymer gels, *J. Appl. Clin. Med. Phys.*, **2**, pp. 85-89 (2001)

[112] GAZA, R., BULUR, E., MCKEEVER, S.W.S., AND SOARES, C.G., Experimental determination of the dose deposition profile of a ^{90}Sr beta source, *Rad. Prot. Dosim.*, **120**, pp. 33-37 (2006)

[113] YUKIHARA, E. K., YOSHIMURA, E. M., LINDSTROM, T.D., AHMAD, S., TAYLOR, K.K., AND MARDIROSSIAN, G., High-precision dosimetry for radiotherapy using the optically stimulated luminescence technique and thin Al_2O_3:C dosimeters, *Phys. Med. Biol.*, **50**, pp. 5619-5628 (2005)

[114] BUCKLEY, L.A., THOMADSEN, B.R. AND DEWERD, L.A., The water-equivalence of phantom materials for ^{90}Sr-^{90}Y beta particles, *Med. Phys.*, **28**, pp. 1010-1015 (2001)

[115] NELSON, W.R., HIRAYAMA, H. AND ROGERS, D.W.O. The EGS4 code system SLAC Report 265, Stanford Linear Accelerator Institute (1985)

[116] KAWRAKOW, I. AND ROGERS, D.W.O. The EGSnrc Code System: Monte Carlo Simulation of Electron and Photon Transport, NRCC Report PIRS-701 Ottawa: National Research Council of Canada (2003)

[117] HALBLEIB, J.A., KENSEK, R.P., MEHLHORN, T.A., VALDEZ, G.D., SELTZER, S.M. AND BERGER, M.J., ITS Version 3.0: Integrated TIGER Series of Coupled Electron/Photon Monte Carlo Transport Codes, Report SAND91-1634, Sandia National Laboratories, NM, USA. (1992)

[118] BRIEMEISTER, J.F., MCNP™ - A General Monte Carlo N-Particle Transport Code, Version 4C Report LA-13709M. Los Alamos, NM, Los Alamos National Laboratory (2000)

[119] WATERS, L.S. MCNPX - User's Manual Version 2.4.0, Report LA-CP-02-408, Los Alamos, NM, Los Alamos National Laboratory (2002)

[120] BROWN, F.B., MCNP - A General Monte Carlo N-Particle Transport Code, Version 5, Vol. I: Overview and Theory, Report LA-UR-03-1987; Vol. II: User's Guide, Report LA-CP-03-0245; Vol. III: Developer's guide, Report LA-CP-03-0284, Los Alamos, NM, Los Alamos National Laboratory (2003)

[121] SALVAT, F., FERNÁNDEZ-VAREA, J.-M. AND SEMPAU, J., PENELOPE - A code System for Monte Carlo Simulation of Electron and Photon Transport, Workshop Proceedings, Issy-les-Moulineaux, France, 7-10 July 2003. Paris, OECD Publications (2003)

[122] AGOSTINELLI S, ALLISON J, AMAKO K, *et al.*, GEANT4 – a Simulation Toolkit, *Nucl. Instr. Meth. Phys. Res.*, **A 506**, pp. 250–303 (2003)

[123] SELTZER, S.M., An Overview of ETRAN Monte Carlo Methods in Monte Carlo Transport for Electrons and Photons, Eds. JENKINS, T.M., NELSON, W.R., RINDI, A. New York, Plenum Press, pp. 153-181 (1988)

[124] BERGER, M.J. AND SELTZER, S.M., Electron and Photon Transport Programs, I. Introduction and Notes on Program DATAPAC 4, NBS Report 9836; and Electron and Photon Transport Programs, II. Notes on Program ETRAN 15, NBS Report 9837. Gaithersburg, MD, National Bureau of Standards (1968)

[125] HALBLEIB, J.A. Structure and operation of the ITS code system in Monte Carlo Transport for Electrons and Photons, Eds. JENKINS, T.M., NELSON, W.R., RINDI, A. New York, Plenum Press, pp. 249-262 (1988)

[126] ICRU Report 37, Stopping powers for electrons and positrons

[127] GOUDSMIT, S. AND SAUNDERSON, J.L., Multiple Scattering of Electrons, *Phys. Rev.*, **57**, pp. 24-29 (1940)

[128] VISED, http://mcnpvised.com/ (2004)

[129] SCHAART, D.R., JANSEN, T.M., ZOETELIEF, J., AND DE LEEGE, P., A comparison of MNCP4 electron transport with ITS3.0 and experiment at incident energies between 100 keV and 20 MeV: Influence of voxel size, substeps and energy indexing algorithm, *Phys. Med. Biol.*, **47**, pp. 1459-1484 (2002)

[130] JERAJ, R., KEALL, P.J., OSTWALD, P.M., Comparisons between MCNP, EGS4 and experiment for clinical electron beams, *Phys. Med. Biol.*, **44**, pp. 705-717 (1999)

[131] REYNAERT, N., PALMANS, H., THIERENS, H. AND JERAJ, R., Parameter dependence of the MCNP electron transport in determining dose distributions, *Med. Phys.*, **29**, pp. 2446-2454 (2002)

[132] NAGEL, H.H., Elektron-Photon-Kaskaden in Blei: Monte-Carlo-Rechnungen für Primärelektronenergien zwischen 100 und 1000 MeV, *Z. Physik*, **186**, pp.319-346 [1965) (English translation Stanford Linear Accelerator Center Report Number SLAC-TRANS-28 (1965)]

[133] FORD, R.L. AND NELSON, W.R., The EGS code system: computer programs for the Monte Carlo simulation of electromagnetic cascade showers (Version 3), Report SLAC-210 Stanford Linear Accelerator Center, Palo Alto (1978)

[134] NELSON, W.R. AND ROGERS, D.W.O., Structure and Operation of the EGS4 code system in Monte Carlo Transport for Electrons and Photons, Eds. JENKINS, T.M., NELSON, W.R., RINDI, A.. New York, Plenum Press, pp. 287-305 (1988)

[135] ROGERS, D.W.O., Low energy electron transport with EGS., *Nucl. Instr. Meth*., **227** pp. 535-548 (1984)

[136] BIELAJEW, A.F. AND ROGERS D.W.O., PRESTA-the parameter reduce electron-step algorithm for electron Monte Carlo transport, *Nucl. Instr. Meth*., **B18**, pp. 165-181 (1987)

[137] KAWRAKOW, I., Accurate condensed history Monte Carlo simulation of electron transport. I. EGSnrc, the new EGS4 version, *Med. Phys*., **27**, pp. 485-498 (2000)

[138] KAWRAKOW, I., Accurate condensed history Monte Carlo simulation of electron transport II. Application to ion chamber response simulations, *Med. Phys*., **27**, pp. 499-513 (2000)

[139] BOEING, N., GEOGHEGAN, S., *et al*., Endovascular brachytherapy: dosimetry and dose-area analysis of various radiation sources, *Australia Phys. Eng. Sci. Med*., **24**, pp. 63-70 (2001)

[140] LI, X.A. AND SHIH, R., Dose effects of guide wires for catheter-based intravascular brachytherapy, *Int. J. Radiat. Oncol. Biol. Phys*., **51**, pp. 1103-1110 (2001)

[141] SEMPAU, J., ACOSTA, E., BARO, J., FERNÁNDEZ-VAREA, J.M. AND SALVAT, F., An algorithm for Monte Carlo simulation of coupled electron-photon transport, *Nucl. Instrum. Methods Phys. Res*., **B132**, pp. 377-390 (1997)

[142] SEMPAU, J., FERNÁNDEZ-VAREA, J.M., ACOSTA, E. AND SALVAT, F, Experimental benchmarks of the Monte Carlo code PENELOPE, *Nucl. Instrum. Methods Phys. Res*., **B207**, pp. 107–123 (2003)

[143] BARCA, G., CASTROVILLARI, F., CHAUVIE, S., CUCE, D., FOPPIANO, F., GHISO, G., GUATELLI, S., LAMANNA, E., LOPES, M.C., PERALTA, L., PIA, M.G., RODRIGUES, P., TRINDADE, A. AND VELTRI, M.A. Powerful simulation tool for medical physics applications: GEANT4, *Nucl. Phys*., **B125** (Proc, Suppl,), pp. 80–84 (2003)

[144] ARCHAMBAULT, L., BEAULIEU, L., CARRIER, J.F., CASTROVILLARI, F., CHAUVIE, S., FOPPIANO, F., GHISO, G., GUATELLI, S., INCERTI, S., LAMANNA, E., LARSSON, S., LOPES, M.C., PERALTA, L., PIA, M.G., RODRIGUES, P., TREMBLAY, V.H. AND TRINDADE, A., Overview of Geant4 applications in medical physics 2003, IEEE Nuclear Science-Symposium Conference Record, **3**, pp. 1743-1745 (2004)

[145] CARRIERS, J.-F., ARCHEMBAULT, L. AND BEAULIEU, L., Validation of GEANT4, an object-oriented Monte Carlo toolkit for simulations in medical physics, *Med. Phys*., **31**, pp. 484-492 (2004)

[146] JAN, S., SANTIN, G., STRUL, D. *et al*., GATE: a Simulation Toolkit for PET and SPECT, *Phys. Med. Biol*., **49**, pp. 4543-4561 (2004)

[147] BRIEMEISTER, J.F., MCNP - A General Monte Carlo N-Particle Transport Code, Version 4B Report LA-12625M, Version 4B. Los Alamos, NM, Los Alamos National Laboratory (1997)

[148] ICRU Report 64, Dosimetry of High Energy Photon Beams based on Standards of Absorbed Dose to Water

[149] HUBBELL, J.H., Review of photon interaction cross section data in the medical and biological context, *Phys. Med. Biol.*, **44**, pp. R1-R22 (1999)

[150] ROGERS, D.W.O., FADDEGON, B.A., DING, G.X., MA, C.- M., WEI, J. AND MACKIE, T.R., BEAM: A Monte Carlo code to simulate radiotherapy treatment units, *Med. Phys.*, **22**, 503 – 524 (1995)

[151] MOLIÈRE, G., Theorie der Streuung schneller geladener Teilchen II Mehrfach- und Vielfachstreuung, *Z. Naturf.*, **A3**, pp. 78-97 (1948)

[152] BERGER, M.J. AND WANG, R., Multiple-Scattering Angular Deflections and Energy-Loss Straggling, Monte Carlo Transport of Electrons and Photons, Eds JENKINS, T.M., NELSON, W.R. AND RINDI, A., New York, Plenum, pp. 21-56 (1988)

[153] ROGERS, D.W.O. AND BIELAJEW, A.F., A Comparison of EGS and ETRAN Monte Carlo Transport of Electrons and Photons, Eds JENKINS, T.M., NELSON, W.R. AND RINDI, A., New York, Plenum, pp 323-344 (1988)

[154] LANDAU, L., On the Energy Loss of fast Particles by Ionization, *J. Phys. (USSR*), **8**, pp. 201-207 (1944)

[155] BIELAJEW, A.F. AND KAWRAKOW, I., The EGS4/PRESTA-II electron transport algorithm: Tests of electron step-size stability, In Proceedings of the XII'th Conference on the Use of Computers in Radiotherapy"(Medical Physics Publishing, Madison, Wisconsin), pp.153-154 (1997)

[156] ICRU Report 50, Prescribing, recording and reporting photon beam therapy

[157] ICRU Report 62, Prescribing, recording and reporting photon beam therapy (Supplement to ICRU Report 50)

[158] CHIU-TSAO, S.-T., Episcleral eye plaques for treatment of intraocular malignancies and benign diseases, in Brachytherapy Physics, 2nd edition (Medical Physics Publ. Corp., Madison, Wisconsin, USA), pp. 673-705 (2005)

[159] BUSCH, M., SAUERWEIN, W., Klinisch-methodische Grundlagen der Brachytherapie, in Strahlentherapie-Radiologisch Onkologie, 4th ed., Eds. SCHERER, E. AND SACK, H. (Springer, Berlin), pp 425-452 (1996)

[160] MESSMER, E.P., SAUERWEIN, W, HEINRICH, T., HÖPPING, W., KLUETER-RECKMANN, D., BORNFELD, N., SACK, H., FÖRSTER, M., HAVERS, W. New and recurrent tumor foci following local treatment as well as external beam radiation in eyes of patients with hereditary retinoblastoma, *Graefe's Archive for Clinical and Experimental Ophthalmology*, **228 (5)**, pp 426-431 (1990)

[161] HERMANN, R.M., PRADIER, O., LAURITZEN, K., OTT, M., SCHMIDBERGER, H., AND HESS, C.F., Does escalation of the apical dose change treatment outcome in β-radiation of posterior choroidal melanomas with ^{106}Ru plaques, *Int. J. Radiat. Oncol. Biol. Phys.*, **52**, pp 1360-1366 (2002)

[162] KAULICH, T.W., ZURHEIDE, J., FLÜHS, D., HAUG, T., NÜSSLIN, F., AND BAMBERG, M. Therapy relevant weak sites in industrial quality assurance of ^{106}Ru eye plaques, *Strahlenth. Oncol.*, **177**, pp 616-626 (2001)

[163] COHEN, G.N., TRICHTER, S., LOVELOCK, M., FUNG, A.Y.C., LOSASSO, T., AMOLS, H.I., ABRAMSON, D., AND ZAIDER, M., Dosimetry and clinical application of ^{106}Ru eye plaques, Proceedings of the 22nd American Brachytherapy Society Meeting, pp. 71-72 (2001)

[164] TRICHTER, S., AMOLS, H., COHEN, G.N, LEWIS, D., LOSASSO, T., ZAIDER, M., Accurate dosimetry of Ru-106 ophthalmic applicators using GafChromic film in a solid water phantom, *Med. Phys*. **29**, p. 1349 (2002)

[165] MENAPACE, R., BINDER, W., CHIARI, A. Results and implications of high-resolution surface dosimetry of Ruthenium-106 eye applicators, *Ophthalmologica* 204, pp 93-100 (1992)

[166] TRICHTER S., ZAIDER M., NORI, D., SABBAS, A., KULIDZHANOV, F., LEWIS, D. AND SOARES, C.G., Clinical dosimetry of ^{106}Ru eye plaques in accordance with the forthcoming ISO beta dosimetry standard using specially designed GAFCHROMIC® Film , *Int. J. Radiation Oncology Biol. Phys*., **69** (Supplement 3), pp. S665-S666 (2007)

[167] ASTRAHAN, M.A., A patch source model for treatment planning of ruthenium ophthalmic applicators, *Med. Phys*., **30**, pp. 1219-1228 (2003)

[168] ROZAN, R., BACIN, F., ALBUISSON, E., DONNARIEIX, D. AND VERRELLE, P., Plaque therapy for uveal malignant melanoma, *Brachyther. J*., Supplement 3, pp. 51-58 (1993)

[169] KIRISITS, C., GEORG, D., WEXBERG, P., POKRAJAC, B., GLOGAR, D., AND PÖTTER, R., Determination and application of the reference isodose length (RIL) for commercial endovascular brachytherapy devices. *Radiother. Oncol*., **64**, pp. 309-315 (2002)

[170] IEC 60601-2-17:2005, *Medical electrical equipment — Part 2-17: Particular requirements for the safety of automatically-controlled brachytherapy afterloading equipment*

[171] ICRU Report 31, *Average Energy Required to Produce an Ion Pair*

[172] ICRU Report 60, *Fundamental Quantities and Units for Ionizing Radiation*

[173] NCS Report 13, *Quality Control in Brachytherapy: Current practice and minimum requirements*

[174] NCS Report 14, *Quality Control of Sealed Beta Sources in Brachytherapy: Recommendations on detectors, measurement procedures and quality control of beta sources*

[175] ISO 2919, *Radiation protection — Sealed radioactive sources — General requirements and classification*

[176] ISO 9978:1992, *Radiation protection — Sealed radioactive sources — Leakage test methods*

ICS 11.040.50; 17.240

Price based on 92 pages